University of Alberta

Experimental PVT Study of the Phase Behavior of CO_2 + Heavy Oil Mixtures

by

Keivan Khaleghi

A thesis submitted to the Faculty of Graduate Studies and Research
in partial fulfillment of the requirements for the degree of

Master of Science
in
Chemical Engineering
Department of Chemical and Materials Engineering

©Keivan Khaleghi
Fall 2011
Edmonton, Alberta

Abstract

Open pit mining can only be used to produce a fraction (15-20 %) of the vast heavy oil and bitumen resources in Canada. Alternative technologies such as gas injection can be used to access the resources trapped in deeper layers of earth. Phase behavior data is instrumental in designing such processes. CO_2 + heavy oil mixtures are opaque to visible light and viscous, and present phase behavior, phase composition and thermo-physical property measurement challenges, especially at high CO_2 mass fractions. X-ray computer-assisted tomography can be used to study such "ill-behaved" materials.

In this work, the phase behavior of Athabasca bitumen + CO_2 and Maya crude oil + CO_2 is briefed. A literature review is presented on the previous research works (mostly experimental studies) done on CO_2 + heavy oil and similar mixtures. Important aspects of phase behavior such as type of phase behavior, the onset CO_2 concentration of LLV behavior, K-point (L1=V, L2) data, two-phase critical point (L=V), CO_2 solubility in liquid phase and asphaltene precipitation are investigated. The experimental technique and data analysis methods are elaborated on in detail wherever needed. Different schemes, inspired by Henry's law and conjugate measurements, to estimate the phase boundaries of mixtures in two-phase region are presented and tested on the literature data. Furthermore, solubility of CO_2 in the liquid phase, type of phase behavior and phase diagrams and new critical points data as well as LLV onset concentration

data for the subject mixtures are presented in a broad range of temperature, pressure and composition. Some liquid-liquid diffusion data for the two subject mixtures are also presented.

Acknowledgments

Table of Contents

List of Tables

List of Figures

Nomenclature

I	(Normalized) Intensity of transmitted beam
I0	(Normalized) Intensity of the incident beam
w_i	Mass fraction of element "i"
Ж	Distance (Thickness)
λ	Wavelength of X-ray beam
λe	Effective wavelength of polychromatic X-ray beam
FOC	X-ray Focus
VLE	Vapor-Liquid Equilibrium
LLV	Liquid-Liquid-Vapor
LV	Liquid-Vapor
L1	Lighter Liquid Phase
L2	Heavier Liquid Phase
V	Vapor
Φ_{HL}	Heavier Liquid Volume Fraction
Φ_{LL}	Lighter Liquid Volume Fraction
v	Volume

DV	Dead Volume
ρ	Density
MW_i	Molecular weight of component "i"
n_i	Number of moles of component "i"
m_i	Mass of component "i"
HH	Heavy Hydrocarbon
T	Temperature
P	Pressure
H	Henry's Constant
x	Mole fraction of CO_2 in liquid phase
w/ w_{CO2}	Mass fraction of CO_2 (global)
s	Henry's constant parameter (s=w/P)
wv	Mass fraction of CO_2 (in the vapor phase)
w_l	Mass fraction of CO_2 (in the liquid phase)

Chapter I: *Introduction*

1.1. Background

Open pit mining can only be used to produce a fraction (15-20 %) of the vast heavy oil and bitumen resources in Canada. Alternative technologies need to be developed or optimized in order to access the balance [1]. SAGD (steam assisted gravity drainage) and EOR (enhanced oil recovery) are among these methods. Enhanced oil recovery (EOR) comprises a range of options. Examples include gas injection where gases such as CO_2, N_2 or natural gas are employed. In gas injection, high-pressure gas is injected into wells and fluid expansion drives a portion of the oil present (that was not recovered by primary and secondary methods) to the production well head [2]. The idea of using carbon dioxide as an oil solvent and viscosity breaker was proposed as early as 1952 and first became commercially viable during the seventies with increasing prices of oil and declining rates of oil recovery [3].

While reservoir geology and the flow and phase behavior of materials in porous media present important challenges for designing an injection process, the first step remains the investigation of the phase behavior of the injectant + reservoir fluid mixtures. The possibility of asphaltene precipitation and rejection in a reservoir and the near certainty of multiphase behavior over possibly narrow ranges of pressure, temperature and/or composition that may or may not intersect the production conditions are some of the issues that contribute to the importance of phase behavior studies. For mixtures of CO_2 + various light crude oil mixtures, the presence of multi-phase zones in phase diagrams is well known [4]. Technical strategies for avoiding multiphase zones during enhanced oil recovery, such as multi-contact processes based on dynamic miscibility have been developed [5]. CO_2 + heavy oil mixtures are opaque to visible light and viscous, and present phase behavior, phase composition and thermo-physical property measurement challenges, especially at high CO_2 mass fractions. Data

quality and data availability in the open literature limit the creation of general-purpose process design and operation optimization tools.

1.2. Experimental Technique

X-ray tomography PVT is a view cell technique developed in the early 90's [6] which enables one to investigate the phase behavior of mixtures opaque to visible light in a variable-volume high-pressure Beryllium PVT cell. In this method, different phases are distinguished based on differences in x-ray absorbance. Phases appearing in heavy oil + diluent mixtures are readily discriminated [7]. The number of phases, their volumes and densities are readily evaluated as are the coexistence pressures and temperatures.

1.3. Theoretical Considerations

A categorization of different types of binary phase behavior was performed by P. H. van Konynenburg and R. L. Scott in 1980 [8],[9]. They identified six types of phase behavior for binary and pseudo binary hydrocarbon and related mixtures. Mixtures of CO_2 + hydrocarbons exhibit Type II or IV (e.g. heptane and tridecane) and Type III phase behavior for heavier hydrocarbons [10]. Typical P-T and P-x (P-w) schematics of Type III behavior for a pseudo-binary mixture are presented in Figure 1.
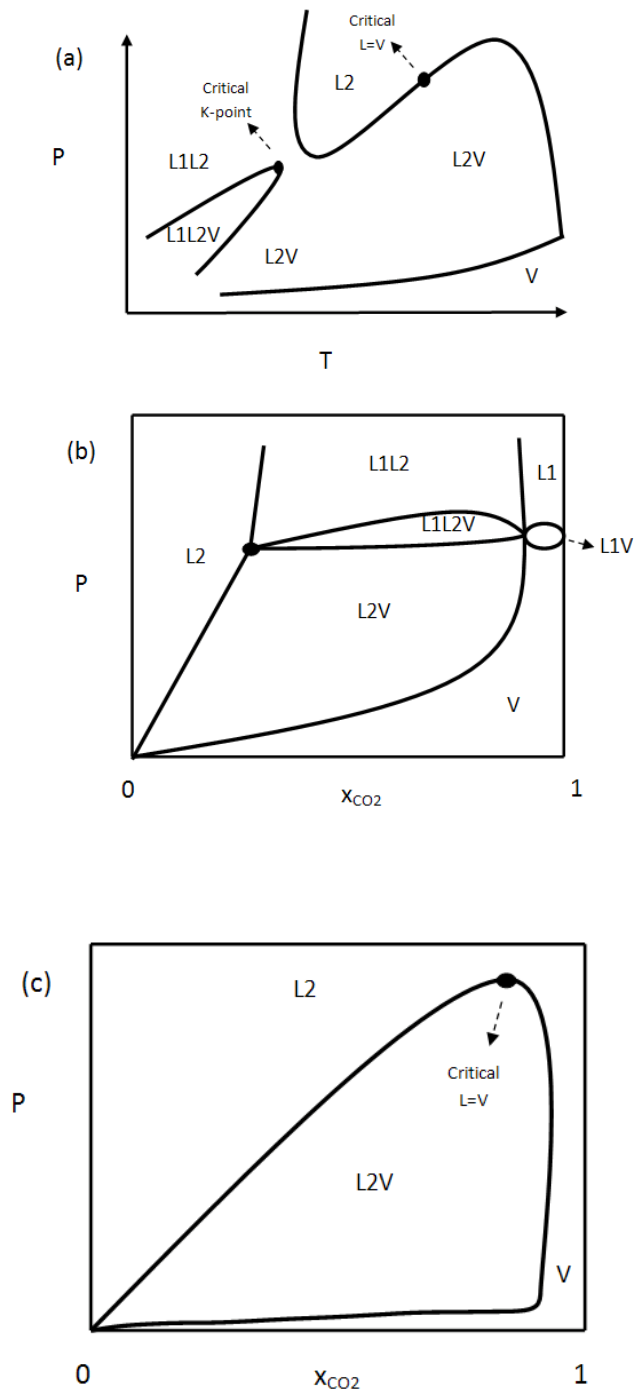
Figure 1: Type III pseudo-binary phase behavior: (a) Pressure-Temperature projection, (b) Pressure-Composition at fixed sub-critical temperature, (c) Pressure-Composition at fixed super-critical temperature [10], [11].

As it can be seen in Figure 1-a, pseudo binary mixtures exhibiting Type III behavior possess a low-temperature critical point, called a K-point (L1=V + L2), in the vicinity of the critical point of the lighter component over a broad range of compositions. At temperatures lower than that of the K-point, the mixture also exhibits multiphase behavior (L1L2V) over a narrow range of pressure with L2V phase behavior below and L1L2 phase behavior above for broad ranges of composition as shown in Figure 1-b. Above the K-point temperature, Figure 1-c, an ordinary critical point (L=V) appears along the L2V-L or V boundary.

1.4. Research Scope

The literature concerning multiphase phenomena and critical points for heavy oil + CO_2 is reviewed. New data related to multi-phase behavior, diffusion, criticality and solubility for the mixtures of Athabasca bitumen + CO_2 and Maya crude oil + CO_2 are presented and then validated by comparison with trends in the extant database.

Chapter II: *Literature Review*

2.1.   Overview

Several research studies have been performed on mixtures of pure materials, synthetic mixtures and oil samples + CO_2. A variety of static PVT experimental set-ups have been employed [12],[13]. The literature contains data on:

1- Bubble and dew point pressures (VLE Data)

2- Solubility data of CO_2 in the oil-rich liquid phase (two-phase region)

3- Multi-phase behavior and criticality (LLVE)

4- Multi-phase onset CO_2 concentration (minimum mass fraction for LLVE to appear)

5- Asphaltene precipitation in CO_2 + oil mixtures

These topics are summarized in a series of tables and figures, which facilitate comparisons. Data for pure compounds + CO_2 are expressed in terms of mole fractions in the literature. As the focus of this work is heavy oil/bitumen + CO_2 where hydrocarbon mean molar masses are unknown, composition data for pure compounds + CO_2 are recast in terms of mass fractions where employed in this work.

2.2.   Phase Behavior Topology

Enick et al. [10] investigated the phase behavior of C12, C13 and C14 alkanes + CO_2 mixtures using a windowed view cell. For C12, Type II phase behavior is observed. For C13, Type IV phase behavior was observed and for C14, Type III phase behavior is observed. Their experimental work illustrates the transition in the type of behavior expected for smaller and larger hydrocarbons. P-T projections showing this transition are depicted in Figure 2. Polishuk et al. [14] performed extensive simulations on the mixtures of CO_2 and several n-alkanes (from undecane (C11) to hexatriacontane (C36)) and compared the results with two other models (the Predictive Soave–Redlich–Kwong (PSRK) and a linear

combination of the Vidal and Michelsen mixing rules (LCVM)). They were able to simulate this phase behavior type transition from type II (C12) to type IV (C13) to type III (C14).
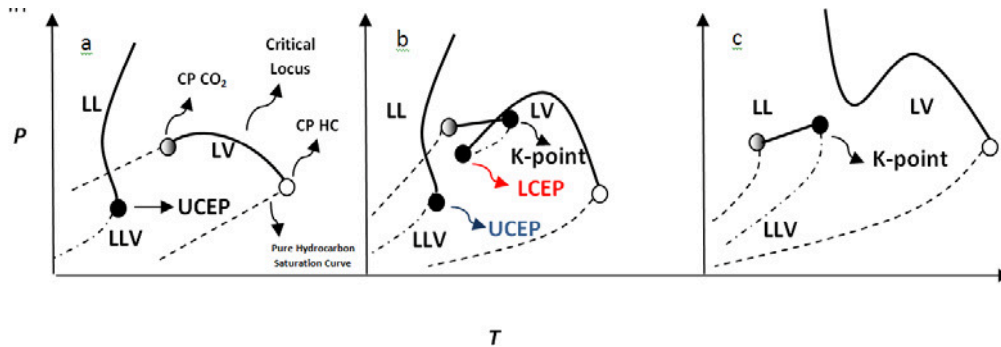
Figure 2: Qualitative P-T Diagram (a): C12H26, (b): C13H28, (c): C14H30; CP: critical point, UCEP: Upper critical end point, LCEP: Lower critical end point [10]

Miller and Luks [15] underscore the effect of carbon number in a hydrocarbon on the type of behavior of CO_2 + hydrocarbon mixtures. The results extend those of Enick et al. [10] to lower temperatures and to both lower and higher carbon number n-alkanes. For example, they traced the low temperature LLV curve from the Q-point (SL1L2V) to the upper critical endpoint (UCEP) for heptane, where the solid is solid heptane. Shaw and Béhar investigated the effect of solidification on phase diagrams in great detail [16], Figure 3. As the number of carbons in the n-alkane was increased to 13 (n-tridecane), a second LLV curve appears with a LCEP (lower critical endpoint) and a K-point – Figure 2-b. For tetradecane the lower and upper LLV curves merge – Figure 2-c. For larger hydrocarbons, the Q-point approaches the K-point, and the LLV curve becomes shorter, and for n-docosane, LLV behavior is no longer observed. This is shown schematically in Figure 4. The alkyl-benzene + CO_2 binary mixtures follow a similar trend. Transition to type III occurs at C14. Naphthenic compounds also appear to exhibit Type III behavior as illustrated by Vito, Jaubert, Pauly and Daridon [17] for cis-decalin + CO_2.
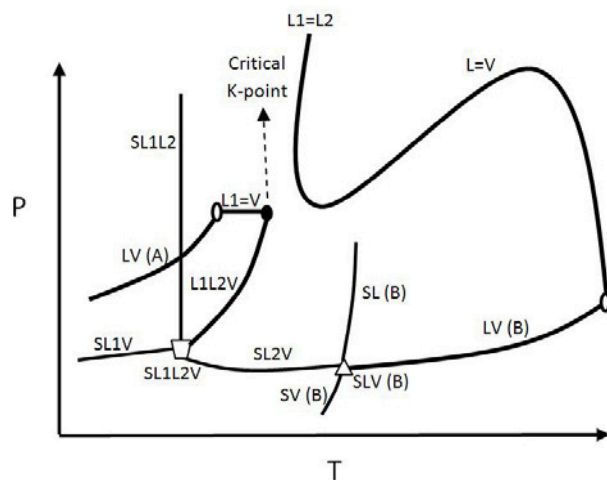
Figure 3: Effect of solidification on P-T critical projection of a type III binary mixture [16]
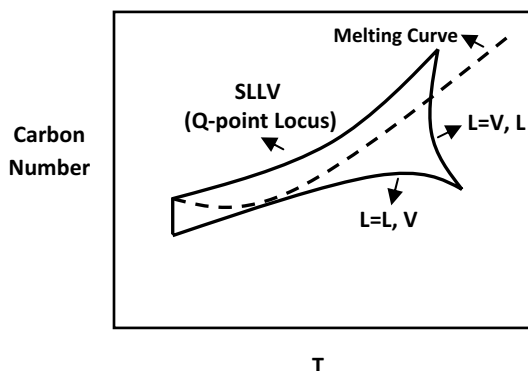
Figure 4: Role of Q-point in the phase behavior of mixtures of CO_2 + n-paraffins by Miller & Luks [15]

In the phase behavior transition region, addition of a third component can alter the phase behavior. For example, Foreman and Luks [18] studied the phase behavior of CO_2 + tetradecane + acetone. Addition of a small mass fraction of acetone, miscible with both constituents, splits the LLV region and UCEP and LCEPs are observed.

Heteroatoms and branching also play a role in phase behavior topology. Florusse et al. [19] investigated the behavior of the mixture of triglycerides + CO_2. They found that tricaprin ($C_{33}H_{62}O_6$) and tricaprylin ($C_{27}H_{50}O_6$), both oxygen rich branched hydrocarbons, Figure 5, exhibit type IV phase behavior with CO_2. Munuklua et al., [20] studied the mixtures: CO_2/Rp70 (hardened rapeseed),

CO2/tripalmitin, CO2/hydrogenated castor oil (HCO) in a Cailletet cell and classified all of them as type III pseudo-binary mixtures.
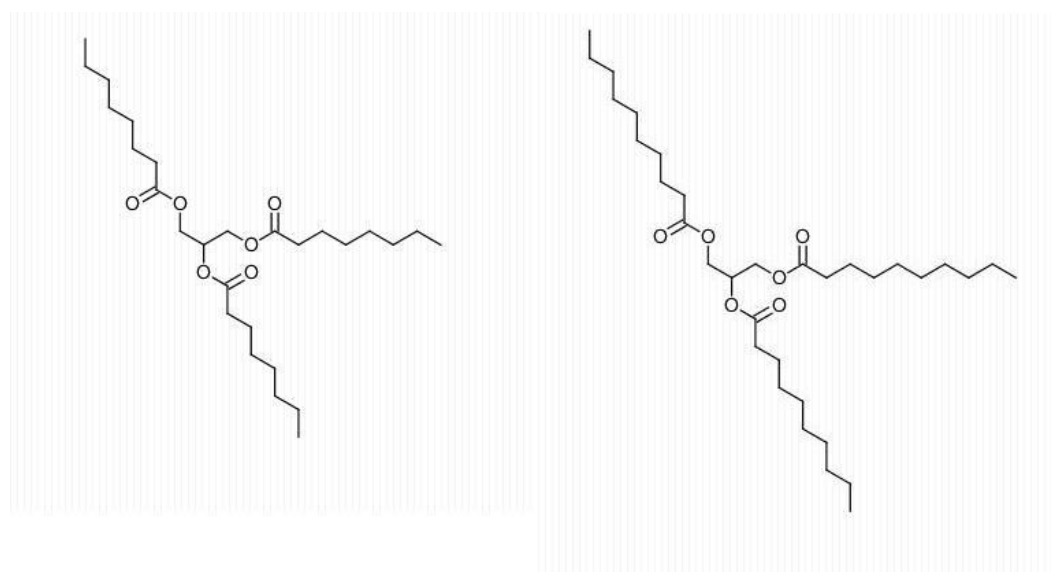
Figure 5: Molecular structure of tricaprylin (left) and tricaprin (right)

Complete phase diagrams for heavy oils, such as Maya crude oil, or Athabasca bitumen are not available. However these feed stocks are more than 50 % liquid at 295 K and more than 80 % liquid at 323 K and only completely solidify below ~ 200 K [21],[22]. As the molar masses of the feed stock constituents are high, typically more than 500 g/mole, Type III pseudo binary phase behavior is anticipated. A K-point is therefore expected in these phase diagrams, at a pressure and temperature greater than the critical pressure and temperature of CO_2 (304.13 K, 7377 kPa) in addition to L1=L2 and L2=V critical points. Given the extreme asymmetry of these pseudo binary mixtures, L1=V critical points, occurring at high CO_2 mass fraction are unlikely to be observable experimentally, and LLV phase behavior is expected to arise over a narrow pressure range at approximately the vapor pressure of CO_2. In subsequent sections, the appearance pressures of L1L2V phase behavior, the compositions of the coexisting phases, and critical points (L2=V, L1=V, L2) are explored in more detail for both pure compound + CO_2

binaries and for complex hydrocarbon mixtures + CO_2 pseudo binary mixtures. These data guided the performance of experiments and data analysis performed in this work. In the interests of brevity, these data are compiled in tables and summarized in figures.

2.3. Two phase criticality (L2=V Critical Points) for CO_2 + hydrocarbon binary and pseudo binary mixtures exhibiting Type III phase behavior

Available two phase critical points for CO_2 + hydrocarbon mixtures are listed in Table 1. Pressure-composition, temperature-composition and pressure-temperature plots, Figure 6, illustrate key trends. While the range of critical pressures is large, the narrowness of the composition range for L2=V critical points from ~310 K to ~380 K is notable. This feature of the data is exploited for data analyses reported in Chapter IV.

Table 1: L=V Critical point data for different hydrocarbons + CO_2 from the literature

Authors/Year/Reference	Method	Heavy Component/Molecular Weight (g/mole)	Temperature (K)	Critical Pressure (kPa)	$w_{critical}$
Vitu et al./2007/[23]	High pressure variable volume cell	Synthetic Oil/111.8	343.15	12300	0.8
			373.15	16000	0.7
Charoensombut-amon et al./1986/[24]	Sapphire Visual Cell	Hexadecane*/226.44	333.15	21700	0.9
Liphard & Schnider/1975/[25]	Sapphire Visual Cell	Squalane/422.81	343.2	43000	0.75
			353.2	38000	0.70
Brunner et al./2009/[26]	High pressure cell	Squalane/422.81	333.15	40000	0.71
Yokozeki/2007/[27]	Data extracted from a work by Youbi-Idrissi et al. [28]	PAG0 oil/400	323	17200	0.84
			333	20000	0.84
Souza et al./2004/[29]	High pressure variable volume cell	Clove oil/172.02	313.2	13500	0.7
			318.2	14500	0.7
Polishuk et al./2003/[14]	Data extracted from different papers	Hexadecane*/226.44	333.15	17500	0.7
			393.2	25000	0.7
Vitu et al./2008/[17]	Sapphire Visual Cell	cis-Decalin/138.25	333.15	19260	0.56
			353.15	21120	0.56

* The critical compositions are approximate.

(a)

(b)

(c)
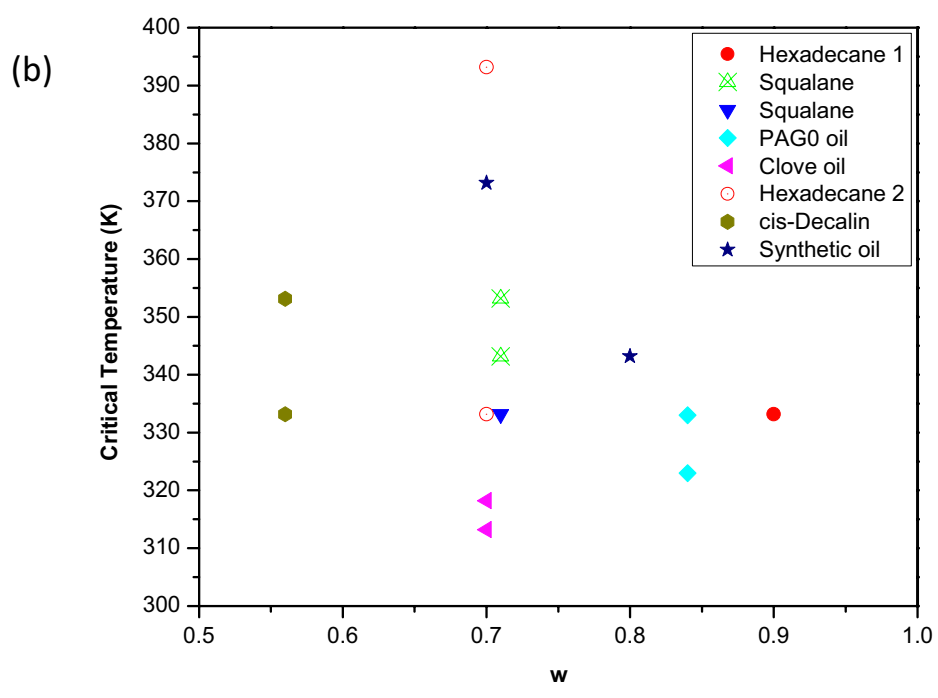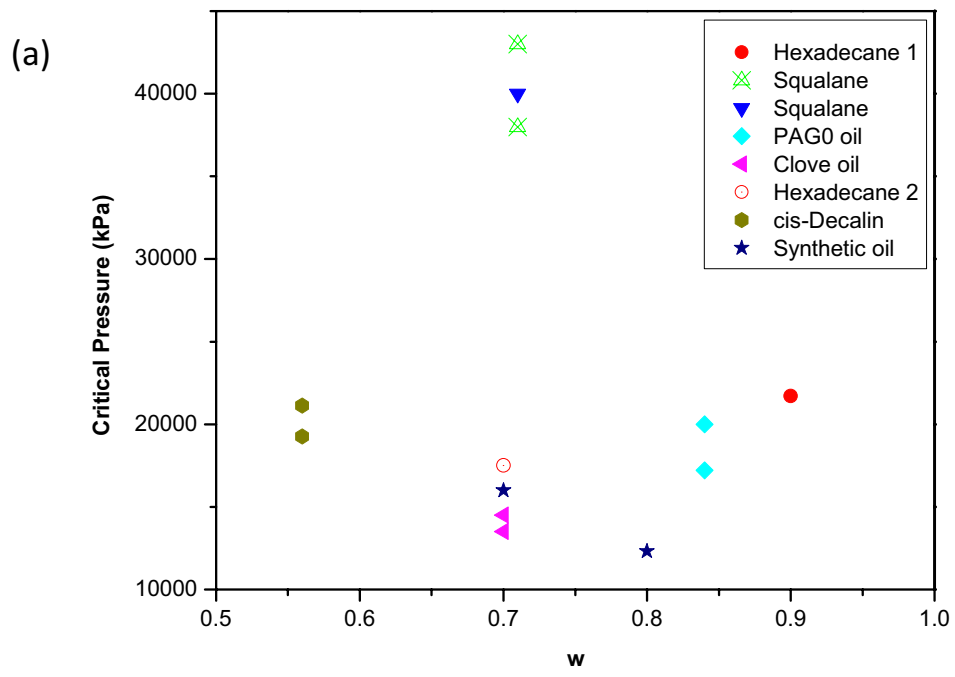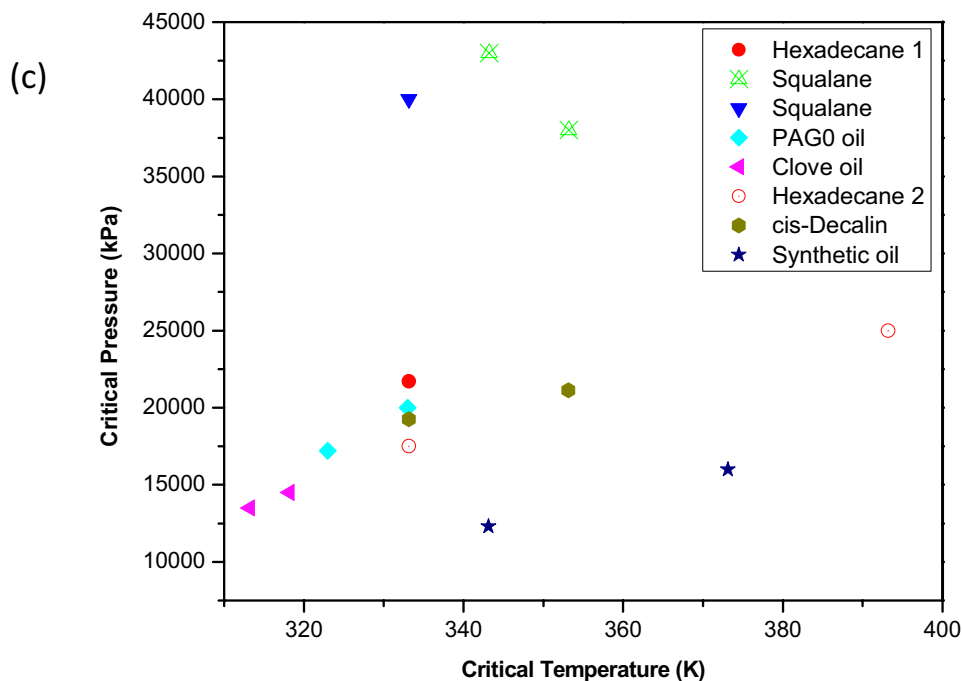
Figure 6: a) critical pressure-composition, b) critical temperature-composition, c) critical pressure- critical temperature trends for CO_2 + hydrocarbon mixtures, L=V 2-phase critical points, see references in Table 1

2.4. K-point data for CO_2 + hydrocarbon binary and pseudo binary mixtures exhibiting Type III phase behavior

K-point data of the mixtures of paraffinic and aromatic compounds + CO_2 are reported in the literature. Limited data for the mixtures of crude oils + CO_2 are also available. The data is presented in Table 2 and Figure 7. All of the K-points fall on a curve that approximates an extrapolation of the pure CO_2 vapor pressure curve.

Table 2: K-point data for CO_2 + hydrocarbon binary and pseudo binary mixtures exhibiting Type III phase behavior

Author/Year/Reference	Heavy Component	Critical Temperature (K)	Critical Pressure (kPa)	Mass Fraction of CO_2
Charoensombut-Amon/1986/[24]	hexadecane (C16)	308.15	7981	0.32
Hottovy et al/1981/[30]	tetradecane (C14)	311.15	8260	0.54
	pentadecane (C15)	309.41	8022	0.43
	eicosane (C20)	305.31	7549	0.27
Miller & Luks/1989/[15]	n-heptylbenzene (C13)	312.67	8499	NA
	n-octylbenzene (C14)	310.17	8167	NA

	tetradecylbenzene (C20)	305.07	7504	NA
Gutierrez & Luks/2001/[31]	1-methylnaphthalene	308.81	7930	NA
Kulkarni et al./1974/[32]	2-methylnaphthalene	309.48	7915	0.21
Lansangan et al/1987/[33]	n-hexylbenzene (C12)*	316.49	9032	NA
Vitu et al./2008/[17]	cis-decalin	312.15	8570	0.24
Larson et al./1988/[34]	C3+C16	309.15	8000	NA
Turek et al./1984/[35]	Oil A	319.2	10300	NA
Huang & Tracht/1974/[36]	A west Texas Crude	317.04<Tc<322.59	Pc>9300	NA
Liphard & Schneider/1975/[25]	Heavy Oil Mixtures**	Tc<322.15	NA	NA
Orr et al./1981/[37]	Heavy Oil Mixtures**	Tc<322.15	NA	NA
Turek et al/1988/[38]	west-Texas crude	Tc<316.5	NA	NA
Bryant & Monger/1988/[39]	Brookhaven Field Oil	Tc<314	NA	NA

*observation in one out of two samples, **estimated values
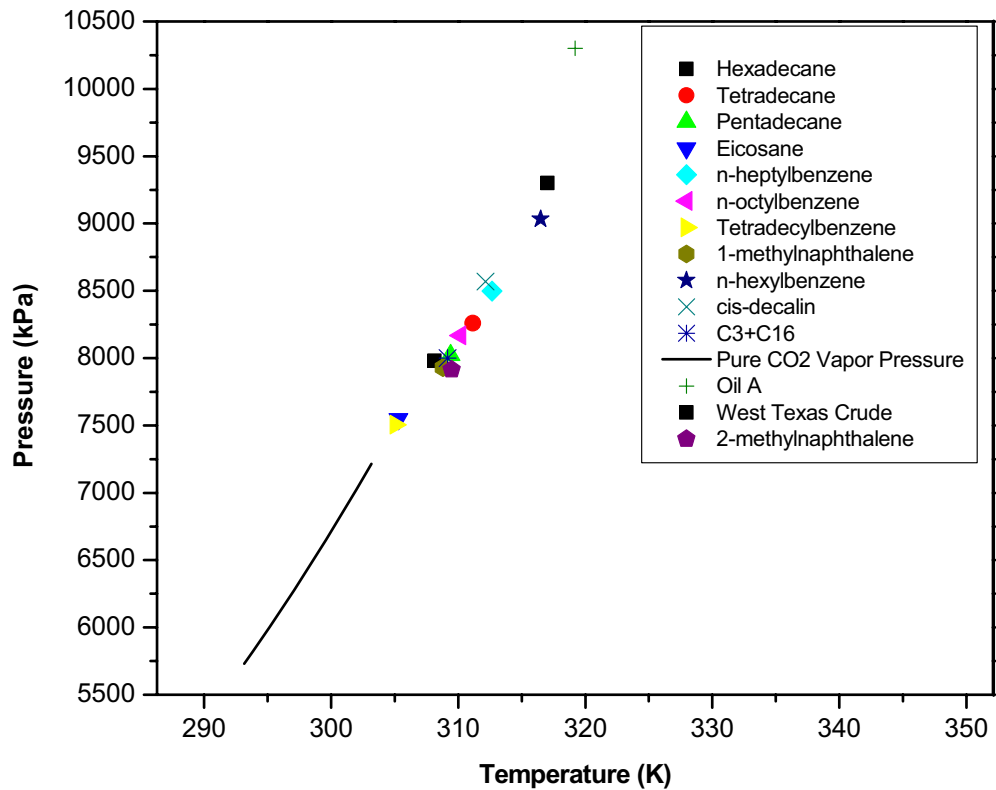
Figure 7: K-points for CO_2 + hydrocarbon mixtures listed in Table 2

2.5.   LLV Pressure for CO_2 + hydrocarbon binary and pseudo binary mixtures exhibiting TYPE III phase behavior

From the phase diagram topology exposition, LLV phase behavior is anticipated to arise at pressures approximating the vapor pressure of CO_2. LLV pressure data for a number of examples is provided in Table 3. These data are plotted against CO_2 vapor pressure in Figure 8. The anticipated behavior is clearly demonstrated. The composition of the saturated L2 phase is variable at fixed temperature 0.1 < w < 0.7 and is temperature dependent. There are no observations of LLV phase behavior above ~ 315 K. This value is lower than Orr et al.[37] provide as an estimate for the highest temperature at which LLV can exist for heavy crude + CO_2 mixtures - **322 K**. Orr and Jensen[40] also note that addition of C1, C2, C3 and C4 raised the saturated mass fraction of CO_2 in Wasson oil. Monger [41], [42] did not observe LLV phase behavior and report on only VLE for all the experimental points at w=0.16-0.17, T=20-40 C and P=28-240 atm in their latter work, even though LLV behavior would be expected to occur. Sako et al. [43] report data for the phase behavior of furfural + CO_2. At 303 K, a plateau in their P-w data suggests the presence of LLV behavior but LLV is not reported. At 323 K, there is no indication of LLV behavior in their data.

Table 3: LLV behavior for mixtures of heavy hydrocarbons + CO_2

Author(s)/Year/Reference	Method	Heavy Component/Molecular Weight (g/mole)	Temperature (K)	Pressure (kPa)	CO_2 Saturation Pressure (kPa)	saturated L2 (wCO_2)	Comments
Orr, et al/1981/[37]	Windowed Cell	Maljamar Separator Oil/183.7	305.35	6550-6620	SC	0.48	
		Recombined Maljamar Oil/102.4	305.35	7580-8270	SC	0.55	
Orr & Jensen/1984/[40]	Windowed Cell	Hexadecane/226.44	294.15 305.15	5900 7300	5865 SC	0.37	
		Wasson Stock Oil/252.04	305.37 313.70	7450 8600	SC SC	0.29 0.31	
		Recombined Wasson Oil (312 scf/bbl)/157.59	305.37 313.70	7600 9000	SC SC	0.39 0.42	
		Recombined Wasson Oil (602 scf/bbl)/116.72	305.37	10700	SC	0.40	
Sayegh & Sarbar/1990/[44]	Two-cell (one windowed, one blind) system	A Canadian heavy crude /628	294.15	6200-8300	5865	0.09	
Creek & Sheffield/1993/[45]	Windowed Cell	Permian basin Oil G/215	307.59	8050	SC	0.25	$w_{Mixture}=0.32$
		Permian basin Oil G/215	307.59	7700	SC	0.25	$w_{Mixture}=0.45$
		Permian basin Oil M/ 250	304.26	7200	SC	0.22	$w_{Mixture}=0.41$
		Permian basin Depleted Oil M/ 252	304.26	6900	SC	0.23	$w_{Mixture}=0.61$
Khan et al./1992/[12]	Unpublished Data from Texaco	West Texas Crude - North Ward Estes (NWE)/229	301.48	≈9000	6944	0.20	LLV pressure: 6200-9000 kPa
		West Texas Crude - Oil G/215	307.59	≈9000	SC	0.20	LLV pressure: 7200-9300 kPa
		West Texas Crude - (JEMA)/248	316.48	≈9000	SC	0.21	LLV pressure: 8200-9000 kPa

Reference	Cell	Oil	T (K)	P	P	Value	Comments
		West Texas Crude - BSB/229	313.71	≈9000	SC	0.21	LLV pressure: 8200-9000 kPa
Eastick et al./1992/[46]	High Pressure Cell	Cold Lake Bitumen	297.85	6500	6390	0.12	
Badamchizadeh et al./2009/[13]	Windowed Cell	Athabasca Bitumen	298.15	6500	6500	0.10-0.12	LL observed up to 313.15 K, 9000 kPa
DeRuiter et al/1994/[47]	High Pressure Cell	Alaskan West Sak reservoir oil A/330	291.45	5520	5500	0.16	
		Alaskan West Sak reservoir oil B/446	291.45	5930	5500	0.11-0.12	
Pollack & Enick/1988/[48]	Ruska Cell	Maljamar oil/200	304	7070	7355	0.3	
Fall & Luks/1986/[49]	Glass Equilibrium Cell	n-Heptylbenzene/176.30	227.67 311.72	817 8319	815 SC*	0.21 0.57	the higher the T, the smaller the immiscibility region over concentration range
Kokal & Sayegh/1993/[50]	Two-cell (one windowed, one blind) system	Lone Rock heavy oil/386	294.15	5800		0.15	The solid fraction (21 wt % of oil) & very light fraction of the oil (20 wt % of oil) have little effect on the solubility of CO_2 in heavy oil.
		Lone Rock heavy oil, De-oil/347	294.15	5700	5900	0.17	
		Lone Rock heavy oil, De-oil, Fraction 2/465	294.15	5650		0.14	
Mehrotra & Svrcek /1988/[51]	Flow-type PVT cell set-up	Cold Lake Bitumen	288.15 299.15	5200 6500	5087 6584	0.12 0.12	
Miller and Jones/1981/[52]	Flow-type PVT cell set-up	Wilmington oil/API=17	297.04	6600	6272	0.15	
Monger/1985/[41]	PVT Cell	Synthetic Paraffinic "Oil P"/183	312.3	7900	SC	0.49	
		Synthetic Paraffinic/Aromatic "Oil P/A"/128	313.3	NA	SC	No LLV	
		Synthetic Blend "Oil P/A+P"/156	311.4	7900	SC	0.61	

Quail et al./1988/[53]	Visual PVT cell	heavy Saskatchewan oil from Senlac field/419	301.1	5520-7580	6884	0.13
Sako et al./1998/[43]	Windowed Cell	Furfural/98.08	303	6400	7189	0.6-0.7
Turek et al./1984/[35]	Variable-volume Windowed Cell	Reservoir Oil A/226	314.2	9900	SC	0.23
Turek et al./1988/[38]	Variable-volume Windowed Cell	West Texas Reservoir Oil A/253	313.71	11500	SC	0.19
		West Texas Reservoir Oil B1/226	314.26	10700	SC	0.20
		West Texas Reservoir Oil B2/233	314.26	9900	SC	0.22
		West Texas Reservoir Oil C2/230	307.59 313.71	9300 10200	SC	0.18 0.21
		West Texas Reservoir Oil C1 (Weathered at 297.04 K)/251	307.59	7500	SC	0.24
		West Texas Reservoir Oil C1 (Weathered at 313.15 K)/290	307.59	7700	SC	0.23
		West Texas Reservoir Oil D/247	313.71	10000	SC	0.21
		West Texas Reservoir Oil E/226	322.04	No LLV	SC	No LLV
		West Texas Reservoir Oil F/243	313.71	11000	SC	0.19
Larson et al./1989/[34]	Visual PVT cell	Hexadecane/226.44	305.37	7400	SC	0.39
		Squalane/422.8	299.82 305.37	6700 No LLV	6686 SC	0.25 NA
Kulkarni et al./1974/[32]	Glass Equilibrium Cell	2-methylnaphthalene/142.2	298.15 304.15	6125 7002	6434 SC	0.24 0.23

*supercritical state, CO_2 vapor pressure does not exist
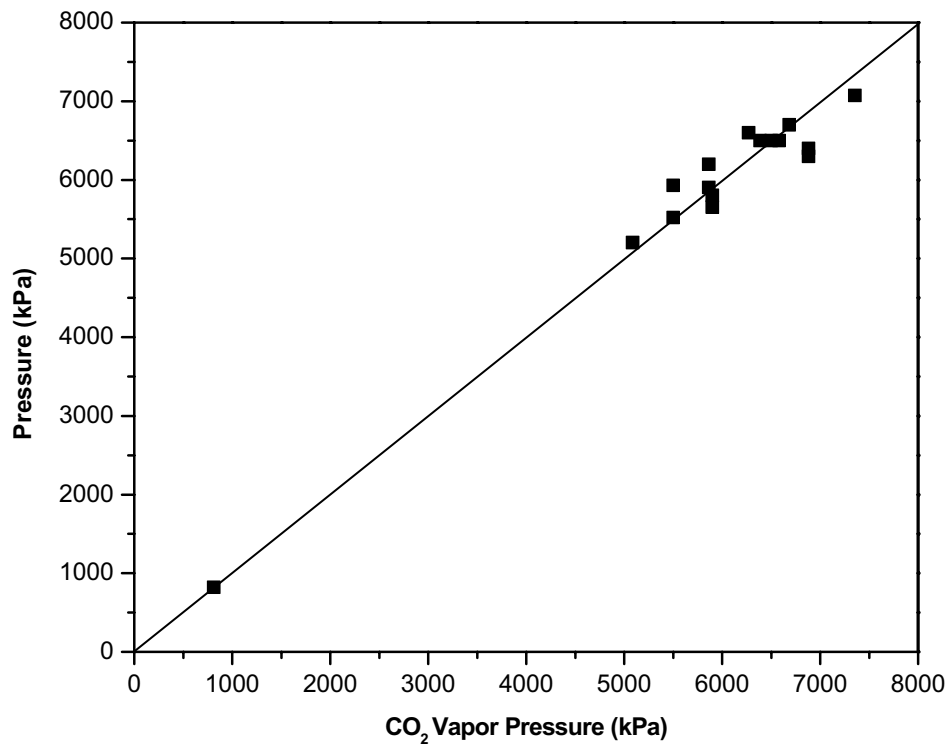
Figure 8: LLV appearance pressure in binary and pseudo binary mixtures of hydrocarbons + CO_2 compared with the vapor pressure of CO_2 at the same temperature, references in Table 3

2.6. L1V Region

At temperatures where L1L2V multiphase behavior arises, an L1V region at high CO_2 mass fractions is expected as shown in Table 4 where onset weight fractions range from 0.87 to 0.97.

Table 4: L1V region data for the mixtures of CO_2 + different hydrocarbons

Author/Year/Reference	Heavy Compound/Molecular Weight (g/mole)	Temperature (K)	Pressure (kPa)	L1V Onset Composition (w_{CO_2})
Enick et al./1985/[10]	Tridecane/184.35	310.8	≈8200-8300	0.87
		311.9	≈8350-8500	0.88
		313	≈8550-8620	0.9
Gutierrez & Luks/2001/[31]	1-methylnaphthalene/142.2	293.14	5581	0.94
		298.13	6246	0.95
		303	6988	0.96
Pollack & Enick/1988/[48]	Maljamar oil/200	304	NA	L1V is not observed
Vitu/2008/	cis-decalin/138.25	293.05	≈7100-7850	0.94

Miller & Luks/1989/[54]	Tetradecylbenzene/260.46	293.19	5717	0.97
Turek et al./1984/[35]	Oil A/226	314.2	≈8000-9000	L1V is not observed
Creek & Sheffield/1993/[45]	Recombined Oil G/215	308	≈7600 Kpa	0.91

2.7. CO_2 solubility in the hydrocarbon rich phase (L2) as a function of pressure and temperature in binary and pseudo binary mixtures exhibiting Type III behavior

Studies related to CO_2 solubility in pertinent hydrocarbons are summarized in Table 5. Molar mass and structure affect CO_2 solubility. The general trends are:

1- Solubility decreases with increasing temperature,

2- Solubility increases linearly with pressure at fixed temperature.

3- Solubility decreases with increasing molar mass and aromatic carbon content at fixed pressure.

However, solubility approaches a maximum near the K-point. Lee and Chao [55] reported on 1-methylnaphthalene + CO_2 and show that solubility increases with temperature. They may have been working below the K-point in their work.

Table 5: VLE data for mixtures of heavy hydrocarbons + CO_2

Author(s)/Year/Reference	Method	Heavy Component/Molecular Weight (g/mole)	Composition Range (w_{CO2})	Pressure Range (kPa)	Temperature (K)
Han et al./1992/[56]	High Pressure PVT Cell	Peace River Bitumen	0.07-0.14	7000-14000	318.15
			0.07-0.14	7000-14000	328.15
Hong et al./1994/[57]	Windowed Cell	Prudhoe Bay oil - Cut A/117	0.03-0.25	1300-7800	360.93
		Prudhoe Bay oil - Cut B/163	0.02-0.20	1100-8000	360.93
		Prudhoe Bay oil - Cut C/215	0.01-0.16	1050-8000	360.93
		Prudhoe Bay oil - Cut D/272	0.02-0.13	1400-8100	360.93
		Prudhoe Bay oil - Cut E/338	0.01-0.13	1300-8150	360.93
Huang & Radosz/1990/[58]	Flow-type Apparatus	Cold Lake Bitumen - Cut 1/201	0.03-0.4	4000-16000	323.5
			0.03-0.26	4000-16000	373.4
			0.03-0.16	4000-16000	473.5
			0.03-0.11	4000-12000	523.2
		Cold Lake Bitumen - Cut 2/304	0.03-0.21	4000-16000	323.3
			0.03-0.17	4000-16000	373.4
			0.03-0.11	4000-16000	473.5
			0.03-0.08	4000-12000	523.2
		Cold Lake Bitumen - Cut 3/572	0.03-0.14	4000-16000	323.3
			0.03-0.12	4000-16000	373.3
			0.03-0.08	4000-16000	473.5
			0.03-0.06	4000-12000	523.2
Inomata et al./1987/[59]	Flow-type Apparatus	Benzene/78.11	0.09-0.6	2000-10000	343.6
			0.09-0.70	3900-15400	343.6
Kim et al./1989/[60]	PVT cell	Tetralin/132.2	0.07-0.82	3200-19200	343.6
			0.05-0.5	3100-22100	373.1
		1-methylnaphthalene/142.2	0.04-0.32	3700-21000	372.6
Gasem et al./1989/[61]	Windowed Cell	Tetradecane/198.39	0.32-0.66	11000-16300	344.3

Reference	Apparatus	Solvent/Molar Mass	Solubility	Pressure	Temperature
Kulkarni et al./1974/[32]	Windowed Cell	1-methylnaphthalene/142.2	0.02-0.19	870-7000	307.15
			0.03-0.13	1500-6600	324.15
			0.02-0.10	1500-6600	348.15
			0.02-0.08	1500-6600	373.15
Huie et al./1973/[62]	Windowed Cell	n-eicosane/282.55	0.01-0.25	500-7600	310.15
			0.01-0.20	500-7600	323.15
			0.01-0.15	500-7600	348.15
			0.01-0.11	500-7600	373.15
Liu et al./1999/[63]	Two-cell Apparatus	Jiangsu Oil	0.04-0.26	2500-14700	328.15
			0.03-0.27	3000-16100	348.15
Mehrotra et al./1988/[64]	Flow-type Apparatus	Athabasca Bitumen - UofC	0.03-0.09	900-10300	352.45
		Athabasca Bitumen - ARC	0.04-0.09	2500-11900	353.15
Mehrotra et al./1989/[65]	Varying–Volume Equilibrium Cell	Peace River Bitumen	0.01-0.07	2000-9400	352.87
			0.01-0.05	2300-10000	393.01
			0.01-0.04	2100-10000	432.77
			0.01-0.04	2200-10000	472.73
Yu et al./1989/[66]	Flow type - Windowed Cell Apparatus	Cold Lake bitumen	0.03-0.12	4000-16000	373.3
			0.02-0.08	4000-16000	473.7
			0.02-0.05	4000-12000	523.1
Mohamed & Holder/1987/[67]	Flow-type Apparatus	m-xylene/106.16	0.12-0.7	2400-7250	312.65
			0.07-0.62	2400-10600	338.15
			0.06-0.6	2400-15400	366.15
		ethylbenzene/106.16	0.09-0.62	2300-7000	312.65
			0.07-0.62	2400-10600	338.15
			0.07-0.62	4000-14000	366.15
		o-xylene/106.16	0.09-0.7	2100-7000	312.65
			0.07-0.62	2300-10500	338.15
			0.06-0.6	2500-15000	366.15
Morris & Donohue/1985/[68]	PVT Cell	1-methylnaphthalene/142.2	0.03-0.23	1500-14400	353.15
			0.01-0.16	1200-14500	413.15
Mehrotra & Svrcek /1988/[51]	Flow-type Apparatus	Cold Lake Bitumen	0.02-0.13	2100-10600	325.62
			0.02-0.11	2500-10900	350.05

			0.01-0.08	2300-10500	371.07
Eastick et al./1992/[46]	High Pressure PVT Cell	Cold Lake Bitumen	0.03-0.11	2850-10200	324.15
			0.02-0.09	2470-10400	347.65
			0.02-0.08	2600-10300	370.05

There appear to be some exceptions to the general linearity of $P - w$ at constant temperature plots. For example, Han et al. [56], report a non-linear trend for Peace River bitumen + CO_2 as shown in Figure 9. Hong et al. [57] report an opposing non-linear trend for Prudhoe Bay oil cuts + CO_2 at 360.93 K (VLE) as shown in Figure 10.
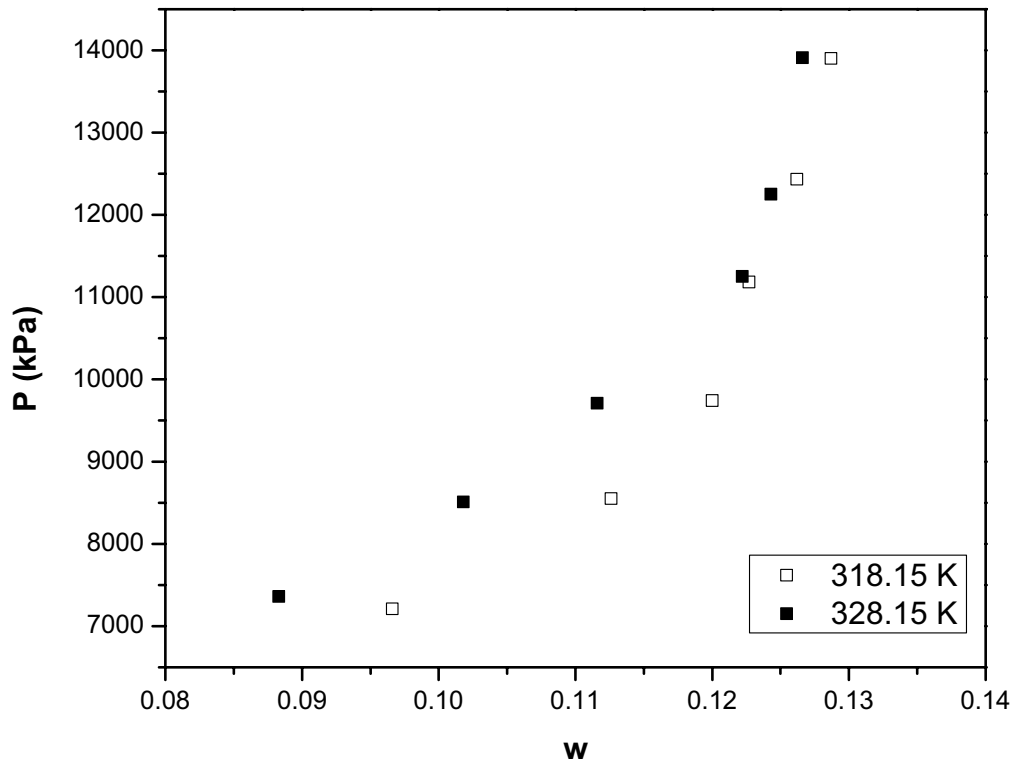
Figure 9: P-w diagram for the mixture of Peace River Bitumen + CO_2 at low concentrations of CO_2 by Han et al. [56]
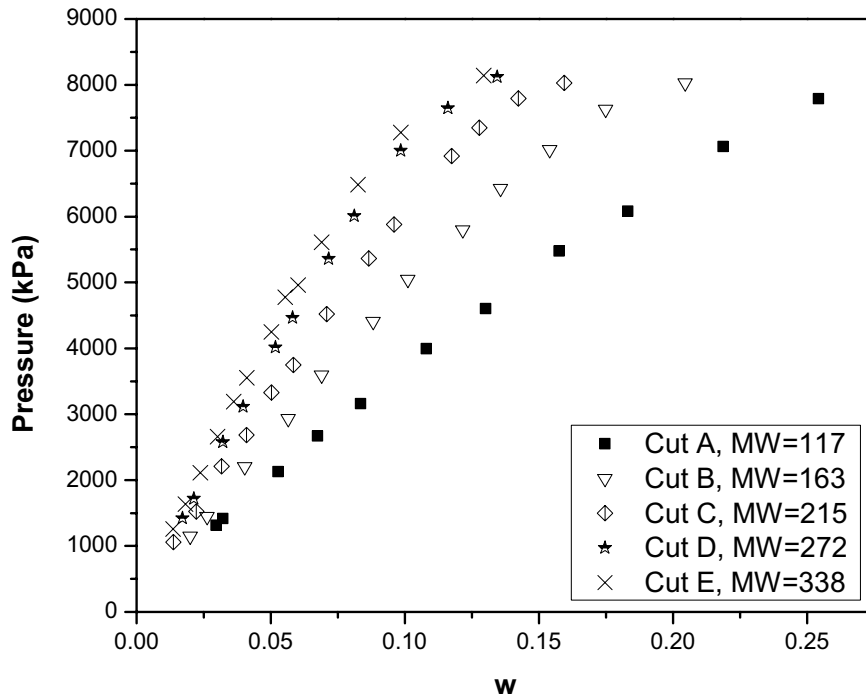
Figure 10: Data of CO$_2$ solubility in Prudhoe Bay oil by Hong et al. [57]

Mehrotra et al. [64] performed a joint investigation between the University of Calgary and Alberta research council (ARC) to measure the solubility of CO$_2$ in Athabasca bitumen to reconcile the differences in their works in the past. The University of Calgary apparatus is a flow-type device while ARC utilized a rocking equilibrium cell to perform their experiments. The results are illustrated in Figure 11 at 352.45 K and 353.15 K for UofC and ARC experiments, respectively. The results are in good agreement; thus the inconsistency in the data of the previous works was attributed to the different bitumen samples used in the experiments. Sample variability based on sample origin, sample preparation, thermal history etc. has a significant effect on the properties of nominally similar materials given the same name e.g. Athabasca bitumen [22].
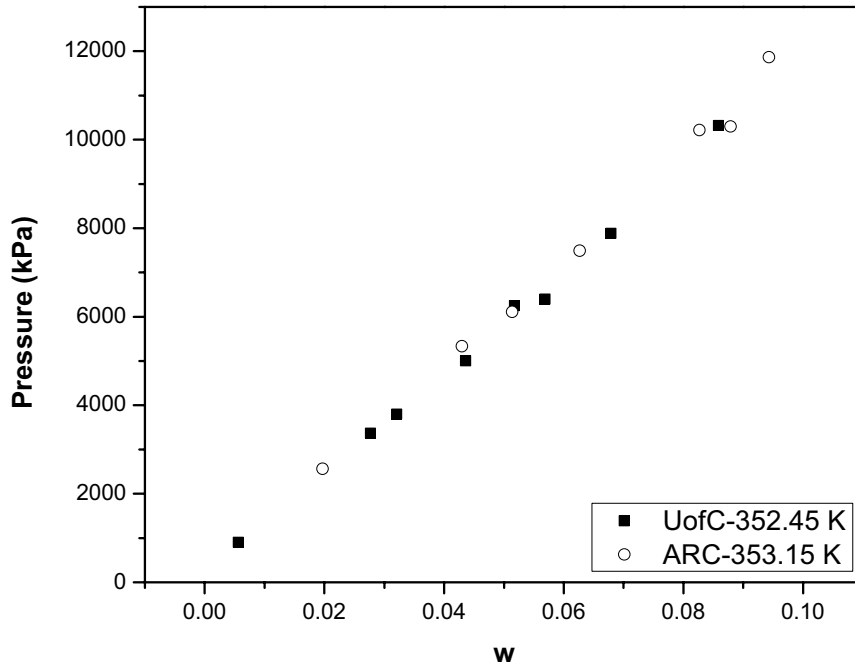
Figure 11: Results of CO$_2$ Solubility in Athabasca bitumen by Mehrotra et al. [64]

2.8. Asphaltene Precipitation in CO$_2$ + hydrocarbon mixtures

Data concerning asphaltene precipitation in the presence of CO$_2$ is diverse and contradictory. A summary of the data in the literature on this subject is provided in Table 6. Depending on the method of study and molecular weight distribution of the heavy oil as well as the temperature, pressure and composition, different results are obtained. In most cases in which deposition is observed, the pressure is near the bubble pressure of the mixtures.

Table 6: Asphaltene precipitation data for the mixtures of crude oils + CO_2

Authors/Year/Reference	Method	Heavy Component/Molecular Weight (g/mole)	Temperature (K)	Pressure (kPa)	w	Asphaltene Precipitation YES/NO
Monger/1985/[41]	PVT Cell	Brookhaven crude/246 (by Freezing Point Depression)	333.2	22000	NA	YES severe asphaltic plugging occurred in displacement test
		Brookhaven crude/212 (by GC)				
Sayegh & Sarbar/1990/[44]	Two-cell Apparatus	A Canadian heavy crude /628	294.15	6200-10300	NA	Indefinite
			413.15	2800	NA	YES
Creek & Shefield/1993/[45]	Windowed Cell	Permian basin - Oil G/215	304.3	6900-8200	NA	YES
		Permian basin Oil M/ 250				
Kokal & Sayegh/1993/[50]	Two-cell (one windowed, one blind) system	Lone Rock heavy oil/386	294.15 413.15	NA	NA	NO
Turek et al/1984/[35]	Variable-volume Windowed Cell	Reservoir Oil A/226*	314.2	5000-10300	0.0-1.0	YES/did not settle out after 48 hrs, dispersed
Simon & Roseman/1977/[69]	Visual Cell	Reservoir Oil A/87.51	327.59	13700-20700	w>0.67	YES
		Reservoir Oil B/239.1	397.04	27600-34500	w>0.31	
Novosad & Costain/1990/[70]	Visual Cell and Titration Set-up	Midale Recombined Reservoir Fluid/259	338.15	11000-13000	w>0.1	YES
Kokal et al./1992/[71]	Micro-model Apparatus	Suffield Oil/NA	298.15	15000	NA	YES
			323.15	17000		YES
			348.15	>20000		Indefinite
			373.15	>20000		Indefinite
		Lindbergh Oil/NA	298.15	>20000	NA	Indefinite
			323.15	20000		YES
			348.15	17000		YES
			373.15	15000		YES

*Molecular weight of C7+

2.8. Liquid-Vapor and Liquid-Liquid Diffusion Data

Data on liquid-liquid mutual diffusion coefficient of hydrocarbons/CO_2 could not be found. Though, some data on liquid-vapor diffusion exist in the literature.

Table 7 compares gas-liquid diffusion coefficients for the mixtures of heavy hydrocarbons/CO_2. The values for different heavy oils fall in the same order of magnitude.

Table 7: Gas-Liquid diffusivity data for CO_2/Heavy hydrocarbons mixtures

Author/Year/Reference	Method	Heavy Compound	Temperature (K)	Pressure (kPa)	Solubility (CO_2 Mass Fraction)	Diffusivity (10^9*m^2/s)
Zabala et al./2008/[72]	Molecular Simulation/PC-SAFT	C16	298	Indefinite	0.08-0.23	2-3
Upreti & Mehrotra/2000/[73]	Pressure-decay Method	Athabasca Bitumen	298.15-363.15	4000	0.00-0.06	0.16-0.47
Song et al./2010/[74]	X-ray Tomography	Heavy Oil (15 Pa.s)	296.15	1180-1670	0.00-0.07	0.03-0.69
Yang & Gu/2008/[75]	Dynamic Interfacial Tension	Weyburn Crude	300.15	100-5000	Indefinite	0.47-2.49
Thanasvian/2006/[76]	Pressure-decay Method	Lloydminster Crude	297.05	3500-4200	0.06-0.09	0.46-0.94
					Gas-Oil Ratio (cm^3/cm^3)	
Zhang et al/2000/[77]	Pressure-decay Method	Heavy Oil (5 Pa.s)	294.15	3741	23.7	4.8
					Solubility (g/cm^3)	
Etminan et al./2010/[78]	Pressure-decay Method	Athabasca Bitumen	323.15	3804.8	0.03934	0.36
			348.15	3239.6	0.03414	0.5

Table 8: Self-diffusion coefficient for carbon dioxide by Gross et al. [79]

P (MPa)	10	20	30
T (K)	D (10^9*m^2/s)		
373	-	-	33.7
333	-	26.9	20.8
298	18.8	15.1	-

The mutual diffusion coefficients of CO_2/Hydrocarbons (Table 7) should not exceed the self-diffusion coefficient of CO_2 (Table 8) at the same conditions.

2.9. Summary

Mixtures of heavy hydrocarbons + CO_2 are expected to exhibit Type III phase behavior if considered as pseudo-binary mixtures. Type III phase behavior

includes LLV phase behavior along a curve adjacent to the vapor pressure of CO_2 that extends from the freezing point of the mixture to a K-point occurring at a pressure and temperature exceeding the critical temperature and pressure of CO_2. For heavy hydrocarbons, the maximum observed K-point temperature is ~ 315 K. At higher temperatures, CO_2 + hydrocarbon mixtures exhibit L2, L2V, and V phase behavior. For the temperature range of 320 K to 380 K, the composition at the L2=V critical point is 0.8 +/- 0.1 wt fraction CO_2.

In general, the solubility of CO_2 increases linearly with pressure and decreases with temperature at fixed pressure. CO_2 solubility in hydrocarbons decreases with molar mass and is lower in aromatic hydrocarbons than in aliphatic compounds. For heavy oil + CO_2 mixtures, critical point data of all types and saturated L1 phase compositions are lacking in the literature.

Chapter III: Materials, Experimental Technique & Methods

3.1. Materials

CO$_2$ provided by PRAXAIR ® (99.999% purity) was used in the experiments. Athabasca bitumen (Alberta, Canada) was obtained from Syncrude Canada Ltd. Maya crude oil (a commercial-blend heavy-oil from Mexico) was supplied by the Mexican Petroleum Institute. Their properties are summarized in Table 9 and Table 10 [22].

Table 9: SARA analysis for Athabasca bitumen and Maya crude oil samples

sample	saturates	aromatics	resins	C5 asphaltenes
	wt. %			
Athabasca bitumen	16.1	48.5	16.8	18.6
Maya crude oil	31.6	42.5	10.2	15.7

Table 10: Elemental composition of Athabasca bitumen and Maya crude oil samples

Element	Athabasca bitumen	Maya crude oil
Elemental analysis, wt. %		
C	83.2	84.5
H	9.7	11.3
N	0.4	0.3
S	5.3	3.3
O	1.7	1.2
Metal analysis, mg/kg		
Al	492	1.0
Ba	6.4	<0.1
K	77	1
Ca	163	29
Cr	2.8	0.8

Fe	762	4.0
Mg	65	0.7
Mn	30	<0.1
Mo	12	3.0
Na	91	112
Ni	93	56
Si	355	80
Ti	24	0.4
V	247	263
Zn	4.4	1.6

3.2. Experimental Technique

3.2.1. Principles of X-ray Tomography

X-ray tomography was used to study the phase behavior of Maya crude oil + CO_2 and Athabasca bitumen + CO_2 mixtures. This technique permits the study of the phase behavior of opaque mixtures that are difficult to examine otherwise. The fundamentals of the method are briefly explained here and illustrated in Figure 12. See Abedi et al. [6] for more details. X-rays emitted from a source are transmitted, absorbed or scattered by a sample. The attenuation or relative attenuation of the transmitted beam elucidate local composition, and local density [6].
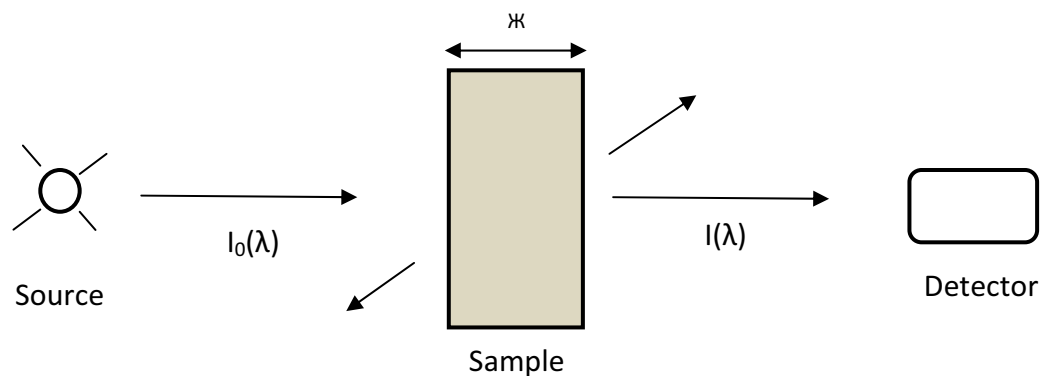
Figure 12: Schematic of x-ray tomography set-up

$$I(\lambda) = I_0(\lambda) * \exp\left(-\rho Ж \mu(\lambda)\right) \qquad \textbf{(1)}$$

$I_0(\lambda)$ is the intensity of the incident beam;

I(λ) is the intensity of the transmitted beam;

ρ is the density of the sample, g/cm^3;

Ж is the width of the sample, cm;

μ (λ) is the apparent mass absorption coefficient of the medium at wavelength λ, cm^2/g.

3.2.2. Experimental Set-up

An X-ray view cell apparatus was used to perform phase behavior measurements. A schematic drawing of the apparatus is shown in Figure 13. It consists of three principle parts: (1) a Phillips MCN-165 tungsten-target bremsstrahlung X-ray source with spectral endpoint energies between 5 and 160 keV, (2) an X-ray view cell (see Figure 13, Figure 14 and Appendix I for details), and (3) an X-ray video capture system comprising a Microphotonics X-ray imager camera, LA 115 mn, with a spatial resolution of 150 μm/pixel and an image capture speed of 33 frames/s. Agilent Pro 8.5 and Image Pro 5.5 software are used for image acquisition. Temperature sensors, comprising RTDs (resistive thermal devices) and pressure transducers are synchronized with the online data acquisition system. A hand-operated high-pressure gas (CO_2) loop was installed and used to meter CO_2 into the view cell.
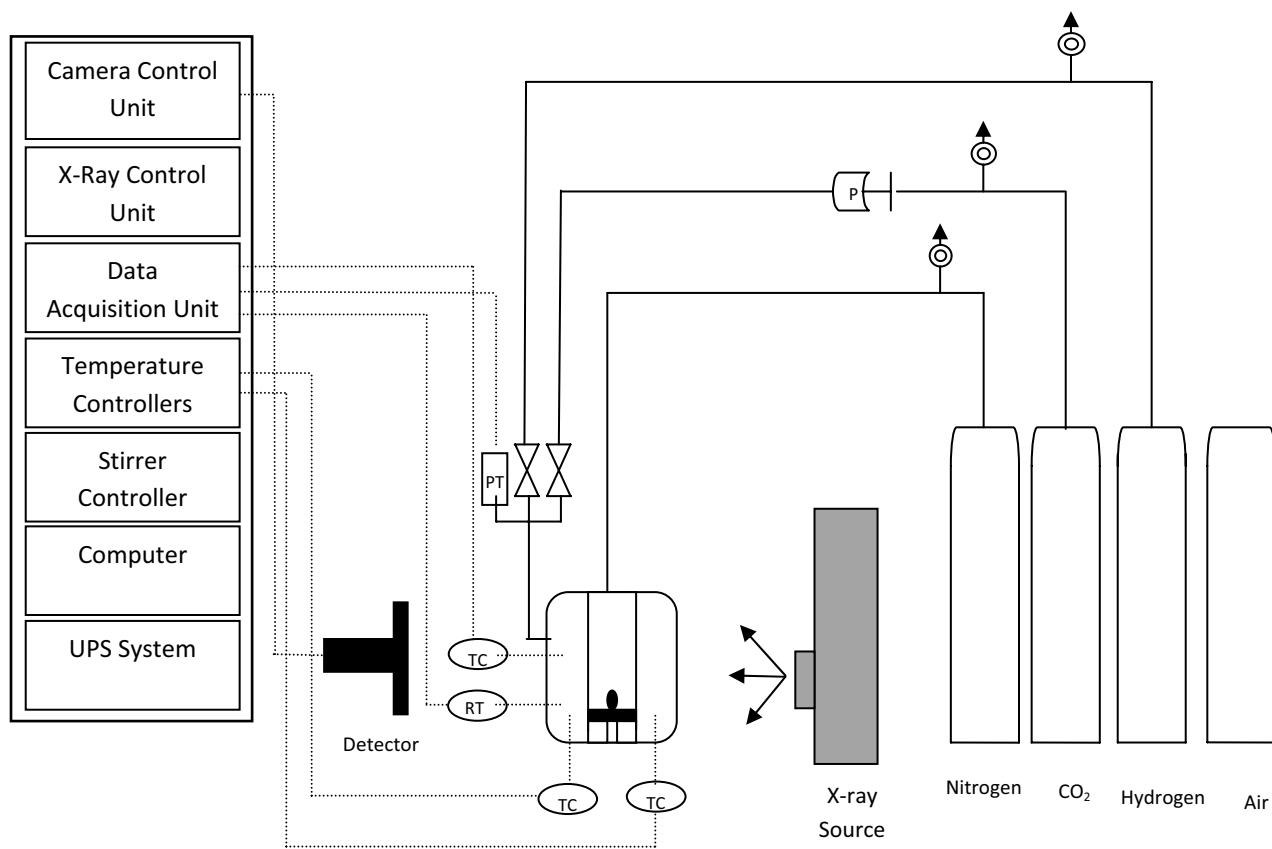
Figure 13: X-ray View Cell Apparatus Schematic

Figure 14: (Photo on the Left) Assembled View Cell, (Photo on the Right) X-ray source

The CO_2 injection line was designed and installed specifically for this project. In Figure 14 to Figure 17, process flow diagram of this line is presented plus some pictures of the actual implementation. Parts and tubing for this line was purchased from Swaglok Company; installation was done according to the standards and instructions provided by Swaglok. The procedure for gas injection, based on Figure 15 is:

1- Open the 3-way valve between the CO_2 cylinder and the hand pump to fill it to the pressure, of the CO_2 gas cylinder.
2- Close the 3-way valve to isolate the hand pump.
3- Spin the pump handle to compress the CO_2 prior to injection into the view-cell.
4- Open the 3-way valve to connect the hand pump and the view cell.
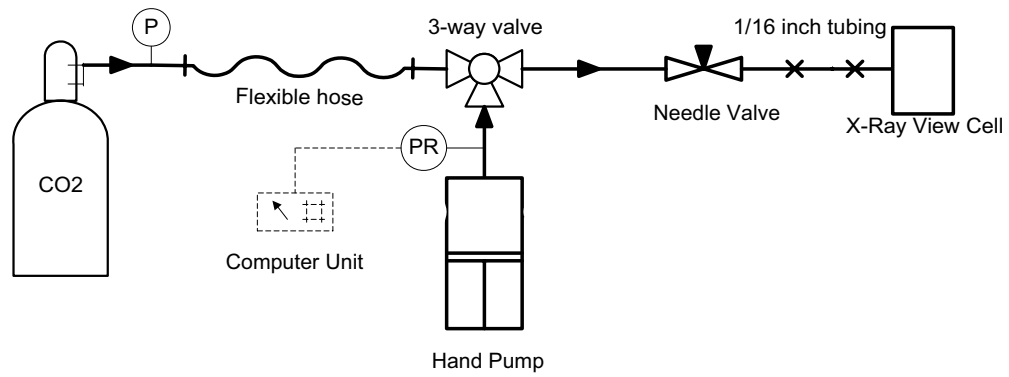
Figure 15: Process Flow Diagram (PFD) of CO$_2$ Injection Line

Figure 16: Front (photo on the left) and Rear (photo on the left) view of the Injection System Control Panel
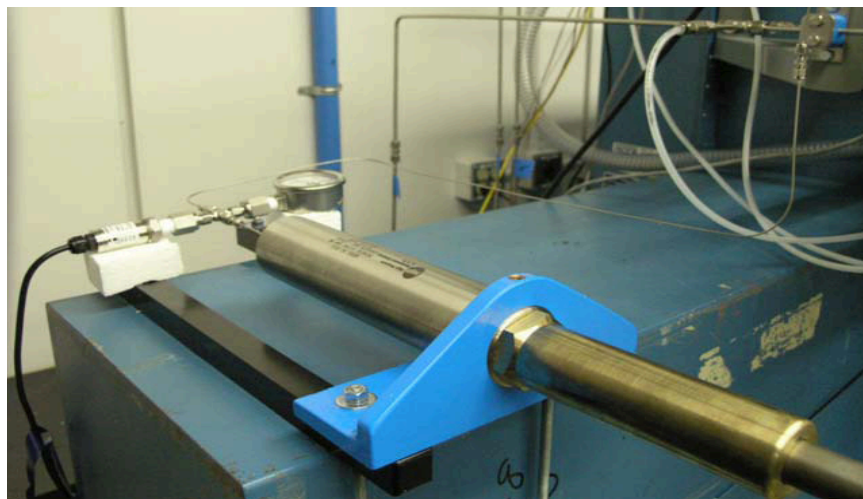
Figure 17: Hand Pump, Pressure Gauge and Pressure Transducer and 1/16" tubing system

3.2.3. Experiment preparation and procedure

A detailed operating manual explaining how to perform experiments with the X-ray view cell apparatus can be found in Appendix I. In summary:

1- Wash and rinse the components of view cell thoroughly with a solvent (toluene or THF) and let them dry. Then assemble the cell.

2- Pour a known amount of heavy oil into the view cell.

3- Close the top with the appropriate gasket and tighten the bolts according to instructions to avoid leakage.

4- Place the cell inside the cabinet and connect the necessary connections.

5- Perform H_2 and N_2 leakage tests and condition the sample to the recommended temperature.

6- Evacuate or purge the cell to remove air.

7- Inject the experimental gas and start the experiments. For equilibrium measurements, a magnetic mixer is used to stir the mixture for at least 1 hour. After stability in pressure at fixed temperature is attained, an image is taken that is used for analysis.

3.3. Data Treatment

3.3.1. Image Analysis

A code was developed to analyze and digitize the X-ray images (Appendix II). Each saved image is an average of 700 video stills taken over approximately 25 seconds. In the code, a number, the shade of gray, is assigned to each pixel. The resultant numerical form is a matrix with the same number of rows and columns as the pixels of the image (640*480). In order to determine the boundaries and the geometry, different cuts and areas of the image are carefully studied and both invariable geometrical attributes (such as shape of the insert, tray and stirrer in addition to outer boundaries of the view cell) and variable ones (such as phase boundaries and position of the bellows) are identified. To determine the variables in each image, a rectangle with 40 pixels in width and the length of the image (640 pixels) (3 mm x 60 mm) is swept.

A sample image is shown In Figure 18-a. The green rectangle in part "b" is the rectangle that is swept by the code. The average intensity of each elevation (~pixel number) is then calculated as the average of intensities of 40 pixels in width divided by the average intensity of the beryllium insert to result in "I", the normalized intensity at that elevation. From left to right, the blue ellipses encompass: L2-insert area, stirrer, L2-above stirrer, L1, Vapor. Three red lines indicate the interfaces and the boundary of the system, from left to right: L1L2 interface, L1V interface and bellows. The two yellow rectangles show the beryllium insert areas that are used to normalize the intensity at each elevation and eliminate/dampen noise.

$$I(elevation) = I(Pixel\ Number) = \frac{Average\ intensity\ at\ each\ elevation}{Average\ intensity\ of\ beryllium\ insert} \qquad (2)$$

In part "c", a normalized intensity profile is presented. Such processed images are analyzed.
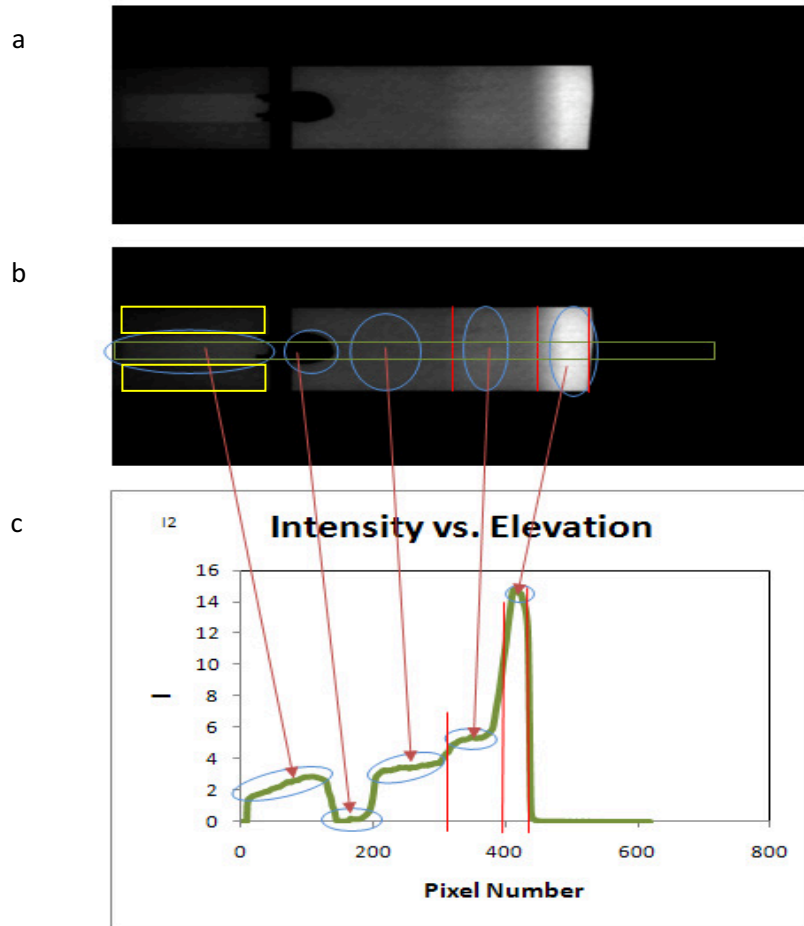
Figure 18: Image analysis and phase detection of a typical LLV mixture, "I" is normalized intensity

3.3.2. Composition Calculation

In order to determine the global composition of a mixture, an image is taken immediately after the injection of CO_2 and at the same time the pressure and temperature of the system are recorded. No dissolution of CO_2 in bitumen is expected in such a short period of time. Either non-equilibrium LLV or LV is observed.

In either case, the volume of the vapor is calculated according to the total volume calibration (see appendix III). The volume of the liquid phase/phases is determined from the volume calibration equations presented in appendix III. The

density values for the vapor phase and less dense liquid phase are calculated based on the assumption that these are pure CO_2. The Advanced Peng-Robinson Equation of State in VMGSim simulation software was used for calculations this approach was validated as shown in section 3.3.6.2. The amount of CO_2 present is given by:

$$m_{CO_2} = \rho_{L1} v_{L1} + \rho_V v_V \qquad \text{(3)}$$

Where ρ_{L1} and ρ_V are the density of lighter liquid and vapor phases, respectively; v_{L1} and v_V are the volumes of lighter liquid and vapor phases, respectively.

The amount of heavy oil is measured separately. Thus the mass fraction of CO_2 in the mixture (global composition) is:

$$w = \frac{m_{CO_2}}{m_{CO_2} + m_{HH}} \qquad \text{(4)}$$

3.3.3. Solubility and Phase Boundary Analysis Methods in the Literature

A number of approaches are tested in this thesis to treat the experimental data and to find phase boundary pressures. First a literature review is presented, and then these approaches are summarized and compared with one another.

3.3.3.1. Henry's Law Approximation

Henry's law is used to correlate VLE for dilute mixtures. At fixed temperature:

$$H = \frac{P}{x} y \qquad \text{(5)}$$

Where H, the Henry's constant, is a function of temperature, P is pressure and y and x are the CO_2 compositions in the gas and liquid phases. Liquid composition can be expressed in terms of molalities, concentrations and mass fraction [80]. The mass fraction form is used in this thesis.

One other assumption can be made in the case of the mixtures in this thesis. The mass fraction of CO_2 in vapor phase is assumed to be 1.00. This assumption is

validated when compared with the data in the literature for similar mixtures (Table 11).

If written in mass fraction form, equation (5) reduces to:

$$H = \frac{P}{w_l} \qquad \text{(6)}$$

Table 11: Mass fraction of CO_2 in the vapor phase of the mixture of CO_2 + hydrocarbons in the literature

Authors/Year/Reference	Heavy Compound	Temperature (K)	Pressure (kPa)	wy (CO_2)
Morris & Donohue/1985/[68]	1-methylnaphthalene	353.15	1815	0.9989
			2930	0.9991
			4980	0.9991
			8280	0.9982
			11265	0.9947
			14425	0.9872
		413.15	1220	0.9816
			2250	0.9877
			4220	0.9915
			6000	0.9921
			8410	0.9910
			11935	0.9873
			14450	0.9826
Han et al./1992/[56]	Peace River Bitumen	318.15	7210	0.9988
			8550	0.9975
			9740	0.9928
			11180	0.9852
			12430	0.9801
			13900	0.9748
		328.15	7360	0.9987
			8510	0.9981
			9710	0.9971
			11250	0.9929
			12250	0.988
			13910	0.9788
Brunner/2009/[26]	Squalene	313.15	10000	0.9993
			15000	0.9981
			20000	0.997
		333.15	12000	0.9998
			16000	0.9985
			20000	0.9971
			25000	0.9955
		343.15	16000	0.9991
			20000	0.9979
			25000	0.9965
		353.15	20000	0.9986
			23000	0.9974
			26000	0.9961
		363.15	23000	0.9978
			26000	0.9965
			29500	0.9949
		373.15	26000	0.9973
			29500	0.9958
		333.15	10000	0.9999

	15000	0.9989
	20000	0.9986
	25000	0.9974
	30000	0.9929
	35000	0.9896
363.15	10000	0.9999
	15000	0.9994
	20000	0.9987
	25000	0.9981
	30000	0.9949
	35000	0.9866

3.3.3.2. Corrected Henry's Constant

The original Henry's law for VLE calculations is to be applied for dilute mixtures. For more concentrated mixtures, a scheme to account for the effect of pressure on the value of the Henry's constant is typically found to be necessary. Rettich et al. [81] and Krichevsky and Kasarnovsky [82] proposed modified correlations. Rettich et al. started from the definition of Henry's constant based on fugacity and using the Virial equation of state, suggested the following:

$$H^{corrected}(P,T) = H(P,T)Z\varphi\exp\left(-\frac{\bar{V}_2^\infty(P-P_1)}{RT}\right) \tag{7}$$

Z is compressibility factor.

φ is the fugacity coefficient.

$\bar{V}_2^\infty$ is the partial molar volume of CO_2 at infinite dilution.

P_1 is the vapor pressure of the solvent.

Gasem and Robinson [61] used the Krichevsky and Kasarnovsky correlation to estimate values of Henry's constant for mixtures of heavy hydrocarbons + CO_2:

$$\ln\left(\frac{f_{CO_2}}{x_{CO_2}}\right) = \ln(H) + \frac{\bar{V}_2^\infty(P-P_1)}{RT} \tag{8}$$

f_{CO_2} is the fugacity of pure CO_2.

Equation (8) works only for mole fractions lower than 0.45. Also the partial molar volume at infinite dilution can be either positive or negative.

3.3.3.3. P-v Extrapolation

P-v measurements at fixed temperature can be used to identify correlations between pressure and volume (vapor volume in the case of LVE) and use that to extrapolate the vapor volume to zero to identify phase boundary pressures. At fixed pressures, variations in phase volume with composition are also used to identify phase boundaries. This scheme is implemented in a work by Fall and Luks [49] as "conjugate measurements" and Zhang [83].

Conjugate Measurements

In order to determine the phase boundaries in phase diagrams such as P-T (fixed w) and P-w (fixed T) projections, a minimum of two experimental points are needed to perform extrapolations [15].

At fixed temperature, measurements are performed by varying the volume (of the vapor phase) and consequently pressure. Assuming that these measurement points are in the two-phase region (Liquid-Vapor), these data can be used to extrapolate to the "LV → L" transition. In 3-phase regions extrapolations to "LLV → LL" and "LLV → LV" transitions can be performed. A linear correlation between pressure and phase volume is used to find the pressure where the volume of one of the phases is zero. This method is effective and accurate if the experimental data are close to the phase boundary.

3.3.4. Proposed Extrapolation Schemes in This Thesis

The conjugate measurements were used in this thesis; this method is named P-v extrapolation in this document. Also, Henry's law is implemented.

Both equation (7) and (8) contain parameters which are hard to calculate in our case, thus a scheme is proposed in this thesis to account for the variation of Henry's constant values with pressure at fixed temperature.

The mass fraction of CO_2 in the liquid phase (solubility) and the corresponding Henry's constant are both obtained indirectly. The total mass of CO_2 is known. The mass of CO_2 in the vapor phase is:

$$m_{CO_2}(vapor) = \rho_V v_V \tag{9}$$

Where v_V is the gas phase **volume** (total volume minus liquid volume from volume **calibration** – appendix III); ρ_V is the **density** of pure CO_2, calculated using the Advanced Peng-Robinson Equation of State.

Subtracting the amount of CO_2 in the vapor phase from the total amount of CO_2 provides in the amount of CO_2 in the liquid phase. The mass fraction of CO_2 in the liquid phase is then calculated according to the following formula:

$$w_l = \frac{Amount\ of\ CO_2\ in\ liquid}{Amount\ of\ CO_2\ in\ liquid + amount\ of\ hydrocarbon\ sample} \tag{10}$$

A "P-w" graph of the experimental data is drawn and the data is linearly regressed (slope of which is H) to w=0.8 to estimate the critical pressure.

$$P_{boundary,Henry's} = Hw \tag{11}$$

$$P_{critical} = H * w_{critical} = 0.8 * H$$

3.3.4.1. Henry's Law Method (Modified)

A new approach based on the parameters dH/dP and dH/dw is discussed here. As it can be seen in Table 12, dH/dP and dH/dw are mainly negative for low-molecular weight pure hydrocarbons + CO_2 mixtures but for heavier compounds and heavy oils, they become positive.

Table 12: dH/dP & dH/dw values calculated for the mixtures of different hydrocarbons + CO_2

Authors/Year/References	Heavy Component/MW	Temperature (K)	Composition Range	Pressure Range (kPa)	dH/dP	dH/dw (kPa)
Vitu et al./2008/[17]	cis-decalin/142.29	373.15	0.03-0.43	3500-22800	-3.21	-97400
Shaver et al./2001/[84]	Decane/138.25	344.3	0.02-0.75	900-12700	-1.62	-29700
Kim et al./1989/[60]	Tetralin/132.2	343.6	0.07-0.82	3200-15900	-1.09	-23200
Occhiogrosso et al./1986/	Cumene/120.19	363.15	0.07-0.92	3000-15000	-2.18	-35500
Morris & Donohue/1985/[68]	1-methylnaphthalene/142.2	353.15	0.03-0.23	1800-14400	-0.32	-20100
		413.15	0.01-0.16	1200-14500	**0.26**	**21853**
Brunner/2009/[26]	Squalene/410.72	313.15	0.25-0.27	10000-20000	**3.36**	**14400**
		333.15	0.25-0.33	12000-25000	**2.14**	**328000**
		343.15	0.29-0.35	16000-25000	**1.68**	**225000**
		353.15	0.31-0.35	20000-26000	**1.48**	**197000**
		363.15	0.34-0.38	23000-29500	**1.22**	**149000**
		373.15	0.35-0.38	26000-29500	**1.05**	**130000**
		333.15	0.21-0.48	10000-35000	**0.85**	**69300**
		363.15	0.15-0.54	10000-35001	**0.09**	**-8200**
Sato et al./1998/[85]	Eicosane/282.55	323.2	0.14-0.64	5900-14800	-0.10	-7000
		373.2	0.14-0.64	8800-30800	-0.61	-28000
		423.2	0.14-0.64	10900-33600	-1.07	-51300
		473.2	0.14-0.64	12200-34400	-1.37	-66900
	Docosane/310.6	323.2	0.17-0.34	6400-12400	-0.05	-3800
		373.2	0.17-0.65	9600-35200	**0.01**	-800
		423.2	0.17-0.65	12200-36600	-0.56	-31800
		473.2	0.17-0.65	13600-37300	-0.86	-48300
	Tetracosane/338.65	373.2	0.16-0.58	9400-38900	**0.24**	**13200**
		423.2	0.16-0.58	12300-38500	-0.37	-23300
		473.2	0.16-0.43	14100-31100	-0.76	-49300
	Octacosane/394.76	373.2	0.16-0.38	9000-22300	**0.10**	**4800**
		423.2	0.16-0.58	11500-40900	-0.06	-4800

Han et al./1992/[56]	Peace River bitumen	318.15	0.10-0.14	7200-13900	**5.27**	**939000**
		328.15	0.09-0.13	7400-13900	**4.05**	**559000**
Huang & Radosz/1990/[58]	Cold Lake Bitumen – Cut 3/	323.3	0.05-0.14	4000-16100	**2.80**	**302000**
	572	373.3	0.03-0.12	4000-16000	**0.27**	**34400**
		473.7	0.02-0.08	4000-16000	-0.87	-170000

a. Correction with $\frac{dH}{dP}$

From the literature review, the mass fraction of CO_2 in the L2 phase is expected to vary linearly with pressure especially at low global CO_2 mass fractions. At higher global CO_2 mass fractions, some deviation is anticipated. This effect, if present, is accounted for in the data analysis using equation 12 and 13:

$$P_{boundary,Henry's} = P_{measured} * \frac{w_{global}}{w_l} \tag{12}$$

$$P_{boundary}^{corrected} = w_{global} \times \left(H_{measured} + \left(P_{boundary} - P_{measured}\right) \left(\frac{dH}{dP}\right)_{average}\right) \tag{13}$$

Where, the derivative of the Henry's constant is obtained from the CO_2 solubility measurements. Henry's constant is assumed to be a linear function of pressure.

The phase boundary pressure is evaluated on the basis of the highest pressure measurements of solubility plus a small correction in this two step procedure.

b. Correction with $\frac{dH}{dw}$

If the correction scheme is based on dH/dw parameter, then the correlations can be developed as the follows:

A line is fitted to the H-w_l data.

$$\frac{dH}{dw} = K \tag{14}$$

K is the slope of the fitted line.

Integrating both sides, we get:

$$\int dH = K \int dw$$

$$H = Kw + b \tag{15}$$

The constant "b" can be calculated via the available experimental data.

$$b = H_{exp} - Kw_{exp}$$

An average value of this so-called intercept is calculated and used in equation 15.

3.3.5. Comparison of the Analysis Methods

The methods presented previously are applied to the three different cases in the literature to compare their accuracy for the prediction of phase behavior (Figure 19).
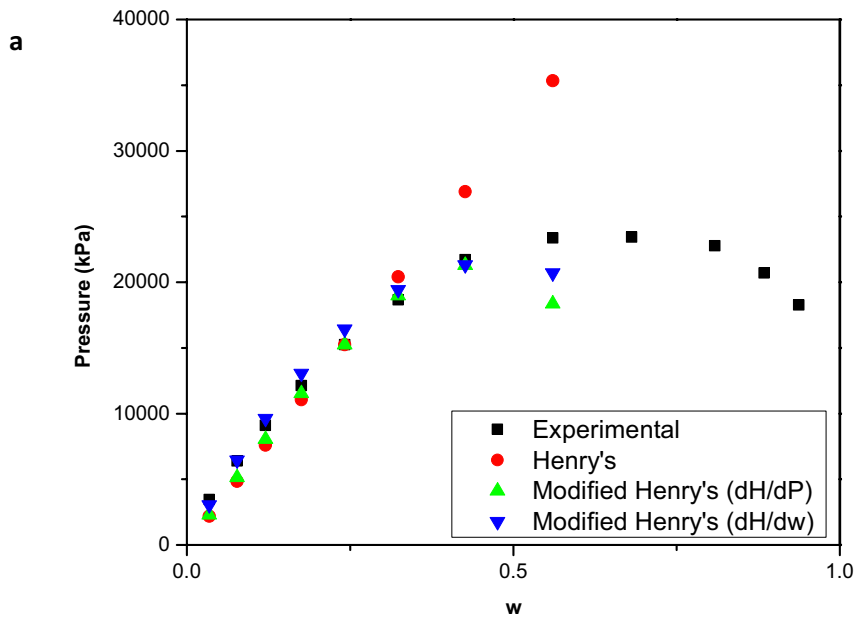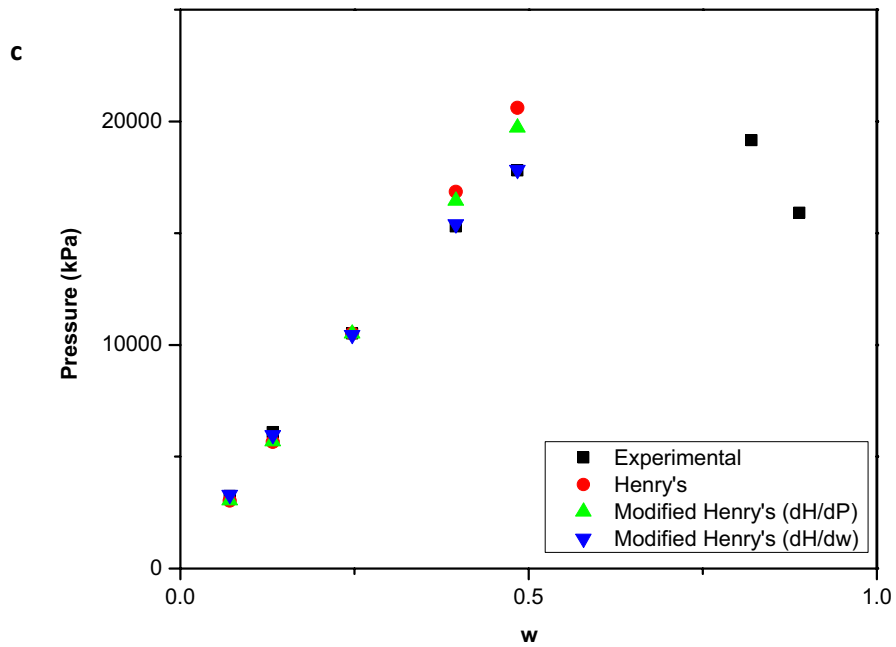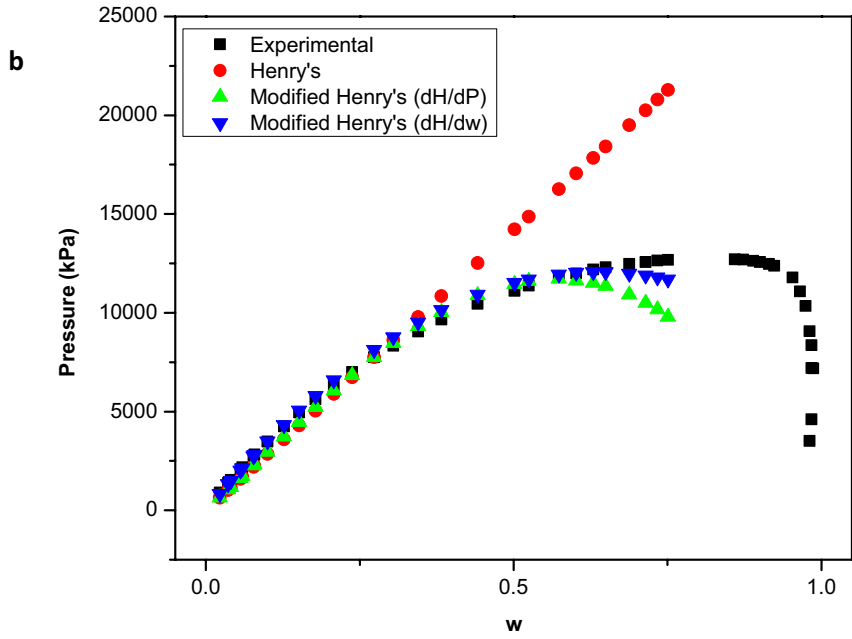
Figure 19: Comparison of the results of the proposed analysis methods on the experimental results in the literature: a: cis-decalin + CO$_2$ at 373.15 K [17], b: Decane + CO$_2$ at 344.3 K [84], c: Tetralin + CO$_2$ at 343.6 K [60]

The modified Henry's law methods predict the phase behavior with great success in the region where the actual experimental data behaves linearly in a P-w diagram. But if a non-linearity occurs, based on the sign of "dH/dP" or "dH/dw", they may overestimate or underestimate the boundary pressure values. This is expected since the prediction of the points at higher concentration is solely based on H and dH/dP values which are calculated for the data at lower concentrations.

Based on this uncertainty and the fact that the experimental data in this work is in a narrow range of concentrations, it was decided to adopt the Henry's law scheme for the Athabasca bitumen and Maya crude + CO_2 data as it produces the most reliable results among the previously discussed methods. Although the modified Henry's law methods, in particular the one with "dH/dw" shows promise if a large number of experimental points at a wide range of compositions is available.

In Table 13, the above 3 methods are compared.

Table 13: Comparison of phase boundary pressure extrapolation schemes

Analysis Method	Strengths	Weaknesses
Henry's Law Method	Consistent with the expected behavior at low concentrations (as P goes to 0, so does solubility)	Only works for dilute mixtures
	Easy to implement and extrapolate	Can only predict linear shape for P-w curve
Modified Henry's Law Method	Considers the variation of H with P or with w at constant temperature	- Margin with the actual bubble pressure values in non-linear P-w curves - Nature of the data (narrow range of concentration in our case) makes this method unfavorable
P-v Extrapolation	It is implemented successfully in previous works in the literature	Assumes the behavior of P-v curve is linear up to the phase boundary point at fixed composition

3.3.6. Error Analysis

3.3.6.1. Phase Volume Error

Image analysis is performed on each image to extract information about the volume of the phases. The volume in the view cell above the stirrer is linearly correlated with the pixel number as is the volume of the insert region.

Pixel number of the phase boundary is extracted from the intensity vs. elevation profile. The middle of the boundary region is selected as the elevation of the interface (Figure 20).
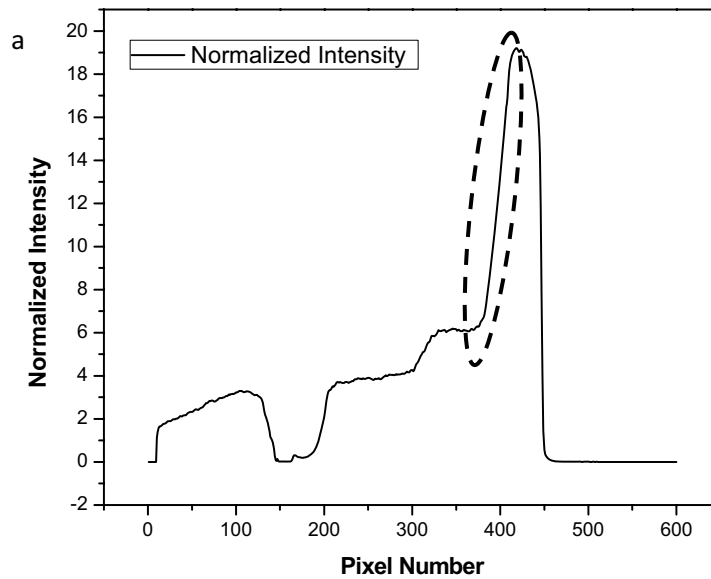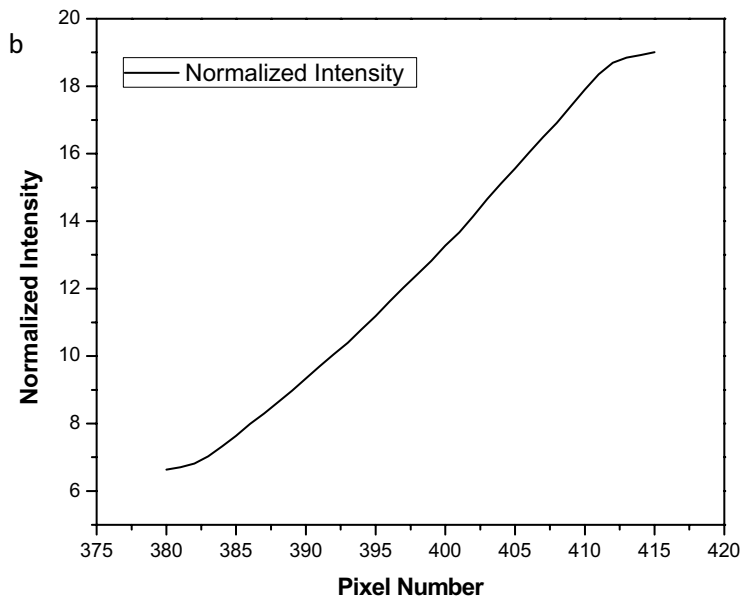
Figure 20: Example phase boundary evaluation (a) overview, (b) detail of the LV interface

From the example above, the interface is assigned an elevation of 398. From the volume calibration, there is 0.1736 ml/pixel below the bellows. Thus the LV interface elevation error corresponds to a volume error of less than 2 ml for the liquid phase.

Gas volume error is linked to uncertainties in the elevation of the bellows. From the geometry, the volume of the annulus is:

Annulus Volume $=(\pi R_{Cell}^2 - \pi R_{Bellows}^2)l_{Bellows}$

R_{Cell} = Internal Radius of the view cell – 25.5 mm

$R_{Bellows}$ = External Radius of the Bellows – 24.5 mm

$l_{Bellows}$ = Length of the Bellows

As the annular volume is less than 1 cm^3 / cm of length, and the elevation error is less than one tenth this value, the error introduced by this uncertainty is negligible compared to the uncertainty of the interface.

49

3.3.6.2. CO_2 Density Accuracy

Advanced Peng-Robinson equation of state was chosen in VMGSim, a commercial simulator, to calculate the density of CO_2. To verify the density values obtained, an accurate equation of state developed by Span-Wagner [86] specifically for CO_2 (recommended by IUPAC [87]) is used to validate the density values calculated. A number of comparative examples are shown in Figure 21. There are small deviations especially near the neighborhood of CO_2 critical point but the uncertainty in density for the range of our experiments is estimated to be less than 1% for the liquid and less than 4% for the vapor phases respectively. Near the critical point, error is less than 7% for the vapor phase.
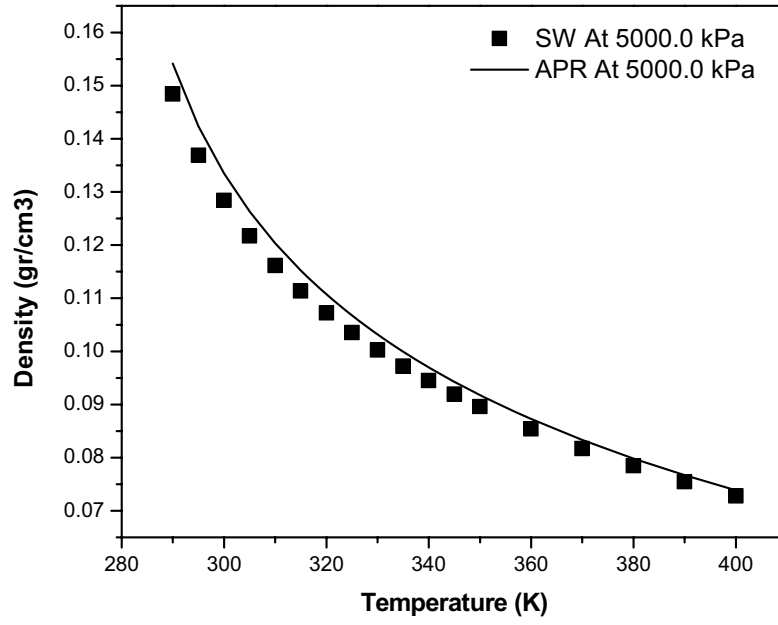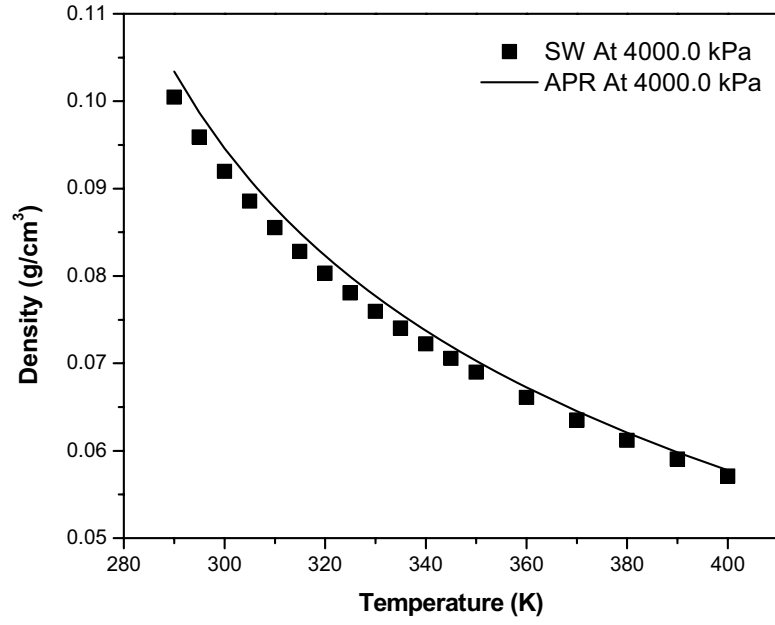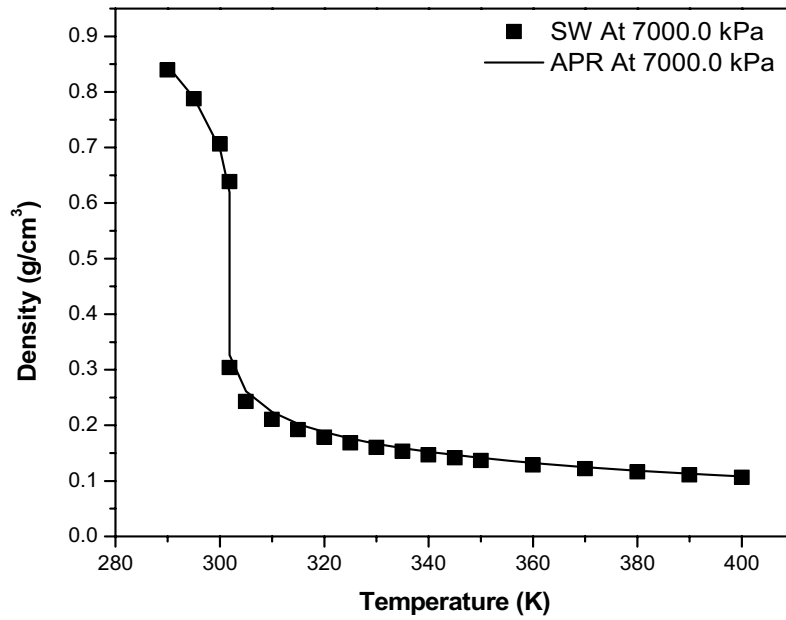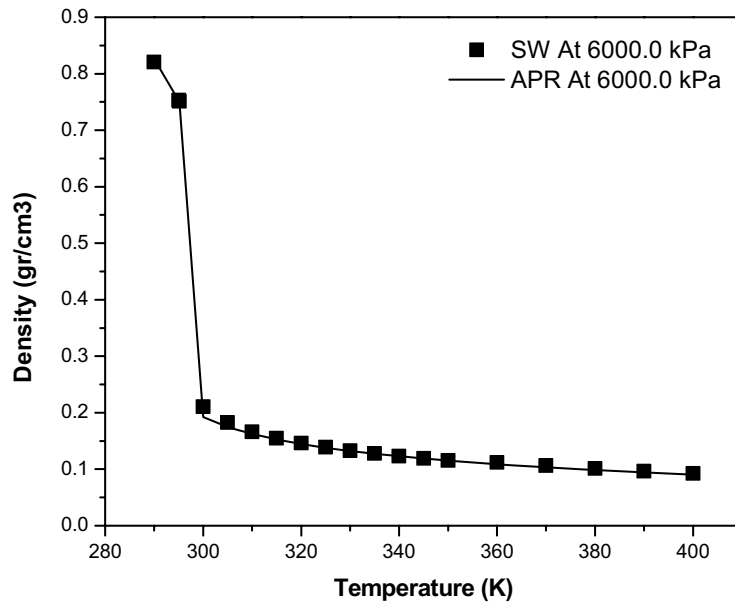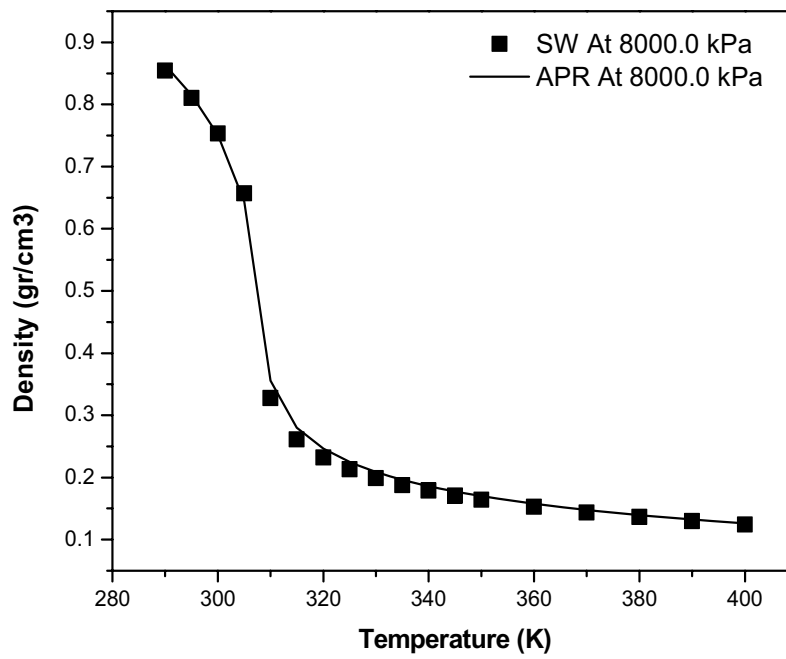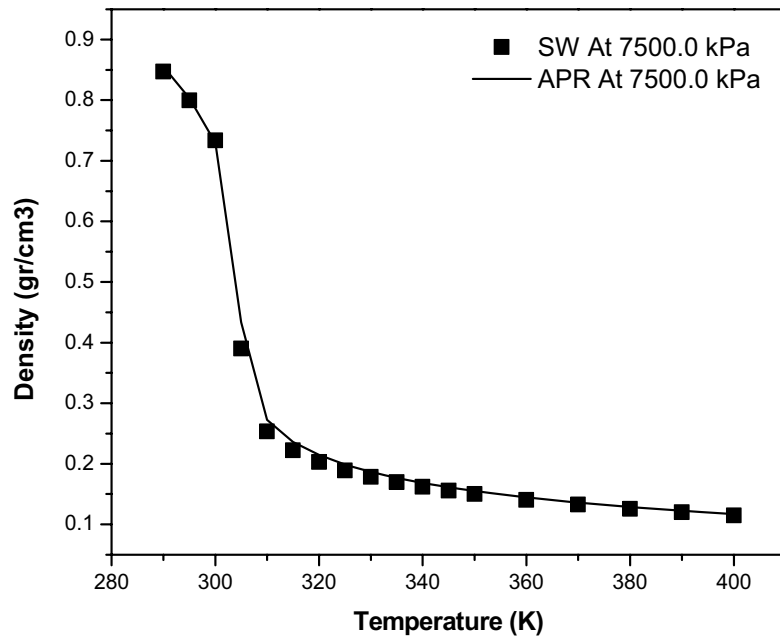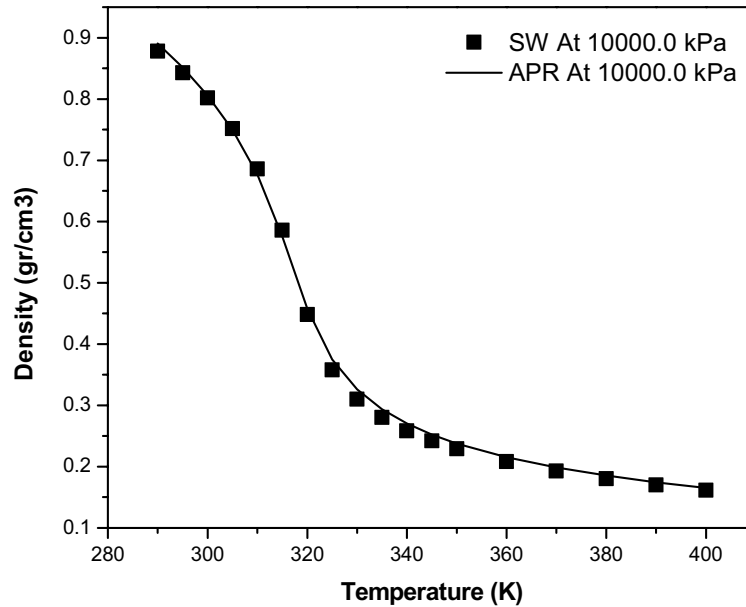
Figure 21: Comparison of CO_2 Densities calculated by APR and Span-Wagner equations of state.

3.3.6.3. Pressure and Temperature Measurement Accuracy

According to the catalogues provided by the manufacturer and lab based calibration:

1- The pressure measurement accuracy is within 1%;

2- The temperature measurement accuracy is $\pm 0.1\ K$.

3.3.6.4. Liquid (L2) Volume Fraction Error

The error in the measurement of saturated hydrocarbon rich liquid (L2) is important since this data is used to evaluate the LLV onset concentration. The propagated error of any parameter is calculated according to the following formula:

$$\Delta f(x_1, x_2) = \sqrt[2]{\Sigma(\frac{\partial f}{\partial x_i})^2 \times (\Delta x_i)^2} \tag{16}$$

Hence:

54

$$\emptyset_{HL}(V_{L1,}V_{L2}) = \frac{V_{L2}}{V_{L2}+V_{L1}} \tag{17}$$

$$\Delta(\emptyset_{HL}) = \frac{\Delta V}{(V_{L1}+V_{L2})^2}\sqrt[2]{V_{L1}^{2} + V_{L2}^{2}}$$

V_{L1}: CO$_2$-rich Liquid Phase Volume

V_{L2}: Oil-rich Liquid Phase Volume

ΔV: Volume Measurement Error

$\Delta\emptyset_{HL}$: Liquid Volume Fraction Error

3.3.6.5.   Mass Fraction and Solubility Error
The mass fraction of CO_2 in the mixture as well as its solubility in the L2 phase is calculated from equations (4) and (10) respectively. Based on the propagation of error formula, the average errors for these parameters were calculated to be:

$$\Delta w = 0.01, \Delta s = 0.03$$

3.3.6.6.   VL – L Boundary Pressure Error
For Henry's law method, the following equations express the truncated error functions:

$$\Delta H = \sqrt{\frac{P^2}{wl^4}(\Delta wl)^2 + \frac{1}{wl^2}(\Delta P)^2} \tag{18}$$

$$\Delta P_{boundary} = \sqrt{H^2(\Delta w)^2 + w^2(\Delta H)^2}$$

The average calculated values are 1000 kPa and 700 kPa respectively for $\Delta H, \Delta P_{boundary}$.

For Henry's law method with dH/dP correction, the error propagation formula for the calculated LV-L boundary pressure is:

$$\Delta P_{boundary} = \sqrt{\frac{P^2}{s^2} \times (\Delta w)^2 + \frac{w^2}{s^2} \times (\Delta P)^2 + \frac{w^2}{s^4} \times P^2 \times (\Delta s)^2}$$ **(19)**

The average error is +/- 3000 kPa which translates to 5% relative error.

For the Henry's law method with dH/dw correction, the variance of the boundary pressure data was calculated. The average error is +/- 1500 kPa.

3.3.6.7.   L=V Critical Pressure Error

As noted in Chapter 2, the composition at which the L=V critical pressure occurs was estimated to be 0.8+/-0.1. In order to calculate the amount of error this assumption introduces, the critical pressure was calculated at w=0.7 and w=0.9 to find the lower and higher values critical pressures can attain.

Chapter IV: Results and Discussions

4.1. Phase Behavior of the Mixture of Athabasca Bitumen + CO_2

4.1.1. Solubility of CO_2 in the Bitumen-rich Liquid Phase:

The solubility of CO_2 is reported as an inverse Henry's constant:

$$s = \frac{w_l}{P}$$

wl is the Solubility of CO_2 in liquid phase.

P is the Pressure (kPa).

s is the solubility/pressure parameter (kPa^{-1}) provides direct access to the mass fraction of CO_2.

The experimental results and average values for solubility/pressure parameter are presented for three compositions in Table 14 and Table 15.

Table 14: Experimental data of CO_2 solubility/pressure parameter for Athabasca bitumen + CO_2

Global Composition of the Mixture, w_{global}	Temperature (K)	Pressure (kPa)	CO_2 Solubility in Athabasca Bitumen, w_l	$s \cdot 10^5$ (kPa^{-1})
0.47	333.0	7681	0.23	2.93
	333.1	7474	0.23	3.02
	333.2	7350	0.22	3.05
	333.2	7246	0.22	2.98
	353.0	7846	0.21	2.66
	353.1	8239	0.22	2.68
	353.2	8632	0.23	2.61
	353.2	8715	0.23	2.59
0.56	307.8	7081	0.19	2.68
	307.8	7171	0.18	2.57
	307.9	6977	0.16	2.32
	332.7	8825	0.22	2.45
	332.8	8694	0.22	2.52
	332.7	8577	0.22	2.57
	352.8	9294	0.24	2.54
	352.9	9915	0.24	2.39

0.62	308.2	7653	0.20	2.56
	308.0	7695	0.19	2.42
	332.6	9915	0.24	2.46
	332.7	9577	0.25	2.57
	352.8	10687	0.26	2.40
	352.7	11149	0.26	2.31
	352.9	11728	0.26	2.19
	397.4	14238	0.27	1.90
	397.1	15541	0.27	1.77

Average values of the solubility data are also presented in Figure 22, where they are compared with available literature data.

Table 15: Average values of solubility/pressure parameter vs. temperature for Athabasca bitumen + CO$_2$

Temperature (K)	$s \cdot 10^5$ (kPa^{-1})
308	2.5±0.4
333	2.7±0.4
353	2.5±0.3
397	1.8±0.2
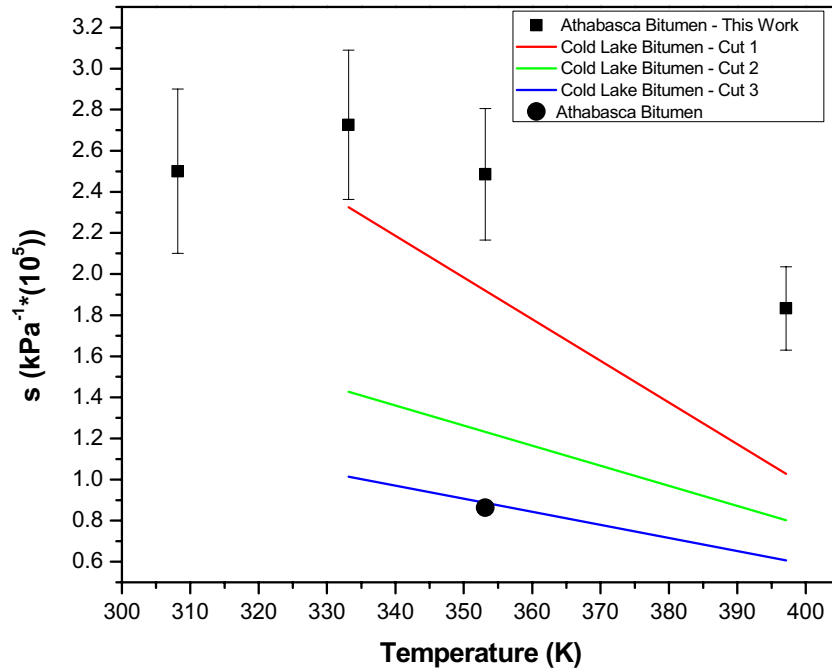
Figure 22: Average solubility/pressure data for Athabasca Bitumen + CO₂ obtained in this work compared with those for Cold Lake bitumen by Huang and Radosz (regressed from data at 323 & 373 K) [58] and Athabasca bitumen by Mehrotra et al [64]

The solubility/pressure parameter decreases as the temperature increases in our work, so does the values in the work by Huang and Radosz [58]. Since Athabasca bitumen is more viscous and heavier oil than Cold Lake Bitumen, it is expected to solubility values closer to the values of cut 3 (the heavy cut). The deviation from the expected behavior requires further study.

Figure 23 and Table 16 present overall perspectives on CO₂ solubility values and trends from the literature and that can be compared with the present results. The trends with temperature are the same.
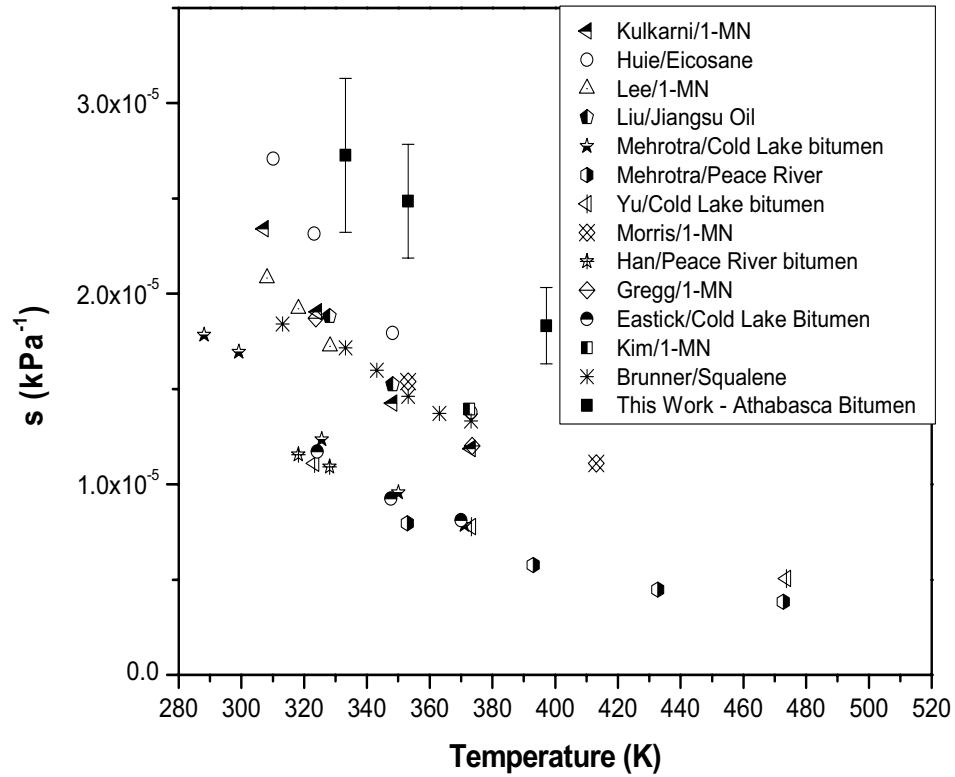
Figure 23: Comparison of CO_2 solubility/pressure data points from the literature with Athabasca bitumen + CO_2 results from this work: Kulkarni [32], Huie [62], Lee [55], Liu [63], Mehrotra [65], Mehrotra [51], Yu [66], Morris [68], Han [56], Gregg [88], Eastick [46], Kim [60], Brunner [26]

Table 16: Average "s" parameter calculated based on the data in the literature

Author(s)/Year/Reference	Heavy Component/Molecular Weight (g/mole)	Temperature (K)	s=w/P (10E5*kPa^{-1})
Han et al./1992/[48]	Peace River Bitumen	318.15	1.11
		328.15	1.06
Hong et al./1994/[49]	Prudhoe Bay oil - Cut A/117	360.93	3.41
	Prudhoe Bay oil - Cut B/163	360.93	2.53
	Prudhoe Bay oil - Cut C/215	360.93	1.97
	Prudhoe Bay oil - Cut D/272	360.93	1.67
	Prudhoe Bay oil - Cut E/338	360.93	1.58
	Cold Lake Bitumen - Cut 1/201	323.5	2.97
		373.4	1.75
		473.5	1.06
		523.2	0.93
	Cold Lake Bitumen - Cut 2/304	323.3	1.28
Huang & Radosz/1990/[50]		373.4	1.08

Reference	Compound/MW	Temperature	Value
		473.5	0.73
		523.2	0.66
	Cold Lake Bitumen - Cut 3/572	323.3	0.8
		373.3	0.73
		473.5	0.51
		523.2	0.47
Inomata et al./1987/[51]	Benzene/78.11	343.6	7.16
		343.6	4.06
Kim et al./1989/[52]	Tetralin/132.2	343.6	4.6
		373.1	2.35
	1-methylnaphthalene/142.2	372.6	1.59
Gasem et al./1989/[53]	Tetradecane/198.39	344.3	6.46
Kulkarni et al./1974/[54]	1-methylnaphthalene/142.2	307.15	2.9
		324.15	2.1
		348.15	1.52
		373.15	1.24
Huie et al./1973/[55]	n-eicosane/282.55	310.15	3.33
		323.15	2.64
		348.15	1.94
		373.15	1.54
Liu et al./1999/[56]	Jiangsu Oil	328.15	1.88
		348.15	1.79
Mehrotra et al./1988/[57]	Athabasca Bitumen - UofC	352.45	0.86
	Athabasca Bitumen - ARC	353.15	0.83
Mehrotra et al./1989/[58]	Peace River Bitumen	352.87	0.82
		393.01	0.53
		432.77	0.52
		472.73	4.14
Yu et al./1989/[59]	Cold Lake bitumen	373.3	0.74
		473.7	0.51
		523.1	0.47
Mohamed & Holder/1987/[60]	m-xylene/106.16	312.65	12.7
		338.15	6.86
		366.15	4.56
	ethylbenzene/106.16	312.65	11.4
		338.15	7.44
		366.15	4.86
	o-xylene/106.16	312.65	13.3
		338.15	6.88
		366.15	4.57
Morris & Donohue/1985/[20]	1-methylnaphthalene/142.2	353.15	1.6
		413.15	1.1
Mehrotra & Svrcek /1988/[41]	Cold Lake Bitumen	325.62	1.25
		350.05	0.98
		371.07	0.82
Eastick et al./1992/[36]	Cold Lake Bitumen	324.15	1.11
		347.65	0.9
		370.05	0.73

4.1.2. Phase Behavior at Low Temperatures (L1V, L1L2V, L1L2)

For the mixture of heavy oil + CO_2 at temperatures below the critical temperature and pressures around the liquefaction pressure of pure CO_2, three phases (two liquid phases and a vapor phase – L1L2V or LLV) may appear in equilibrium in a narrow range of pressure at fixed temperature. The region is bounded by an LLV to LL transition (LLV-LL) and two LLV to LV (L1L2V-L1V, L1L2V – L2V) transitions.

4.1.2.1. *L1L2V-L2V transition*

The composition of saturated L2 (the dense bitumen/heavy oil-rich phase) was not observed directly. Since the pressure does not change significantly in the LLV region, the L1L2 – L2 boundary can be found by assigning the material in the vapor phase - assumed to be pure CO_2 – to the L1 phase where L1L2V behavior is observed. Thus the volume of the L1 phase along the L1L2 boundary can be evaluated. The volume fraction of the heavier liquid along the LLV-LL phase boundary, calculated as $VF_{L2} = \frac{V_{L2}}{V_{L2}+V_{L1}}$, versus global concentration is shown in (Figure 24). The composition at which $VF_{L2} = 1$ is a measure of the L2 composition and the composition at $VF_{L2} = 0$ is a measure of the L1 composition. Table 17 contains data used to perform these extrapolations.

Table 17: Heavy Liquid Volume Fraction (HLVF) Calculated at LL region for the mixture of Athabasca bitumen + CO_2

Global Composition (w)	Temperature (K)	Pressure (kPa)	L2 Volume (cm^3)	L1 Volume (cm^3)	V Volume (cm^3)	V Density (g/ cm^3)	L1 Density (g/ cm^3)	L1+V Pseudo Volume (cm^3)	Φ_{HL}	Δ(Volume)	Δ(Φ_{HL})	Δ(Φ_{HL})%
0.47	295.3	6068.77	26.90	0.35	82.65	0.22	0.75	25.17	0.52	2.00	0.03	6.51
0.47	295.31	6103.93	26.90	0.53	77.39	0.22	0.75	23.94	0.53	2.00	0.03	6.57
0.56	295.75	6152.19	26.90	2.12	82.65	0.23	0.74	27.54	0.48	2.00	0.03	6.60
0.56	295.73	6158.40	26.90	3.70	77.39	0.23	0.74	27.28	0.46	2.00	0.03	6.88
0.74	297.05	6320.42	13.67	16.75	78.03	0.24	0.72	43.15	0.24	2.00	0.03	12.17
0.74	296.86	6265.27	13.67	3.53	134.75	0.24	0.72	48.47	0.22	2.00	0.03	12.28
0.91	293.72	5797.11	3.14	1.06	105.12	0.21	0.77	29.64	0.10	2.00	0.06	58.18
0.91	293.46	5790.22	3.14	2.54	88.80	0.21	0.77	26.30	0.11	2.00	0.06	57.65
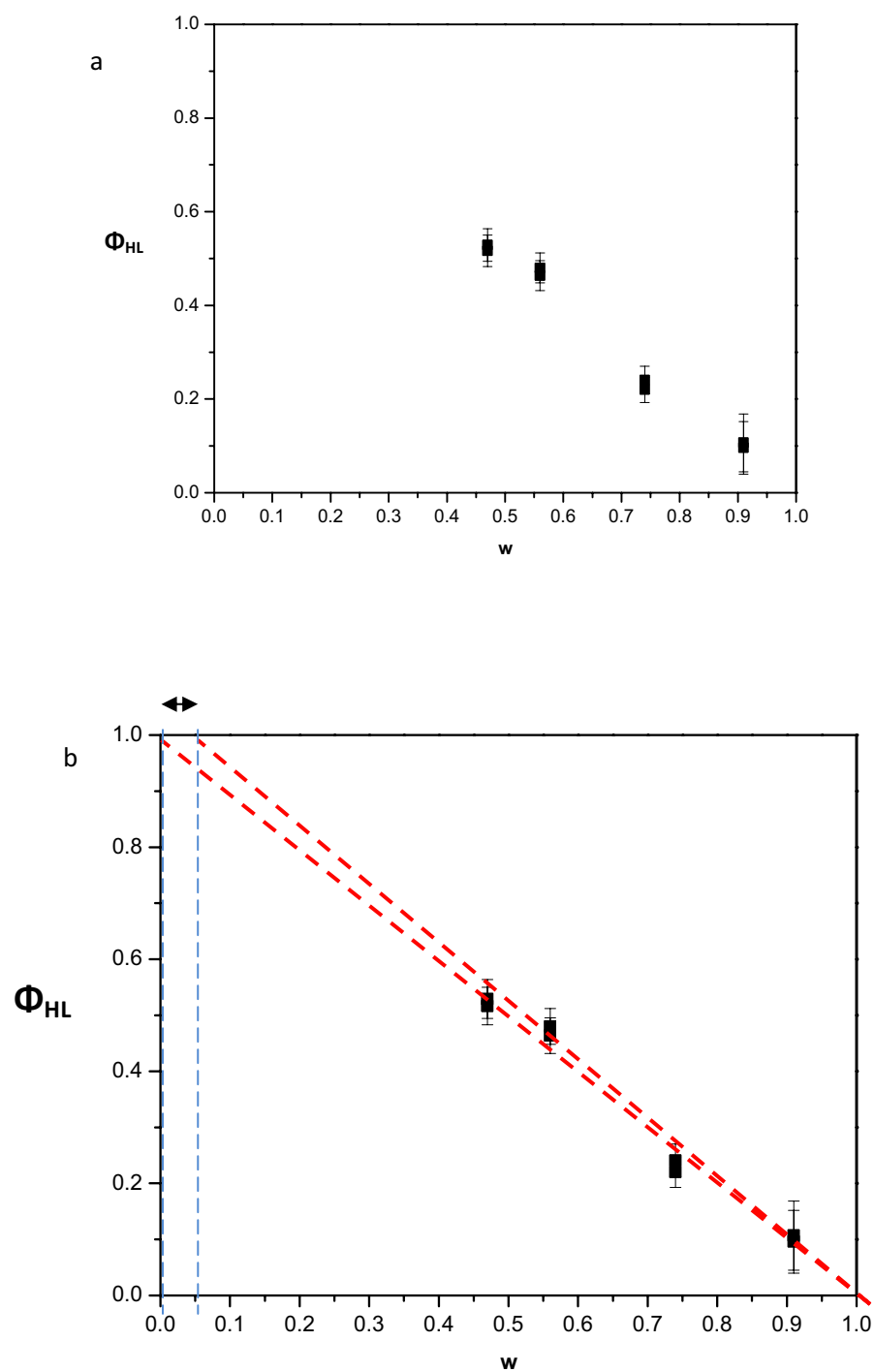
Figure 24: Diagram of heavier liquid (L2) fraction vs. global composition of Athabasca bitumen + CO₂ mixture, (b): Extrapolation lines to find the interval of LLV onset concentration

The value for the global composition for the L2-L1L2 transition is in the range 0.0-0.10 and for the L1-L1L2 transition in the range 0.96-1.0 (Figure 24-a). From the literature review, the composition of the L1 phase is expected to be well approximated as pure CO_2 to two or more significant figures. From the solubility of CO_2 in the L2 phase within the LLV region, Table 18, which is based on this assumption, the L2-L1L2 transition occurs at 0.10 +/- 0.05. By combining these constraints, the CO_2 composition in Athabasca bitumen (the L2 phase) is more narrowly defined as 0.08+/-.02 at room temperature. This value is in close agreement with L2-L1L2 transition compositions for bitumen and heavy oil reported in the literature - Table 3.

Table 18: CO_2 solubility in the bitumen-rich phase (L2) in L1L2V region and at room temperature

Global Composition	Temperature (K)	Pressure (kPa)	CO_2 Mass Fraction - wl
0.47	295.3	6068	0.09
	295.3	6103	0.12
	295.2	5624	0.07
0.56	295.8	5867	0.05
	295.8	6152	0.15
	295.7	6158	0.15
0.62	295.8	5867	0.08
	295.8	6152	0.06
	295.7	6158	0.10
0.74	296.9	6265	0.14

4.1.2.2.   L1V Region

At very high CO_2 concentrations L1V behavior appears. L1V Data from the literature is reported in Table 4. Based on it, it was concluded that for heavier hydrocarbons, the concentration at which L1V appears (w_{CO2}) approaches ~ 1 and it is not possible to perform meaningful experiments.

4.1.2.3.   L1L2V to L1L2 and L1L2V to L2V transitions at Room Temperature

Now, we investigate the transitions of the upper and lower boundaries of liquid-liquid-vapor region. Table 19 shows the experimental data acquired at room

temperature which are in the three-phase region. Conjugate method was applied to these data points to estimate the phase boundary pressures for LLV to LV (lower boundary) and LLV to LL (upper boundary) transitions – Table 19 and Figure 25. Some of the data in Table 19 are repeated from Table 18.

Table 19: Experimental data in LLV region utilized to estimate the boundaries LLV to LV and LLV to LL

w	Temperature (K)	Pressure (kPa)	LL Interface Pixel Number	LV Interface Pixel Number	Bellows Position Pixel Number	L1+L2 Volume (cm^3)	L1 Volume (cm^3)	L2 Volume (cm^3)	V Volume (cm^3)
0.47	295.30	6069	285	287	342	27.2	0.35	26.9	82.6
0.47	295.31	6104	285	289	307	27.6	0.7	26.9	77.4
0.56	295.75	6152	283	295	349	28.7	2.1	26.5	82.3
0.56	295.73	6158	284	305	320	30.4	3.7	26.7	76.3
0.62	296.42	6256	287	330	360	34.8	7.6	27.2	77.6
0.62	296.35	6252	287	328	342	34.5	7.2	27.2	75.4
0.74	297.05	6320	210	305	332	30.4	16.7	13.6	78.0
0.74	296.86	6265	210	230	631	17.2	3.5	13.6	134.7
0.91	293.72	5797	90	112	338	4.2	1.1	3.1	105
0.91	293.46	5790	90	140	236	5.7	2.5	3.1	88.8
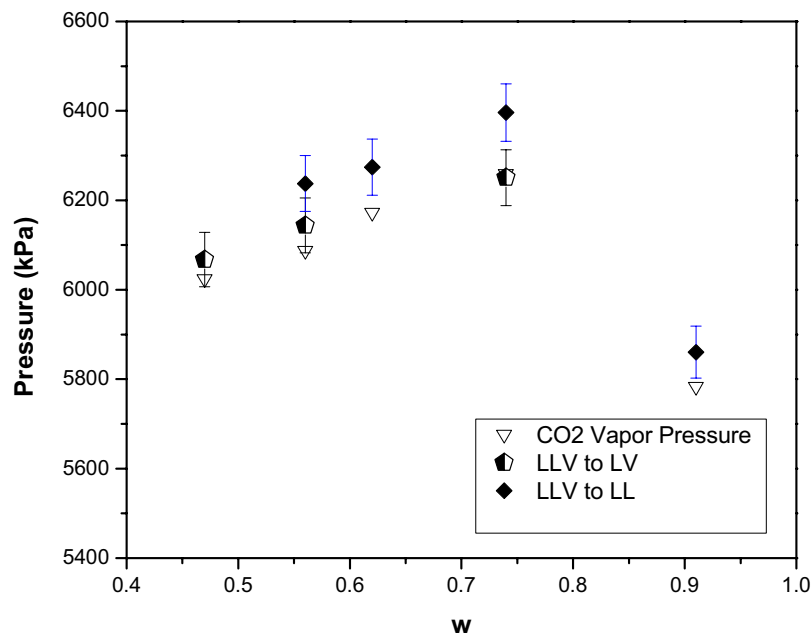
Figure 25: Estimated LLV phase boundaries on P-w diagram at room temperatures (the average value is 295.54 K)

Table 20: Estimated LLV phase boundaries at room temperatures calculated by the conjugate method

w	Temperature (K)	Pure CO_2 Vapor Pressure (kPa)	LLV-LV Pressure (kPa)	LLV-LL Pressure (kPa)
0.47	295.3	6024	6067*	--
0.56	295.7	6087	6144	6238
0.62	296.3	6173	--	6274
0.74	296.9	6259	6251	6396
0.91	293.5	5783	--	5861**

*Boundary was directly observed.

**Suspected to be the phase boundary.

The LLV-LV transition occurs almost at the vapor pressure of CO_2. The upper transition occurs at slightly higher pressures. Both are sensitive to temperature due to the proximity of the critical point for CO_2. This effect becomes apparent when pressure is normalized as $\frac{P}{P_{CO_2}^{sat}}$, as shown in Figure 26.

67
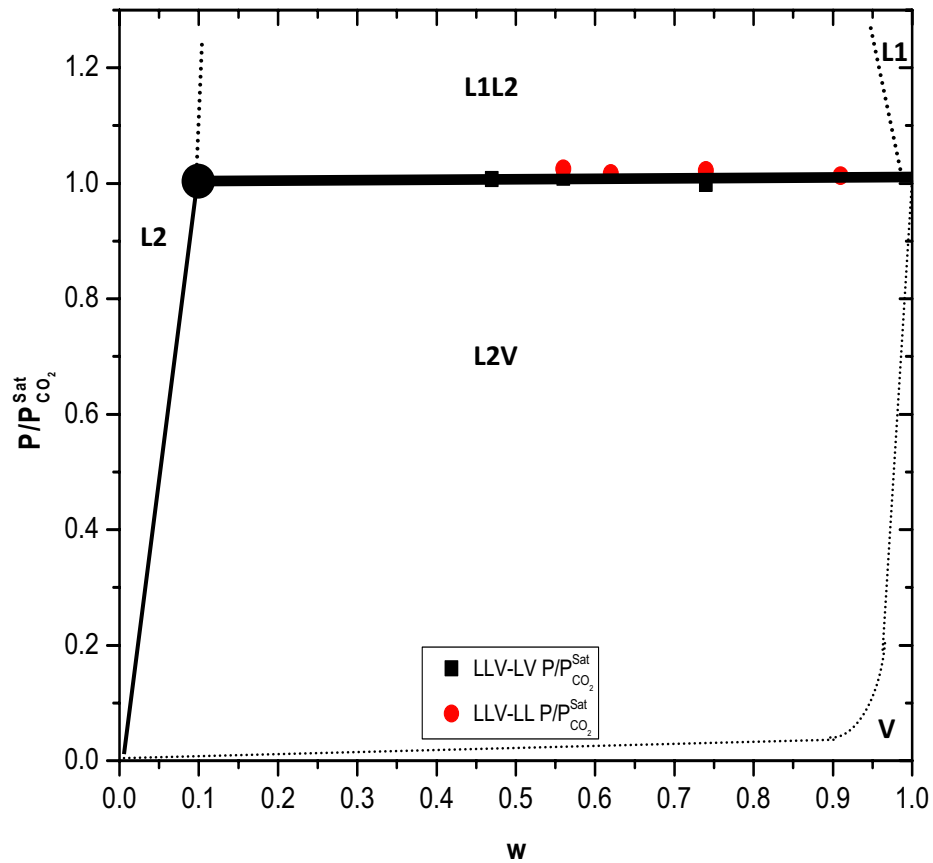
Figure 26: P/P^{sat}-w diagram of Athabasca bitumen + CO$_2$ at room temperature: solid lines are experimental observations from this work, dashed lines are expected boundaries.

The results are in agreement with the theory and with the literature. Badamchizadeh et al.[13] studied the mixture of Athabasca bitumen + CO$_2$ at low CO$_2$ concentrations and found that the LLV region appears around the vapor pressure of CO$_2$. At 298.15 K, about 6000 kPa and around 10% CO$_2$ (mass), evidence of multiphase equilibrium is observed in their experiments. In another work by DeRuiter[47], similar results are obtained: at 291.45 K, for an Alaskan West Sak reservoir oil, the second phase appears at 5500 kPa, almost equal to the vapor pressure of CO$_2$ at this temperature which is 5504 kPa.

4.1.3. Phase Behavior in Two-Phase Region (L2V, L2)

4.1.3.1.   *Henry's Law Analysis*

At temperatures above the critical temperature of pure CO_2, and below the vapor pressure of CO_2 at low temperatures, liquid-vapor equilibrium occurs (L2V). The boundary is the transition of L2V to L2. The Henry's constant method (explained in chapter III) is used to estimate the phase boundary pressure. Figure 27 shows the solubility data at three different temperatures. Points at 292 K are calculated through normalization of data at room temperatures (291-296 K). The original data was obtained in the two-phase region (LVE) at room temperature. This data can be found in Table 21. The rest of the data can be found in Table 14.

Table 21: Normalized pressure vs. LVE solubility data at 291.83 K

Global Composition	Temperature (K)	Pressure (kPa)	CO$_2$ Vapor (Saturation) Pressure (kPa)	saturated CO$_2$ Mass Fraction (wl)	P/Psat
0.38	291.83	5287	5554	0.04	0.95
0.47	295.23	5624	6014	0.07	0.94
0.56	295.82	5867	6097	0.05	0.96
0.62	296.53	6052	6198	0.08	0.98
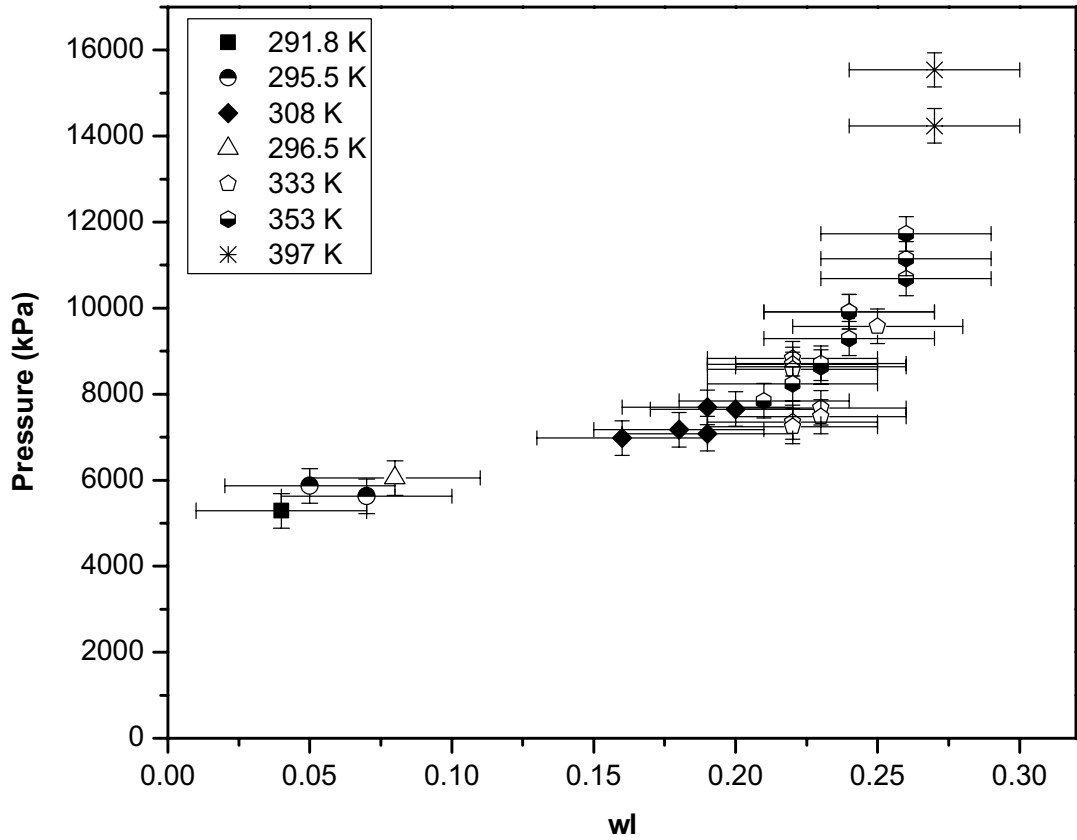
Figure 27: Saturated CO$_2$+Athabasca compositions. Temperature is a parameter.

Lines are fitted to these data to be able to predict the phase behavior at higher concentrations (see Table 22).

Table 22: Regressed lines to the solubility data

Temperature	P vs. wl Equation	Regression Accuaracy
291.8	P = 132175wl	$R^2 = 1$
295.5	P = 92842wl	$R^2 = 0.8972$
296.5	P = 75650wl	$R^2 = 1$
308	P = 39631wl	$R^2 = 0.9843$
333	P = 36785wl	$R^2 = 0.9251$
353	P = 40261wl	$R^2 = 0.9616$
397	P = 55146wl	$R^2 = 0.9943$

The same method is applied to the data at w=0.91 which is on the dew curve. Results are presented in Table 23.

Table 23: Dew point data calculated from the data at w=0.91

w	Temperature (K)	Pressure (kPa)
0.91	333.15	10300
	353.15	10700

P-w curves can be found in Figure 28.
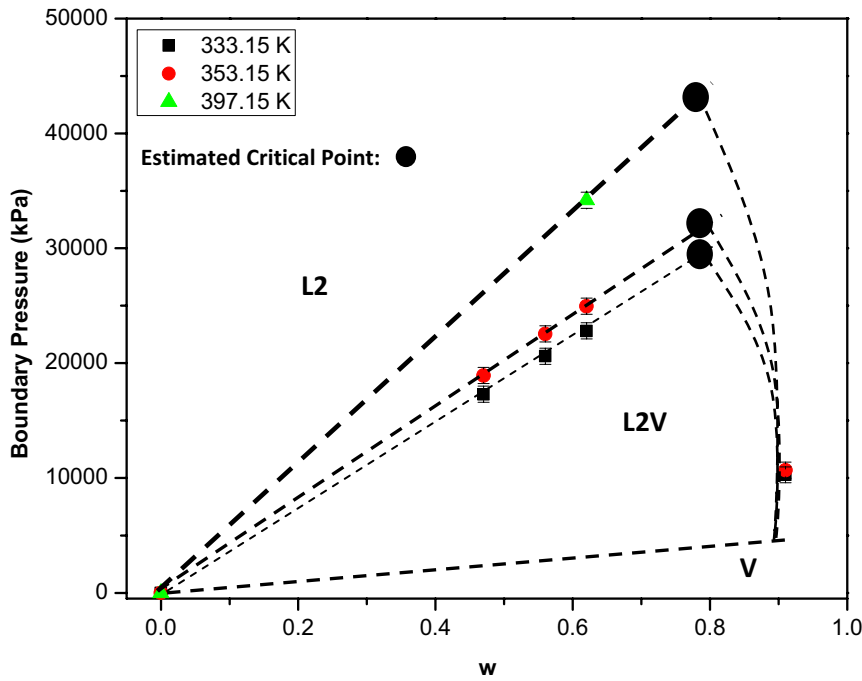
Figure 28: P-w diagram for the mixture of Athabasca bitumen + CO_2 at 333.15, 353.15 and 397.15 K

4.1.3.2. *Critical Points (L2=V)*

At temperatures above the K-point temperature, first order critical points where (L2=V) are expected to arise. From the literature data these are expected to arise at approximately ($w_{critical} = 0.8$). Computed pressure - temperature points are reported in Table 24.

Table 24: Critical points in 2-phase region

Temperature (K)	333.15	353.15	397.15
Critical Pressure (kPa)	29400	32200	44100

The estimated critical pressures in Table 24 can be compared with the extrapolated critical point data from the literature. These computed pressure-temperature values are reported in Table 26. The values in Table 26 at 333.15 and 353.15 K are regressed based on the data presented in Table 25 at different temperatures.

Table 25: Extrapolated critical pressures of the mixtures of hydrocarbons + CO_2 in the literature

Author(s)/Year/Reference	Heavy Component/Molecular Weight (g/mole)	Temperature (K)	Extrapolated Critical Pressures at w=0.8 (kPa)	R^2 (P-w)
Han et al./1992/[48]	Peace River Bitumen	318.15	72000±9000	0.9014
		328.15	75400±9400	0.9434
Hong et al./1994/[49]	Prudhoe Bay oil - Cut A/117	360.93	24100±3000	0.9945
	Prudhoe Bay oil - Cut B/163	360.93	32300±4000	0.9803
	Prudhoe Bay oil - Cut C/215	360.93	41200±5000	0.9839
	Prudhoe Bay oil - Cut D/272	360.93	48700±6000	0.9789
	Prudhoe Bay oil - Cut E/338	360.93	51400±6300	0.9664
Huang & Radosz/1990/[50]	Cold Lake Bitumen - Cut 1/201	323.5	29300±3600	0.9817
		373.4	46900±5700	0.9984
		473.5	76100±9400	0.9986
		523.2	86500±10700	0.9991
	Cold Lake Bitumen - Cut 2/304	323.3	60800±7800	0.9427
		373.4	74600±9300	1
		473.5	109700±13600	0.9998
		523.2	120800±15000	0.9999
	Cold Lake Bitumen - Cut 3/572	323.3	97300±12500	0.9205
		373.3	108700±13600	0.9977
		473.5	156400±19500	0.9998
		523.2	170100±21200	0.9998
Inomata et al./1987/[51]		343.6	12800±1400	0.9773
	Benzene/78.11	343.6	22400±2500	0.9572
Kim et al./1989/[52]		343.6	21600±2200	0.8466
	Tetralin/132.2	373.1	35700±4300	0.9938

Reference	Substance/MW	Temperature	Value±Error	R^2
	1-methylnaphthalene/142.2	372.6	51400±6300	0.9973
Gasem et al./1989/[53]	Tetradecane/198.39	344.3	18900±1500	0.9738
Kulkarni et al./1974/[54]	1-methylnaphthalene/142.2	307.15	28100±3400	0.9947
		324.15	38400±4800	0.9965
		348.15	53000±6600	0.9994
		373.15	64400±8000	0.9995
Huie et al./1973/[55]	n-eicosane/282.55	310.15	24600±3000	0.9904
		323.15	30700±3800	0.9971
		348.15	41400±5100	0.9984
		373.15	52100±6500	0.9994
Liu et al./1999/[56]	Jiangsu Oil	328.15	42400±5300	0.9822
		348.15	45800±5600	0.9995
Mehrotra et al./1988/[57]	Athabasca Bitumen - UofC	352.45	92800±11600	0.996
	Athabasca Bitumen - ARC	353.15	97000±12100	0.9937
Mehrotra et al./1989/[58]		352.87	97200±12100	0.9972
		393.01	149100±18700	0.9964
		432.77	153800±19100	0.8571
	Peace River Bitumen	472.73	193500±24100	0.9963
Yu et al./1989/[59]		373.3	107500±13500	0.9971
		473.7	156800±19600	0.9999
	Cold Lake bitumen	523.1	171600±21400	0.9989
		312.65	8300±800	0.9426
		338.15	13700±1600	0.9622
	m-xylene/106.16	366.15	19600±2200	0.9785
		312.65	9000±900	0.9267
Mohamed & Holder/1987/[60]		338.15	13200±1300	0.9806
	ethylbenzene/106.16	366.15	18600±2100	0.9681
		312.65	8100±800	0.9132
		338.15	13700±1500	0.9587
	o-xylene/106.16	366.15	19600±2200	0.98
Morris & Donohue/1985/[20]	1-methylnaphthalene/142.2	353.15	50100±6200	0.9995
		413.15	72500±9100	0.9994
Mehrotra & Svrcek /1988/[41]		325.62	64000±8000	0.9969
		350.05	81600±10200	1
	Cold Lake Bitumen	371.07	97200±12100	0.9992
Eastick et al./1992/[36]		324.15	71500±9000	0.9932
		347.65	88900±11100	0.9961
	Cold Lake Bitumen	370.05	108000±13600	0.9983

The error is calculated based on the assumption that the critical point can occur within w= 0.7-0.9 (previously explained in chapter III).

Table 26: Estimated critical pressures at 333.15 & 353.15 K for the mixtures of heavy hydrocarbons + CO_2

Author(s)/Year/Reference	Heavy Component/Molecular Weight (g/mole)	Estimated Critical Pressure At 333.15 K (kPa)	Estimated Critical Pressure At 353.15 K (kPa)	R^2 (P-T) if Applicable	Number in Figure 29-**b,c**
Han et al./1992/[56]	Peace River Bitumen	72000±9600	83800±10400	NA	1
Mehrotra et al./1989/[65]	Peace River Bitumen	89700±11200	104500±13100	0.9209	2
Huang & Radosz/1990/[58]	Cold Lake Bitumen - Cut 1/201	33800±4100	39500±4800	0.9939	3
	Cold Lake Bitumen - Cut 2/304	63500±8000	69700±8800	0.9952	4
	Cold Lake Bitumen - Cut 3/572	98200±12500	105900±13400	0.9865	5
Mehrotra & Svrcek /1988/[51]	Cold Lake Bitumen	69400±8700	84000±10500	0.9999	6
Eastick et al./1992/[46]	Cold Lake Bitumen	78200±9800	94300±11800	0.9977	7
Yu et al./1989/[66]	Cold Lake bitumen	91300±12300	100100±13300	0.9886	8
Liu et al./1999/[63]	Jiangsu Oil	43300±5400	46700±5700	NA	9
Mukhopadhyay & Du/1995/[89]*	cis-Decalin/138.25	10500±600	11800±800	NA	10
Huie et al./1973/[62]	n-eicosane/282.55	34800±4300	43500±5400	0.9997	11
Kulkarni et al./1974/[32]	1-methylnaphthalene/142.2	43200±5400	54400±6800	0.9954	12
Morris & Donohue/1985/[68]	1-methylnaphthalene/142.2	42600±5300	50100±6200	NA	13
Mehrotra et al./1988/[64]	Athabasca Bitumen - UofC	NA	92800±11600	NA	14**
	Athabasca Bitumen - ARC	NA	97000±12100	NA	15**

*Quadratic Form Extrapolation

**Figure 29 -c

a

75

333.15 K

b

Legend:
1- Peace River Bitumen
2- Peace River Bitumen
3- Cold Lake Bitumen - Cut 1/201
4- Cold Lake Bitumen - Cut 2/304
5- Cold Lake Bitumen - Cut 3/572
6- Cold Lake Bitumen
7- Cold Lake Bitumen
8- Cold Lake bitumen
9- Jiangsu Oil
10- cis-Decalin/138.25
11- n-eicosane/282.55
12- 1-methylnaphthalene/142.2
13- 1-methylnaphthalene/142.2
14- This Work - Henry's Constant
15- This Work - dH/dw

c
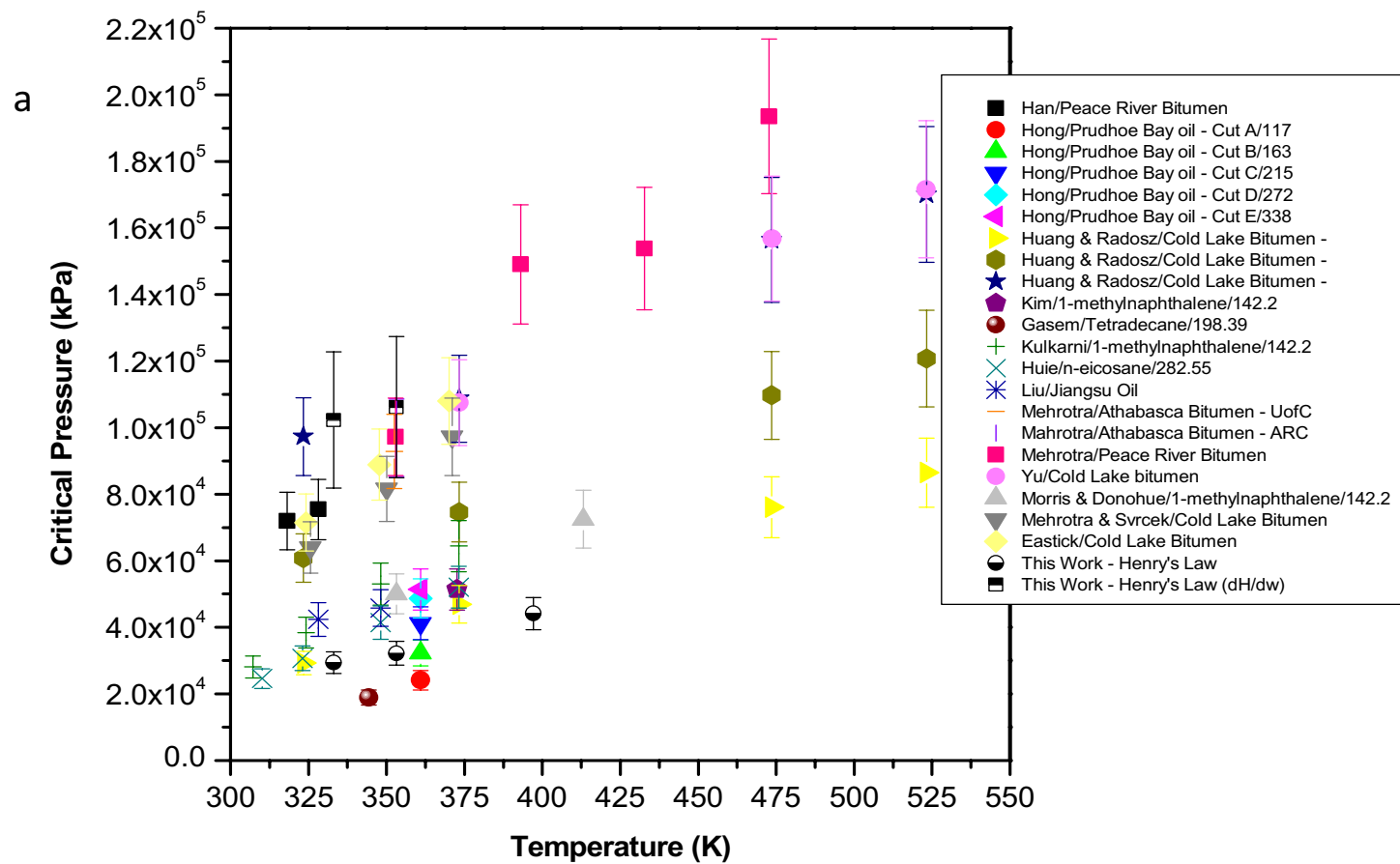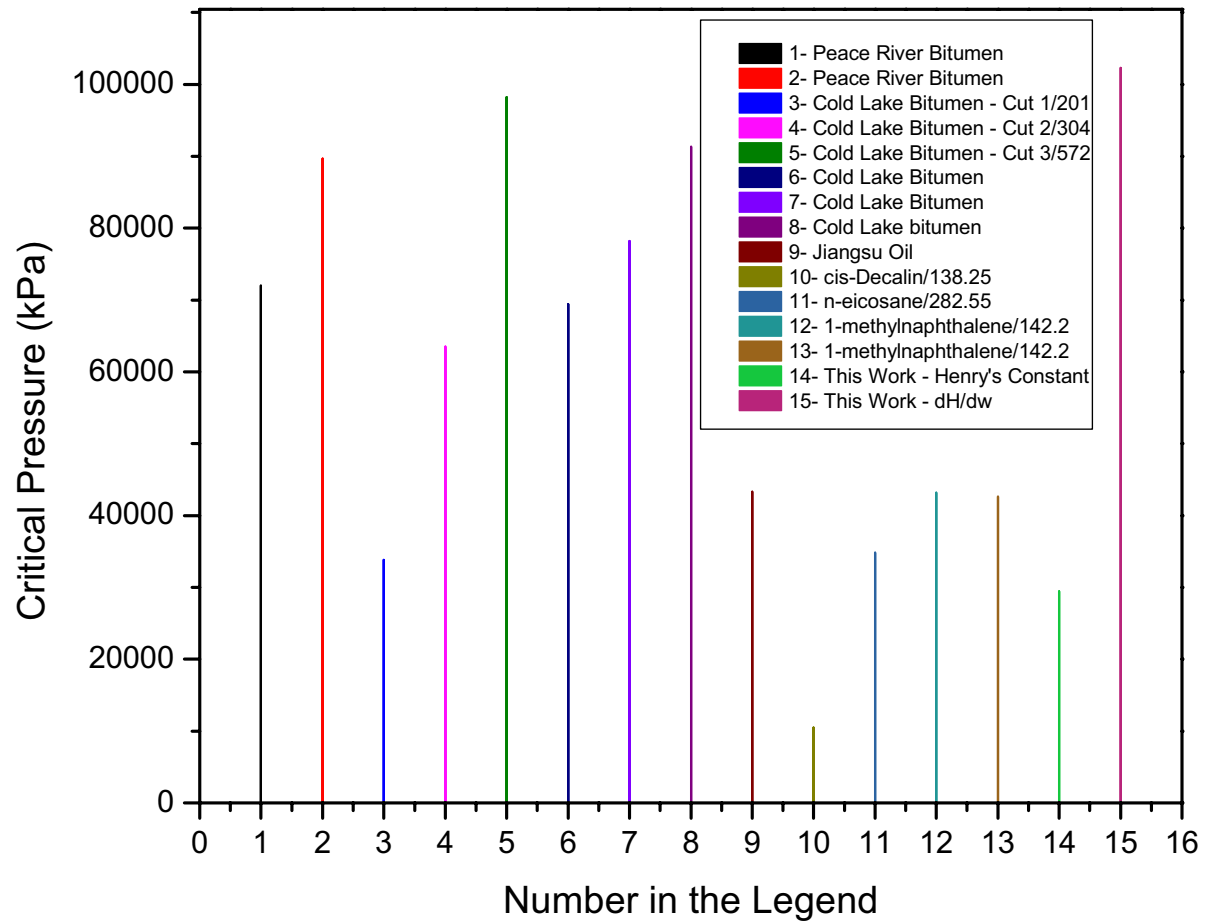
353.15 K
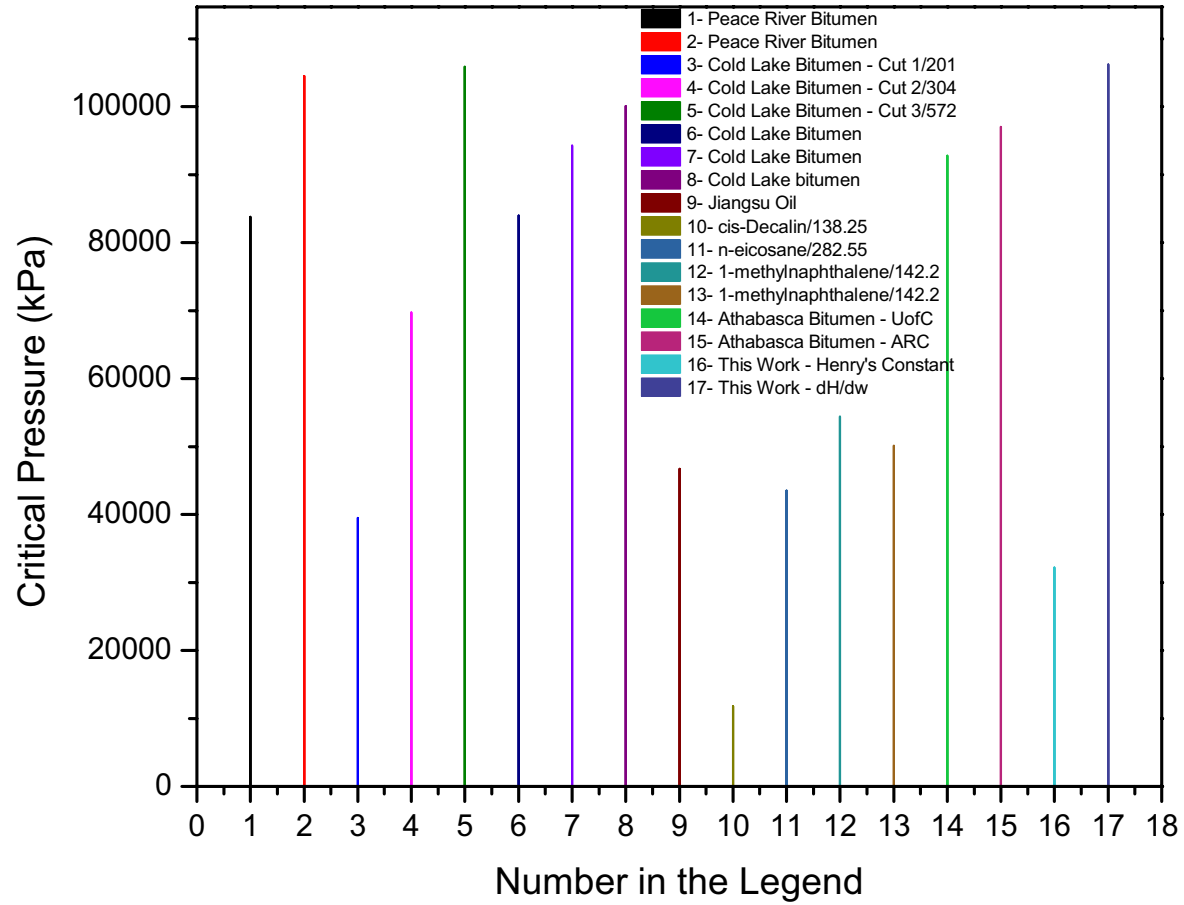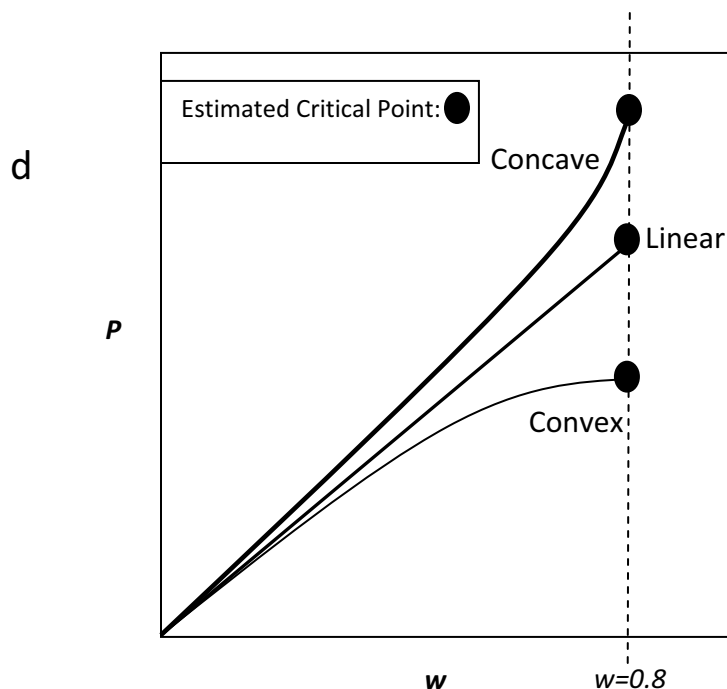
Figure 29: a: Critical Pressure P-T Map of the type III mixtures in Table 25/ b & c: Comparison of the extrapolated critical pressures at w=0.8 for the literature data in Table 26 and this work/ d: Possible P-w behavior for different hydrocarbons + CO_2 (qualitative)

Number "14 and 15" & "16 and 17" in Figure 29-b & c, respectively, are the critical pressures calculated based on Henry's law method and the modified (dH/dw) Henry's law for the mixture of Athabasca bitumen + CO_2 at 335 & 353 K. As noted previously, because the solubility values fall in a narrow range of concentration, the estimated values by the modified Henry's law method are considered less reliable in comparison with the Henry's law data.

Based on the literature review, three general types of behavior are possible for P-w diagram. Figure 29-d demonstrates these possibilities. The Henry's law models the linear curve while dH/dw in our case resulted in a concave curve, a case rarely encountered in the literature, which predicts a higher amount for the critical pressure.

4.1.4. P-T Diagrams

Since all the characteristics of phase behavior for the mixture of CO_2 with Athabasca bitumen are identified, the next step is the construction of P-T diagrams at fixed composition given the P-w diagrams and critical point data. Figure 30 to Figure 32 are constructed based on the data from the previous sections; the dashed lenses are the qualitative representation of LLV region.
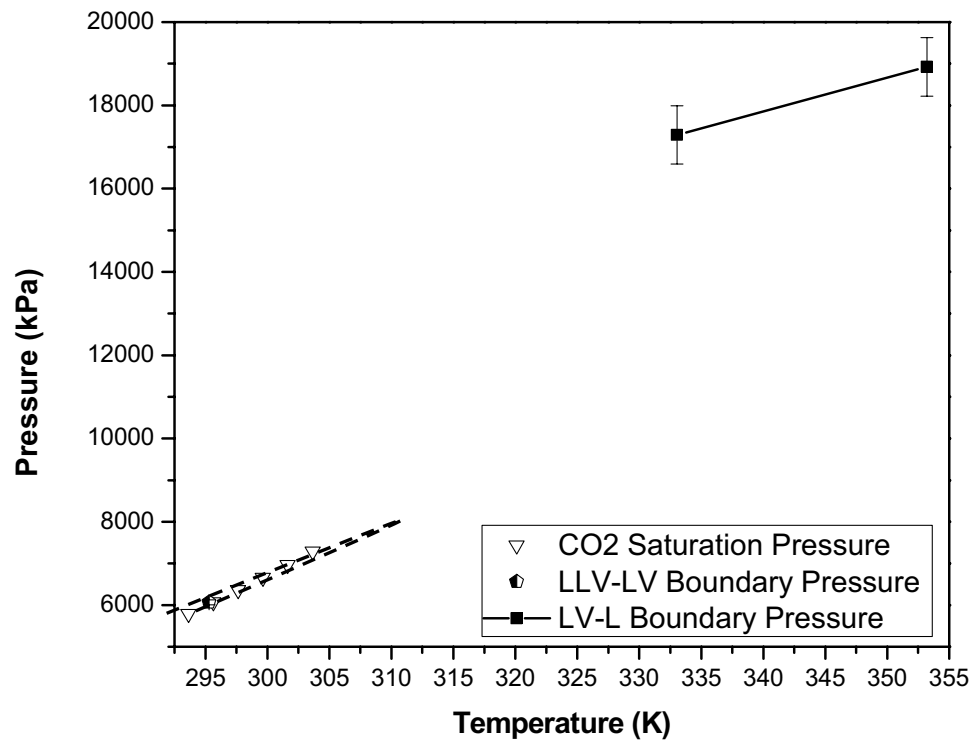
Figure 30: P-T diagram at w=0.47
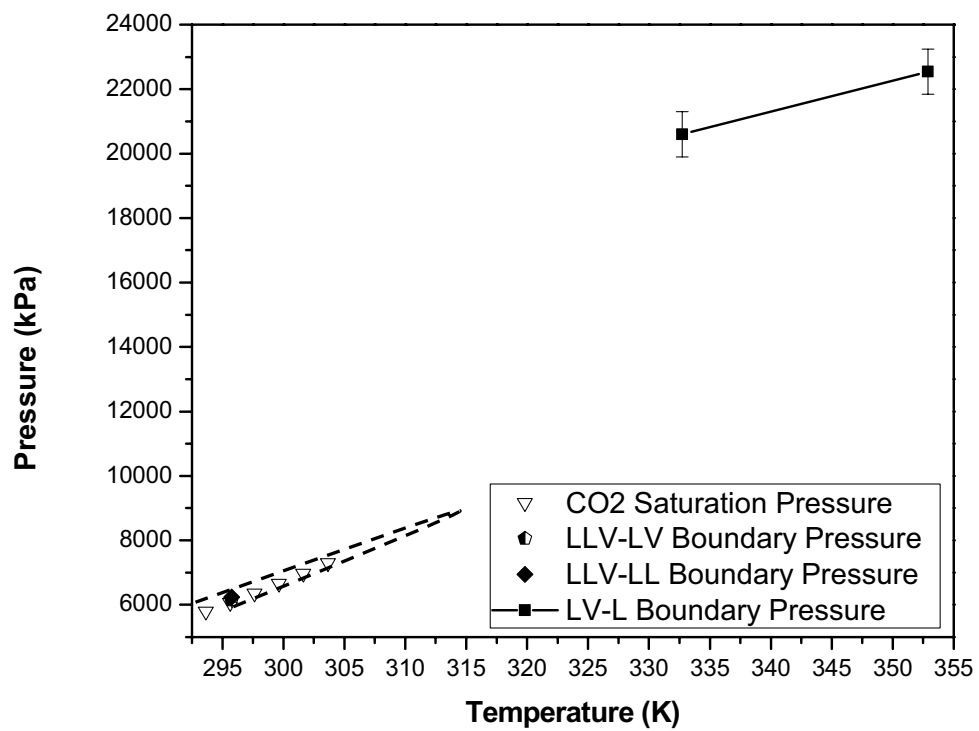
Figure 31: P-T diagram at w=0.56
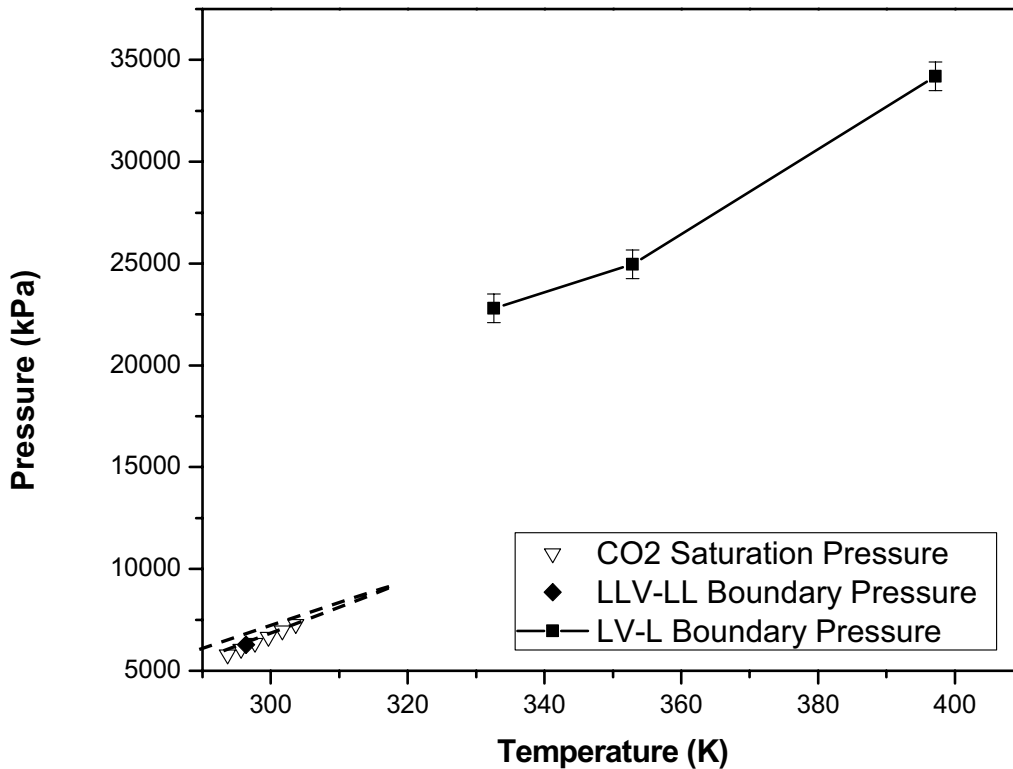
Figure 32: P-T diagram at w=0.62

In all cases the 3-phase region is bounded by the dashed lense displayed in the figures. The end point of this lense (which is the K-point) is not experimentally determined in this study but is less than 320 K [37].

4.1.4.1.   *Critical Curves on P-T projection:*

Different characteristic points of the mixture are now identified. A pressure-temperature projection of the critical points of Athabasca bitumen + CO_2 is given containing the important highlights of phase behavior. P-T critical projection can be seen in Figure 33. Occurrence of a K-point at the inversion point (maximum point) of LLV lense at which L1 and V come to a critical state in the presence of L2 (L1=V, L2) is also another notable characteristic of this mixture. The

temperature range for the critical point is expected to be 308-320 K.
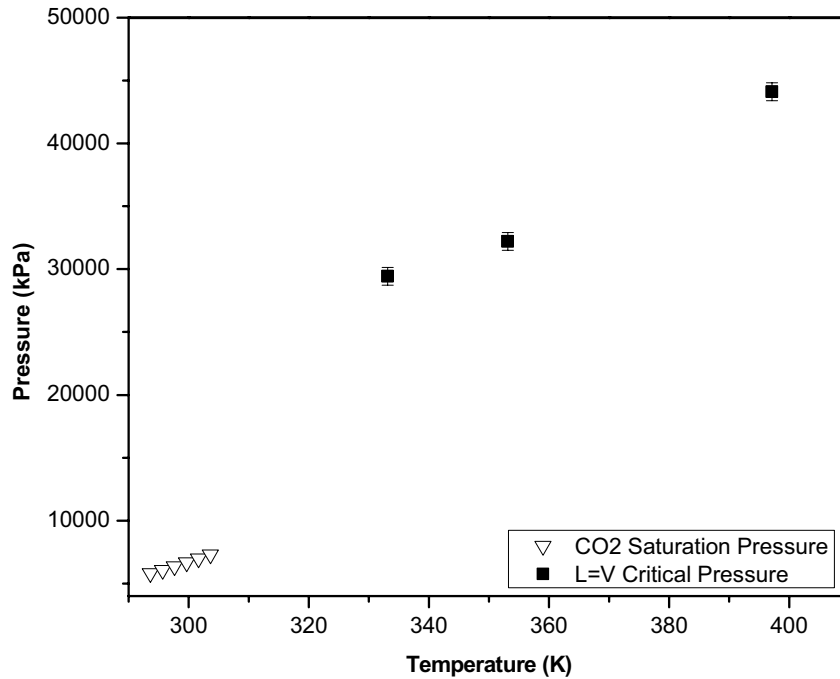
Figure 33: P-T critical projection for Athabasca bitumen + CO_2 mixture

4.1.5. Comparison with the Literature Data and Discussion:

4.1.5.1. P-w Diagram at 333.15 K

For the purpose of comparison, the bubble pressure data calculated at 333.15 K

are compared with some of the literature data, Table 27.

Table 27: VLE Data used for comparison with those of CO_2 + Athabasca bitumen measured in this work at 333.15 and 353.15 K

Author/Year/Ref	Heavy Component	Molecular Weight (g/mole)	Composition Range (w)	Extrapolation Procedure
Vito/2008/[17]	cis-decalin	138.25	0.03-0.93	NA (available data at 333.15 & 353.15 K)
Chou/1990/[90]	Tetralin	132.202	0.05-0.6	Extrapolation between 344.25 & 377.55 K
Brunner/2009/[26]	Squalane	422.81	0.05-0.6	Extrapolation between 343.15 & 373.7 K
Brunner/2009/[26]	Squalene	410.72	0.25-0.33	NA (available data at 333.15 & 353.15 K)
Bamberger/1994/[91]	Cumene	120.19	0.22-0.66	NA (available data at 333.15 & 353.15 K)
Morris/1985/[68]	1-Methylnaphthalene	142.2	0.03-0.23	NA (available data at 353.15 K)

82

Eastick/1992/[46]	Cold Lake bitumen	NA	0.05-0.5	Henry's Constant Extrapolation* based on the data at 51,74.5 and 96.9 C and at 0<w<0.1
Huang/1990/[58]	Cold Lake bitumen - Cut 3	573	0.05-0.5	Henry's Constant Extrapolation* based on the data at 50 and 100 C and at 0<w<0.15

*Henry's constant parameter is estimated at 333.15 & 353.15 K from the values at other temperatures.
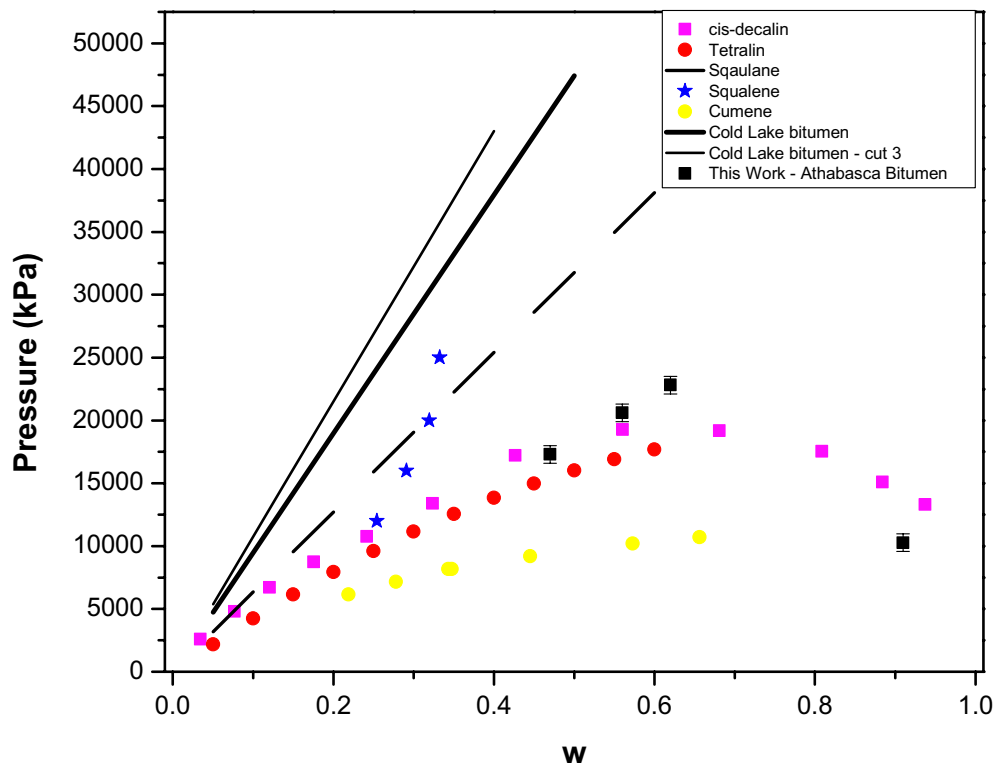
Figure 34: Pressure-composition diagram for Athabasca bitumen + CO$_2$ and similar mixtures at 333.15 K, cis-decalin [17], tetralin [90], squalane [26], squalene [26], cumene [91], 1-methylnaphthalene [68], Cold Lake bitumen [46], Cold Lake Bitumen – Cut 3 [58], lines are extrapolations based on the data at lower concentrations, points are experimental data

A general trend can be observed in Figure 34: As the molecular weight of the heavy component increase, so does the bubble pressure of the mixture. The predicted phase transition points calculated in the case of Athabasca bitumen is not close to those values for other bitumen + CO$_2$ data in the literature as excepted. Two points are to be mentioned here:

1- The calculated data points from Henry's law scheme are presented.

2- The extrapolations of the bitumen data in the literature are based on data at extremely lower concentrations coupled with the assumption of linearity, the scheme implies uncertainty in their case.

Data at 353.15 follows the same trend.
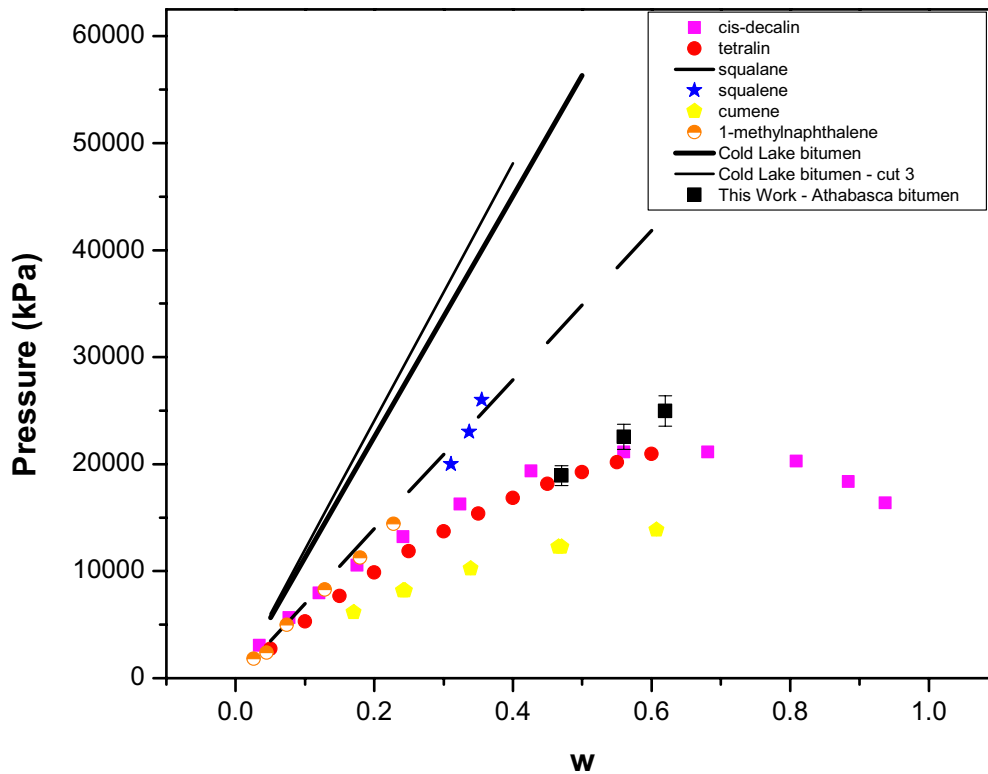
Figure 35: Pressure-composition diagram for Athabasca bitumen + CO₂ and similar mixtures at 353.15 K, cis-decalin [17], tetralin [90], squalane [26], squalene [26], cumene [91], 1-methylnaphthalene [68], Cold Lake bitumen [46], Cold Lake Bitumen – Cut 3 [58], lines are extrapolations based on the data at lower concentrations, points are experimental data

4.1.6. P-v Extrapolation Method for Phase Boundary Determination

Before adopting a Henry's constant method to estimate the phase boundary, another method was tested to perform this task (method is explained in detail in

Chapter III). The data obtained directly from our set-up was considered for this purpose. At fixed temperature and by varying the volume, the corresponding pressures are recorded at each point. As a result, a set of 2-4 points at each fixed temperature in pressure-vapor volume (P,V_v) co-ordinates was provided. We assume that at "LV-L" boundary, vapor phase is disappearing and the liquid phase is incompressible. Thus, the extrapolation (either linear or higher degrees polynomials) of "vapor phase volume versus pressure" to zero results in the coordinates of the points on the phase boundary. Different combinations of this method was used and finally the method with pressure and specific volume of the vapor phase (inverse of density) "(P,v)" was considered the most consistent. The results are presented in Table 28-Table 33.

Table 28: Experimental data at w=0.38 and the estimated boundary pressures from P-v method

w	Temperature (K)	Pressure (kPa)	Density (g/cm^3)	Specific Volume (cm^3/g)	Boundary Pressure (kPa)
0.38	314.06	5863	0.1485	6.732	8880
0.38	312.93	5421	0.1325	7.547	
0.38	313.33	4825	0.1110	9.013	
0.38	333.37	5080	0.1031	9.702	9920
0.38	333.02	5760	0.1223	8.180	
0.38	333.34	6412	0.1419	7.047	
0.38	353.05	6829	0.1339	7.468	11400
0.38	353.44	6100	0.1154	8.665	
0.38	353.61	6856	0.1341	7.455	
0.38	373.15	7150	0.1261	7.933	11700
0.38	373.35	6355	0.1090	9.173	
0.38	373.45	5675	0.0952	10.51	

Table 29: Experimental data at w=0.47 and the estimated boundary pressures from P-v method

w	Temperature (K)	Pressure (kPa)	Density (g/cm^3)	Specific Volume	Boundary Pressure (kPa)

				(cm³/g)	
0.47	308.19	6482	0.1946	5.140	9510
0.47	308.29	6742	0.2125	4.706	
0.47	308.17	6866	0.2229	4.486	
0.47	333.05	7681	0.1878	5.326	12100
0.47	333.15	7474	0.1794	5.573	
0.47	333.18	7350	0.1747	5.725	
0.47	333.18	7246	0.1708	5.854	
0.47	353.01	7846	0.1617	6.185	14200
0.47	353.15	823	0.1730	5.781	
0.47	353.21	8632	0.1848	5.412	
0.47	353.19	8715	0.1874	5.337	

Table 30: Experimental data at w=0.56 and the estimated boundary pressures from P-v method

w	Temperature (K)	Pressure (kPa)	Density (g/cm³)	Specific Volume (cm³/g)	Boundary Pressure (kPa)
0.56	307.76	7081	0.2455	4.074	9420
0.56	307.83	7171	0.2545	3.929	
0.56	307.88	6977	0.2345	4.265	
0.56	332.67	8825	0.2403	4.161	13400
0.56	332.82	8694	0.2333	4.287	
0.56	332.73	8577	0.2279	4.389	
0.56	352.82	9294	0.2066	4.840	15600
0.56	352.88	9915	0.2276	4.393	
0.56	352.82	8667	0.1865	5.363	

Table 31: Experimental data at w=0.62 and the estimated boundary pressures from P-v method

w	Temperature (K)	Pressure (kPa)	Density (g/cm³)	Specific Volume (cm³/g)	Boundary Pressure (kPa)
0.62	308.23	7653	0.3218	3.108	9120
0.62	307.97	7695	0.3377	2.961	
0.62	307.68	7281	0.2594	3.855	

0.62	332.37	8894	0.2450	4.082	14300
0.62	332.6	9915	0.3023	3.308	
0.62	332.69	9577	0.2812	3.556	
0.62	352.84	10690	0.2557	3.910	18300
0.62	352.75	11150	0.2737	3.654	
0.62	352.87	11730	0.2961	3.377	
0.62	397.45	14240	0.2590	3.862	26700
0.62	397.15	15540	0.2891	3.459	

Table 32: Experimental data at w=0.74 and the estimated boundary pressures from P-v method

w	Temperature (K)	Pressure (kPa)	Density (g/cm^3)	Specific Volume (cm^3/g)	Boundary Pressure (kPa)
0.74	305.85	7019	0.2548	3.925	8740
0.74	305.48	7536	0.3958	2.527	
0.74	305.02	6494	0.2087	4.791	
0.74	307.32	6661	0.2108	4.743	9320
0.74	307.47	7205	0.2619	3.818	
0.74	307.58	7632	0.3329	3.004	
0.74	314.21	7991	0.2863	3.492	10500
0.74	313.86	6851	0.1979	5.054	

Table 33: Experimental data at w=0.91 and the estimated boundary pressures from P-v method

w	Temperature (K)	Pressure (kPa)	Density (g/cm^3)	Specific Volume (cm^3/g)	Boundary Pressure (kPa)
0.91	303.15	6842	0.2596	3.852	8770
0.91	302.79	6420	0.2141	4.670	
0.91	303.09	6138	0.1901	5.260	
0.91	309.21	6378	0.1847	5.414	9280
0.91	308.02	6884	0.2253	4.438	
0.91	307.88	7219	0.2596	3.852	
0.91	313.44	6881	0.2011	4.973	10100
0.91	313.40	7336	0.2323	4.304	

0.91	313.43	6206	0.1651	6.057	
0.91	332.86	7012	0.1628	6.141	12600
0.91	333.22	7460	0.1788	5.593	
0.91	333.36	8563	0.2252	4.440	
0.91	353.01	9584	0.2159	4.631	14500
0.91	353.04	8501	0.1810	5.524	
0.91	353.28	7522	0.1523	6.568	
0.91	373.25	8170	0.1490	6.712	16700
0.91	372.82	9363	0.1783	5.610	
0.91	373.10	10800	0.2155	4.641	

4.1.6.1.   A Comparison between Two Repetitions (P-v Method)

Results in a repetition experiment (w=0.46) were compared to those of w=0.47 for verification. At T=353.15 K, the calculated phase boundary for these two compositions can be seen in Table 34. As it can be seen the results are virtually identical within the uncertainty of the experiment (5% in pressure).

Table 34: Comparison of the results of different experiments with similar CO_2 concentration at 353.15 K

w	Temperature (K)	Calculated Boundary Pressure (kPa)
0.46	353.01	*14000*
0.47	353.14	*14200*

4.1.6.2.   P-v Method Evaluation

The reason this method is underestimating the pressures of the phase boundary is because of the nature of our experiments i.e. high amount of residual vapor volume (constant dead volume) causes the data points to be distant from the actual phase boundary. Since as the vapor volume goes towards zero, the change of pressure is not necessarily linear or quadratic as it was assumed in the extrapolations for this method, our extrapolation method is therefore not close to expected values.

4.1.7. Comparison of the Proposed Methods

Table 35 and Figure 36 compare the extrapolated phase boundaries predicted by P-v method, Henry's law method and the modified Henry's at 353.15 K.

Table 35: Comparison between the results of Henry's constant method with alternative method at T=353.15 K

Henry's Constant Method		Modified Henry's Constant Method (dH/dw)		P-v Extrapolation Method	
w	Boundary Pressure (kPa)	w	Boundary Pressure (kPa)	w	Boundary Pressure (kPa)
0.47	18900	0.47	36700	0.38	11400
0.56	22500	0.56	52100	0.47	14200
0.62	25000	0.62	63800	0.56	15600
0.91	10700	0.91	23400	0.62	18300
				0.74	20800
				0.91	14500
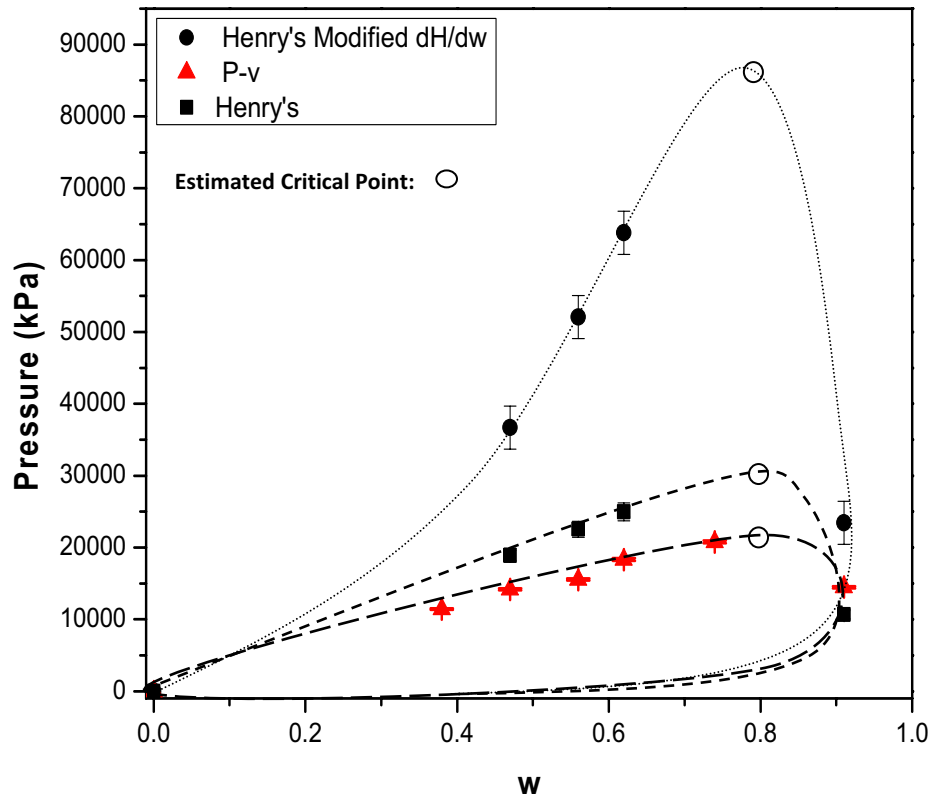
Figure 36: Comparison of the values of phase boundary at 353.15 K calculated by Henry's constant and alternative methods

The dashed lenses are approximate representation of calculated phase envelopes.

4.1.8. Comments on the Calculated Boundary Pressures

The Henry's law method is the accepted method in this thesis based on the discussion given before. Yet in Figure 36, the results obtained via applying the different extrapolation schemes in this thesis are compared at 353.15 K:

1- The results of P-v method are underestimated.

2- The modified Henry's law method (dH/dw) is unreliable in our case because of narrow range solubility in the experimental data, yet the estimated boundary pressures are closer to the expected values.

4.2. Phase Behavior of the Mixture of Maya Crude + CO_2

The phase behavior of this mixture is similar to that of Athabasca bitumen + CO_2. Some of the characteristics are:

1- At lower temperatures and near the vapor pressure of pure CO_2, a three phase liquid-liquid-vapor region appears over a narrow range of pressure at each temperature.

2- A K-point (L1=V+L2) is expected to occur in the proximity of the critical point of pure CO_2.

3- At temperatures above the K-point, 2-phase equilibrium (L2V) with an LV-L transition is expected.

4- A small L1V zone is expected at very high concentrations of CO_2 at sub-critical temperatures.

In Figure 37 and Table 37, the estimated phase boundaries at low temperature range where three-phase LLV behavior is expected are given. The phase boundary pressures are calculated similarly to those of Athabasca bitumen + CO_2 mixture. Using the same method for the case of Athabasca bitumen + CO_2, the L2V-L2L1V transition was calculated for Maya crude + CO_2. The data are reported in Table 38. The solubility of CO_2 in the oil-rich phase is calculated in a similar fashion to that of the mixture of Athabasca bitumen + CO_2. See Table 36. This can be used as a constraint to better pinpoint the concentration for L2V-L2L1V transition. Thus L2V-L2L1V transition is approximately at w_{CO2}= 0.07±0.03. The L1L2V - L1V transition is w_{CO2} = 1.00.

Table 36: The solubility of CO_2 in Maya crude oil-rich phase in LLV region and at room temperatures

Global Composition	Temperature (K)	Pressure (kPa)	CO_2 Mass Fraction - wl
0.47	294.9	6003	0.02
	297.6	6391	0.02
0.63	294.4	5676	0.08
	294.4	5694	0.14

A sketch of a phase diagram for Maya crude oil + CO_2 is presented in Figure 39, where phase boundaries are also labeled.

Table 37: Estimated 3-phase to 2-phase phase boundaries at room temperature

w	T (K)	Pure CO_2 Vapor Pressure (kPa)	LLV-LV Pressure (kPa)	LLV-LL Pressure (kPa)
0.47	297.64	6357		6428
0.63	294.38	5896	5680	5979
0.63	307.32		7591	
0.91	297.57	6349		6589
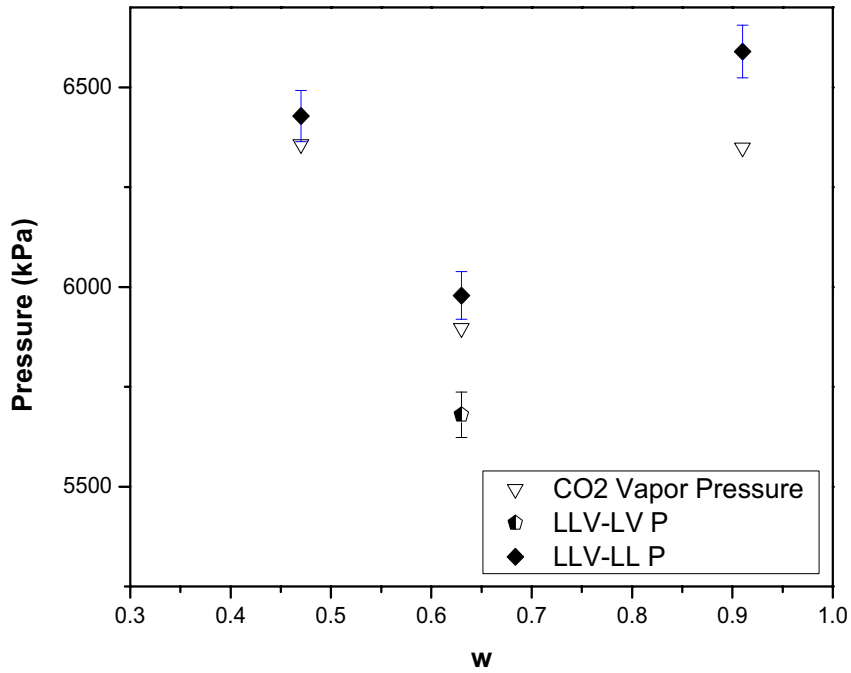
Figure 37: Estimated phase boundaries on P-w diagram at room temperature

It is noteworthy that at 307.32 K (above the critical temperature of pure CO_2), second liquid phase was directly observed (LLVE) which is in agreement with the literature data i.e. K-point temperature is greater than the temperature of the critical point of pure CO_2.

Table 38: Heavy Liquid Volume Fraction (HLVF) Calculated at LL region for the mixture of Maya crude + CO$_2$

Global Composition (w)	Temperature (K)	Pressure (kPa)	L2 Volume (cm^3)	L1 Volume (cm^3)	V Volume (cm^3)	V Density (g/ cm^3)	L1 Density (g/ cm^3)	L1+V Pseudo Volume (cm^3)	Φ$_{HL}$	Δ(Volume) (cm^3)	Δ(Φ$_{HL}$)	Δ(Φ$_{HL}$)%
0.47	294.94	6003.27	33.07	11.81	87.87	0.22	0.75	37.58	0.47	2.00	0.02	5.14
0.47	297.64	6391.44	33.07	13.58	73.74	0.25	0.71	39.65	0.45	2.00	0.02	5.10
0.63	294.38	5676.45	11.21	15.87	98.11	0.22	0.76	43.64	0.38	2.00	0.03	8.06
0.63	294.35	5693.69	11.03	19.39	80.35	0.22	0.76	42.14	0.42	2.00	0.03	7.58
0.91	297.62	6252.86	1.94	5.49	94.77	0.25	0.71	38.94	0.05	2.00	0.05	98.58
0.91	297.57	6288.02	2.00	5.73	84.86	0.25	0.71	35.57	0.05	2.00	0.05	94.99
0.91	297.94	6370.76	2.13	5.18	87.62	0.26	0.71	36.88	0.05	2.00	0.05	89.27
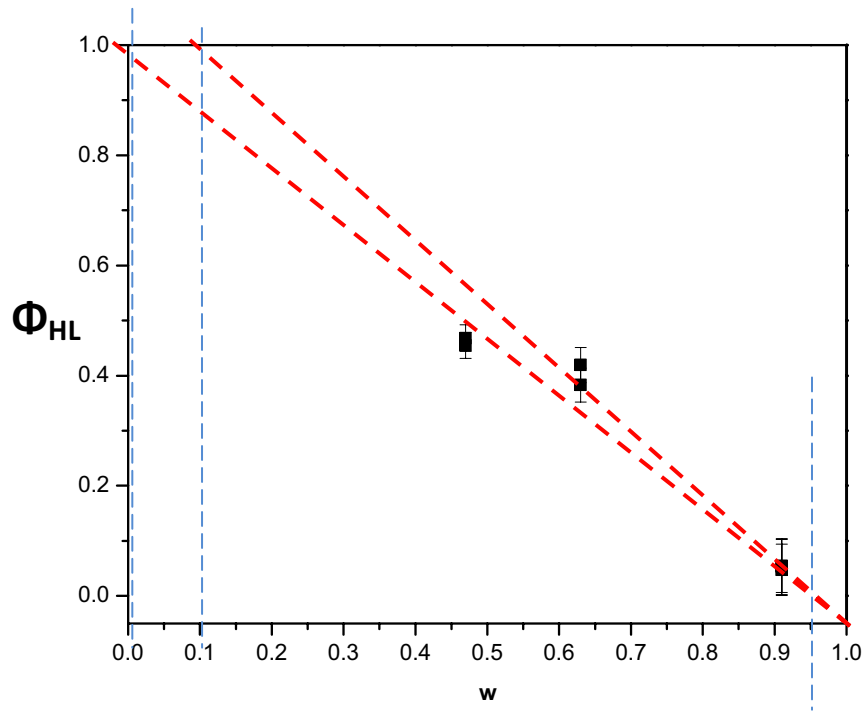
Figure 38: Diagram of heavier liquid (L2) fraction vs. global composition of Maya Crude + CO$_2$ mixture
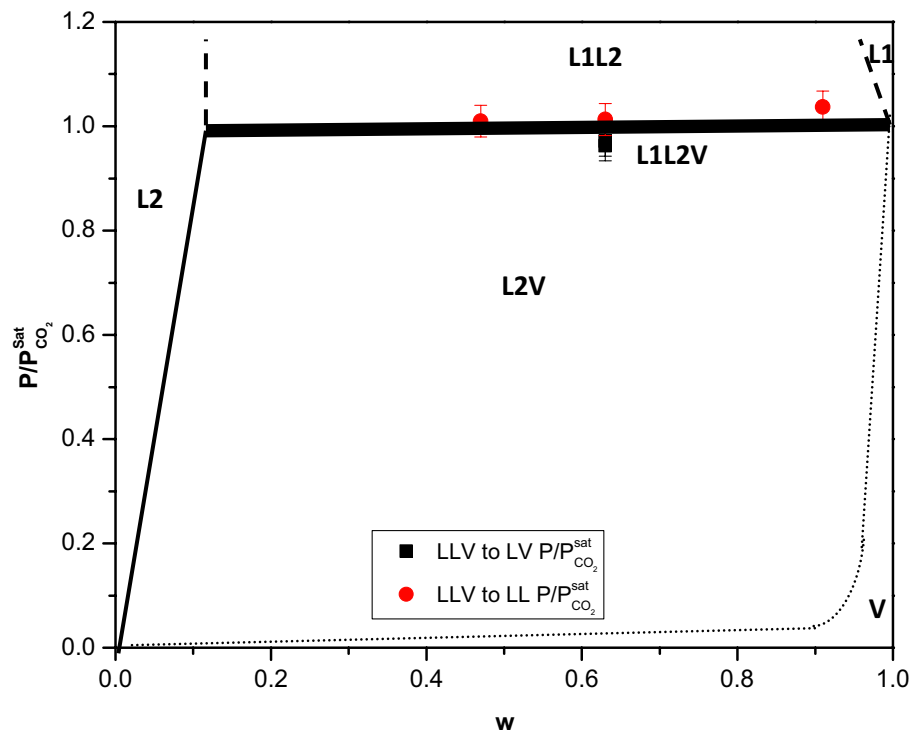
Figure 39: $\frac{P}{P_{CO_2}^{sat}}$-w diagram of Maya crude + CO_2 at room temperature

Now, the pressure-temperature diagrams can be constructed (Figure 40).
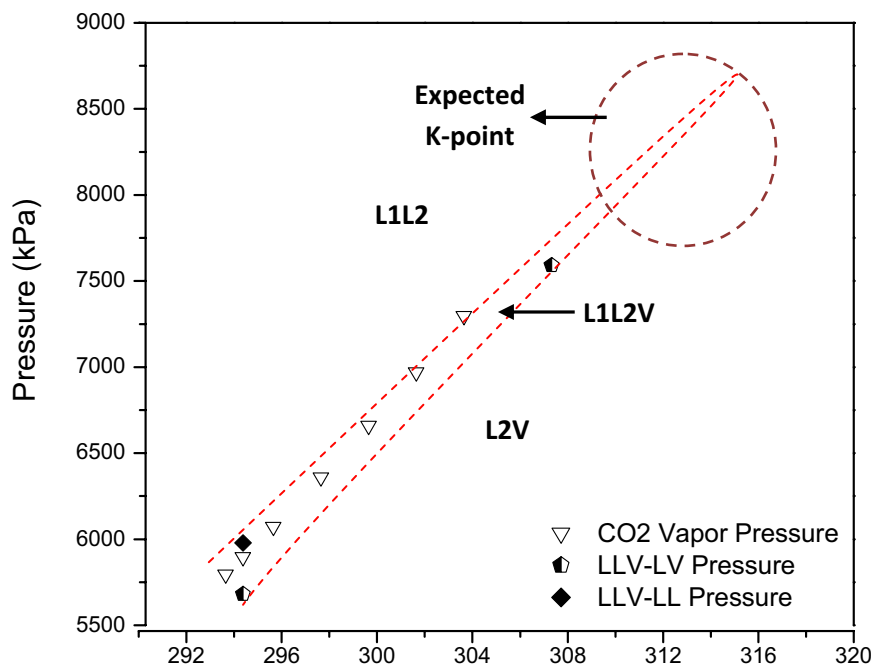
Figure 40: P-T projection containing the L=V critical points for the mixture of Maya crude oil + CO_2 (upper left mini-diagram is zoomed in on the LLV region)

4.3. Diffusion Measurement

Liquid-liquid diffusion measurements for Athabasca bitumen and Maya crude + CO_2 were performed at room temperature; CO_2 was injected until a CO_2-rich liquid phase formed (t=0s) above the heavy feed stocks. Then intensity profiles at the liquid-liquid interface were measured over time. Diffusion is associated with a broadening of the interfacial region as the composition gradient at the interface becomes less sharp. Figure 41 and Figure 42 show time sequences for intensity profiles for Maya + CO_2 and Athabasca + CO_2 respectively. In both cases, the interfacial region remains 2 mm wide even up to 28 hrs of contact. By contrast, mutual diffusion of pentane + Athabasca bitumen [92] proceeds much more rapidly as shown in Figure 43. The interfacial region broadens to more than

20 mm within 24 hours. The difference in behavior reflects the presence of the L1-L2 interface for CO_2 + heavy feed stocks. Liquid-liquid mass transfer is much slower than diffusion within a liquid phase, and is slower than gas-liquid mass transfer.
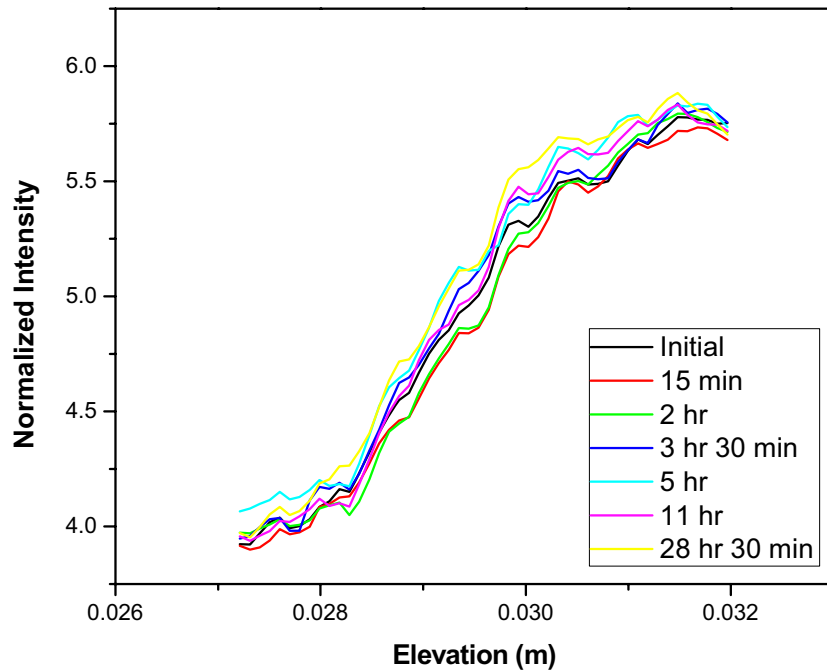
Figure 41: Diffusion profiles for Maya crude + CO_2 over the period of 29 hrs, average temperature 294.8 K, 5900 kPa, approx. 29 g CO_2 & 32 g Maya crude
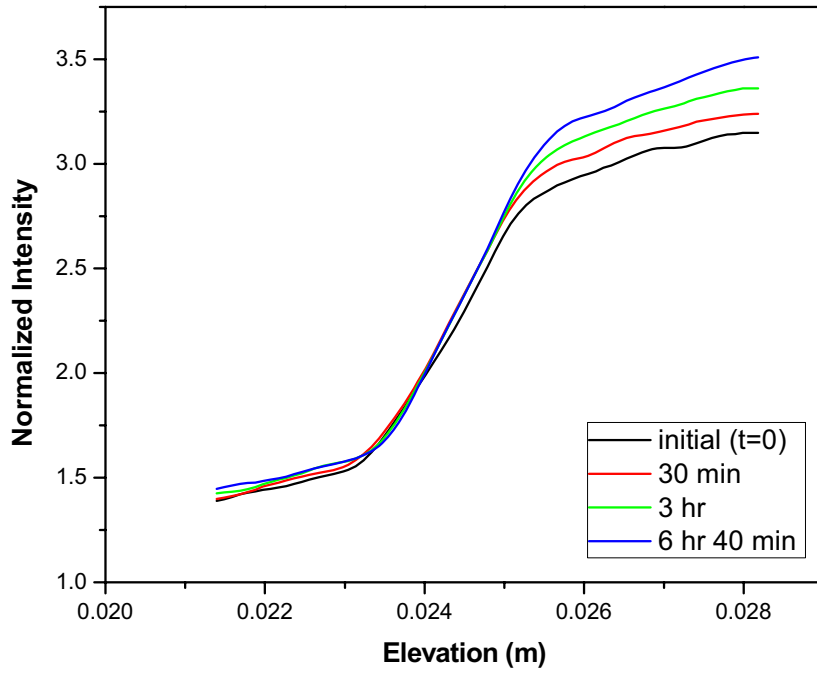
Figure 42: Diffusion profile of Athabasca bitumen + CO_2 over the period of 7 hrs (smoothed), between 295.52 - 297.14 K & 6082 – 6349 kPa, approx. 25 g CO_2 & 22 g Athabasca bitumen
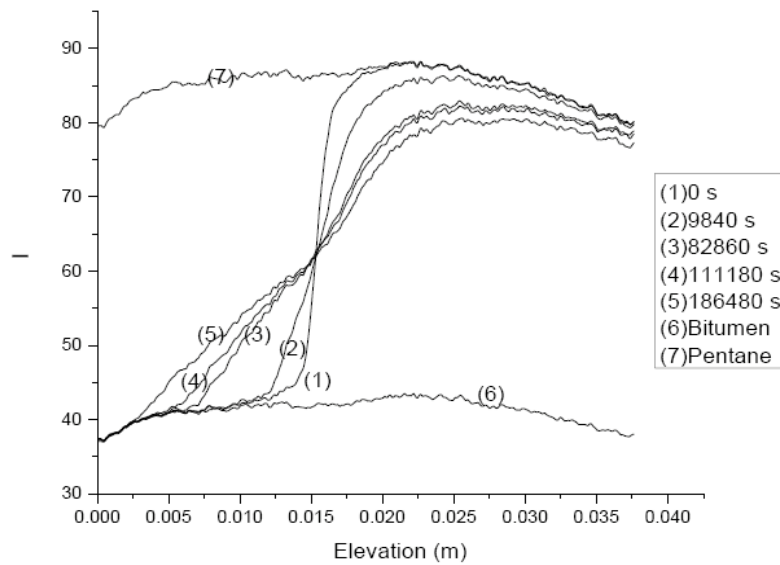
Figure 43: Diffusion of Pentane + Athabasca Bitumen at 24ºC and atmospheric pressure.

by Sadighian et al. [92]

Chapter V: Conclusions and Future Work

5.1. Conclusions

The following points can be made as results of this study:

1. Athabasca bitumen and Maya crude oil + CO_2 mixtures exhibit type III phase behavior according to the Van Konynenburg and Scott naming scheme if these mixtures are treated as pseudo-binary mixtures.

2. The results are in agreement with the phase behavior found for similar mixtures in the literature.

3. L2V-L1L2 transition was estimated to occur at w_{CO2} =0.08±0.02 for the mixture of Athabasca bitumen + CO_2 at room temperature (297.15 K); the L1L2V - L1V transition occurs at w_{CO2} ~ 1.00. For Maya crude + CO_2, the corresponding compositions are w_{CO2} =0.07±0.03 and w_{CO2} ~ 1.00.

4. The L1L2V - L1V transition occurs at high CO_2 mass fractions and cannot be observed reliably with the view cell.

5. Observed CO_2 solubility trends in Athabasca bitumen + CO_2 mixtures follow the trends in the literature i.e. it decreases as temperature increases and increases with pressure but the values appear to be too high.

6. At higher temperatures, vapor-liquid equilibrium VLE is observed in both mixtures. The solubility data was used to estimate the bubble point pressure at different compositions using based on conjugate measurements and Henry's law. Also, new modified Henry's law methods are proposed based on the parameters $(\frac{\partial H}{\partial P})_T, (\frac{\partial H}{\partial w})_T$.

7. Critical points (L2=V) are expected to appear at high pressure at temperatures greater than the K-point temperature. From trends in the literature, the w CO2 =0.80 +/- 0.1 is associated with these points. Critical points were identified on this basis. Experimental verification is the

subject of future work as these arise outside the maximum operating pressure of the view cell.

8- Due to the presence of a L1L2-L1 boundary adjacent to the pure CO_2 axis, and the consequent slowness of mass transfer across interface, diffusion of liquid CO_2 into Maya crude and Athabasca bitumen could not be detected.

9- Asphaltene precipitation/rejection was not observed in these experiments, a result consistent with expectation because this phenomenon is associated with pressures higher than those employed here.

5.2. Future Work

1- A more detailed investigation of the mixture of Maya crude + CO_2, especially at higher temperatures, will help to better identify the characteristics of its phase behavior.

2- Identify ways to decrease the dead volume of the view cell.

3- Identify ways to increase the upper pressure limit of the view cell in order to perform phase behavior experiments at higher pressure to enhance the accuracy of phase boundary extrapolations.

4- Attempt to measure L2=V critical points directly.

5- One can compare the experimental results from this study with simulation results of a cubic equation of state and try to tune the parameters such as k_{ij} to improve the equation of state method's accuracy.

Appendices

Appendix I: Operating Manual of X-ray View Cell

Safety Warning:

It is recommended to wear gloves, safety glasses and X-ray dosimeter while working with the view cell equipment and related materials.

Preparations:

The following images (Fig A1) show the initial configuration of the valves on the outside panel and cylinder:
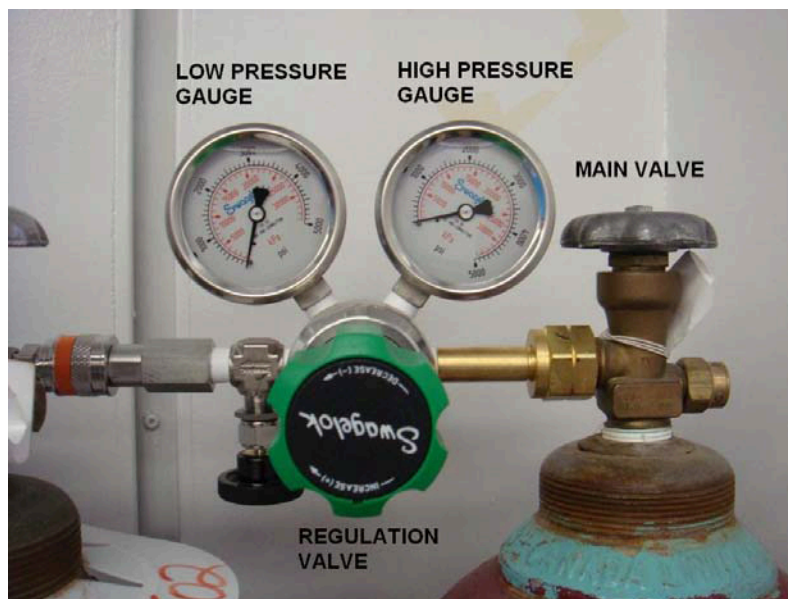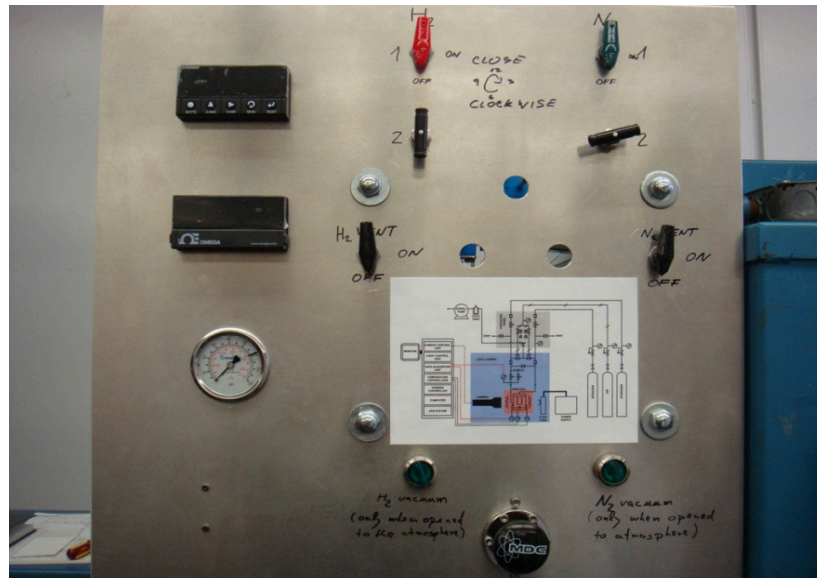
Fig A1: Closed valves configuration at the start of the experiment

- Gas cylinders:

- Green valve on the cylinders should be loose (closed).
- The main valve on the cylinder and the black valve should be closed as well.

- X-Ray:

  - **Important:** Before using x-ray, turn on the cooling water. The cooling system is installed behind the cabinet. (<u>Note</u>: the last task to do in an experiment before leaving the lab is to turn off the water 5-10 min after turning off the x-ray).

  - Check the level of re-circulating cold water in reservoir. Top up with de-ionized water if required (<u>Note:</u> This unit is mounted on the shelf behind the cell cabinet).

  - Before using the x-ray, conditioning of the x-ray gun is required. Block the x-ray gun with the yellow lead brick to make sure the camera is protected (Don't forget to wear gloves).

  - Turn on cold water supply to the wall-mounted heat exchanger. Use a modest flow rate so hose does not pop out of the drain.

  - A conditioning procedure for the X-ray gun is the following:

  a. Turn the x-ray control key (on XYLON panel) to stand by (~). Ensure that the access door to the chamber is closed.

  b. <u>Note</u>: the x-ray source will need to be conditioned if it is being turned on for the first time today. Accept this by making the appropriate entry using the key pad (the default voltage for conditioning is 120 kV).

  c. The system chooses the time for conditioning automatically based on amount of inactivity period. Use key pad on control unit to enter the number of days since last use of x-ray source.

  d. Turn control key to the on position (⚡).

  e. **<u>If the green safety circuit light is not illuminated check whether the access door to the chamber is closed.</u>**

  f. Press "I" to turn on x-ray source for conditioning. Countdown of conditioning time remaining begins.

o   Once conditioning of the x-ray source is complete, press "I" again to turn on the x-ray source. Suitable parameters are given in table A1.

Table A1: Ideal Operational Condition

V (kv)	I (mA)	Focus
045.0	03.35	0.5

Loading and pressure testing

Assembling of view cell

o   Wear personal protective equipment (nitrile gloves, safety glasses).

o   All cell parts that would come in contact with the test sample should be thoroughly cleaned and dried. Do not expose the plastic electrical connectors to any solvents!

o   Eight bolts should be sitting in the holes of the lower base plate. The Cell Mount (attached to Lower Base Plate of the cell) should be securely mounted onto the assembly scaffold by three screws. It should be left in this position after it is disassembled.

o   Assemble the view cell in the sequence shown in Figure A2.
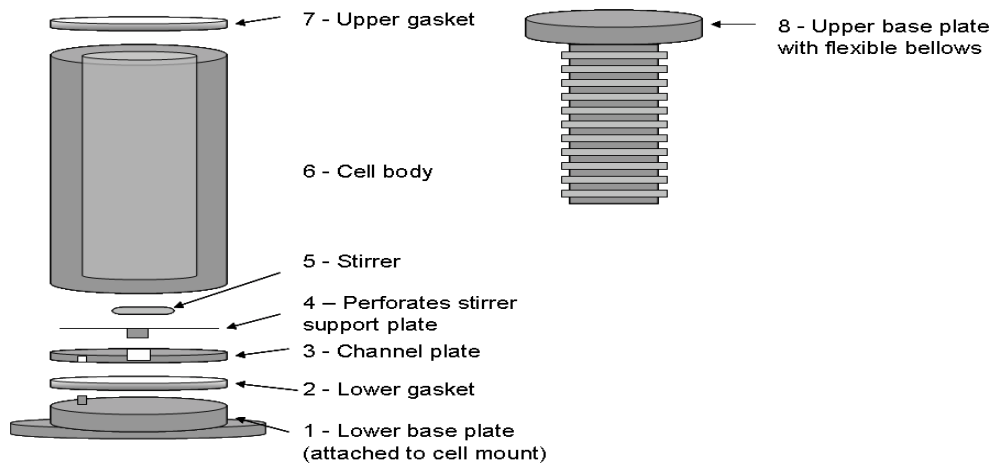
Fig A2: View cell assembly sequence

a. The Beryllium Insert with the channel has a notch which matches a pin in the Lower Base Plate. Ensure the pin is in the notch.

b. Position of the channel with respect to the bolts and groove in the Cell Mount with a punching mark **P** (Port – sample tubing and thermometers

attached to the view cell should be aligned with this groove) must correspond to the configuration in Figure A3.
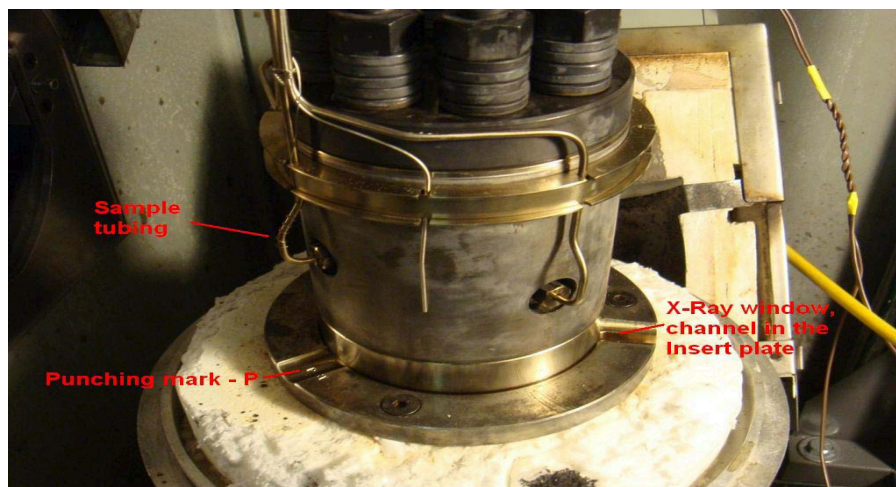
Fig A3: Position of the view cell with respect to its base

    c. The Perforated Stirrer Support Plate has a pair of tongues which must be fitted in the channel of the Beryllium Insert.

    d. Gaskets – Upper and lower gaskets must be of the same type!

    e. Lower Kalrez o-ring is fitted into the groove in the Lower Base Plate.

    f. Before installing the upper gasket and Upper Base Plate with flexible bellows, add a known mass of solid or semi-solid sample. If a low dense liquid sample will be used, complete the cell assembly without sample addition. The liquid sample will be added at a later stage.

    g. Install the upper Kalrez o-ring on the top of the view cell body between inner and outer retaining metal rings.

    h. Do not forget to place the magnetic stirrer in the view cell.

    i. Install the Upper Base Plate with flexible bellows.

o Lightly coat the bolts with molybdenum sulfide grease.

o Add and finger-tighten the eight numbered sets of nuts and washers to the eight bolts. Correct configuration of washers is shown in figure A4.

Fig A4: Correct configuration of washers
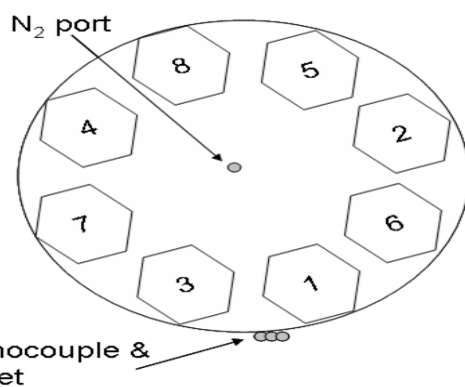
o   Torque each bolt in sequence, 1 to 8 (see Figure A5).

Fig A5: Bolt tightening sequence

o   For Kalrez® gaskets begin tightening at 10ft-lb set on ratchet wrench and increase torque in steps of 5 ft-lb till 25 ft-lb.

o   Attach the VCR Silver-Plated Gasket with Retainer to the VCR fitting (DO NOT SRATCH THE ROUNDED SEALING SURFACE)

Installation in the Shielded Enclosure (CABINET)

o   Ensure that magnetic stirrer block is installed on the cell support block in the cabinet.

o   Loosen the 3 locking screws (Cell Mount) from the assembly scaffold in the fume hood.

o   Transport the view cell to the cabinet (use a cart). Make plenty of space in the cabinet for comfortable safe manipulation. Position the view cell over the three holes for locking the screws. Always hold view cell with two hands (one hand at

107

the bottom of the assembly, the other on the 8 bolts positioned at the other end of the structure). Do not touch or stress the sample tubing and thermometers. The Inlet Port and thermometers attached to the view cell determines the position of the view cell in the cabinet.

o   Attach the VCR Silver-Plated Gasket with Retainer to the VCR fitting at the end of the tubing supplying Hydrogen to the view cell.

o   Bring the fork attached to the "Crane" assembly back to its position and adjust the fork-shaped structure to be face-to-face with Inlet Port attached to the view cell.

o   Attach inlet lines for sample-side (2 VCR fittings - FORK) and bellows-side (SWAGELOK TUBE FITTING) of the view cells. Finger-tighten it and then tighten with wrenches to a very little extent (for VCR fittings: less than 1/8 of a turn from the finger-tight position, for normal tube fittings: less than quarter of a turn from the finger-tight position).

o   Attach the marked thermocouple leads.

o   Figure A6 shows the correct configuration of the view cell.

Fig A6: Correct configuration of the view cell

Checklist before the start of the experiment:

- o Check the cold trap and clean it with solvent (THF). Then rinse it and dry it with air. Detach it from the vacuum hose and under the fume hood start rinsing it by the solvent and then decant the solvent and dry the trap with air.
- o Check to make sure all the valves on the panels (outside and inside) are closed.
- o Push the button beneath the computer keyboard to turn on the instrument power.
- o Turn on Agilent control panel (white panel below the X-ray panel).
- o In case of high temperature experiment, install the heating jacket then turn on the T-control for heating jacket (It is below the X-ray control panel) by hitting its switch. After setting the set point and attaching its thermocouples, heating jacket will start automatically. Tip: For installing the heating jacket, lean the half parts a little bit and fit it slowly. Try to align it with the slot on view cell base.
- o Put the white plastic part (it can be found in the cabinet) underneath the thermocouple on top of the heating jacket to protect the thermocouples above the heating jacket (it covers the hole made for passing the tubing).

Image Acquisition Software:

Note: Images are taken when the stirrer is off.

- o For taking pictures, "Image Pro" software is used. Start the program and in main tab menu, follow the procedure mentioned below:

    Acquire→video captioning→new image & no integration & number of images 800 (or 700)

- o Incremental display means averaging the images onto a single image. In this way the quality of images are better and noises are omitted to a great extent.
- o In case where change of contrast is needed follow the procedure mentioned below:

    Enhance→Display range→change the position of arrow

Data Acquisition Software:

"VEE Pro 8.5" software is used for this purpose.

Disassembling the view cell:

- o Before starting the disassembling process, make sure the pressure in bellows and view cell is equal and both gases in bellows and view cell are vented to atmosphere to assure there would be no sudden depressurization and movement in bellows. There is a black valve on inside panel that connects the bellows and view cell together. By opening that and closing the red and green valve on the inside panel, basically, we are isolating the view cell and bellows from the outside and connecting the two together.

- o To make sure that the above procedure was done properly, open the Nitrogen vent valve and see whether position of the bellows changes or not. If it does, open the valves till the system reaches atmospheric pressure.

- o Open the connectors between tubing by means of two wrenches. For opening and closing nuts and bolts of connections: figure A7 shows the way in which wrenches should be exerted on connections.

Close	Open
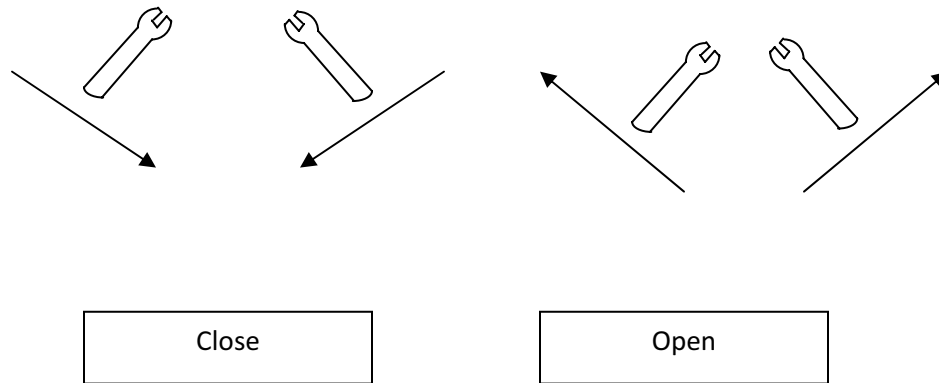
Fig A7: Direction of movement for two wrenches

- o disassembling procedure is as the following:

- a. Open the connections to the view cell (Figure A8): 2 on top of the fork and 1 at the bottom part. Every single time, you need to change the gaskets in two places (bolts).

Fig A8: 3 VCR connections on the fork-shaped structure (specified by green circles)

> Note: Do treat the fork shaped connection with extreme care. It is an expensive piece of equipment.

b. Open three bolts connecting the view cell to its base and then detach any wire connections to it and lean the view cell (put one of your hand bellow the view cell and the other one on the big 8 bolts (Do not touch the O-rings in order to prevent deformation). Then pull it out, put it on the cart. Move it to the fume hood.

c. Tighten cell again into the box under the fume hood. Start loosening the 8 bolts on the view cell with Ratchet wrench on top (determine the mode for loosening with knob) and French wrench at the bottom. Pay attention to the configuration of the nuts and Washer. Also note that these bolts should be tightened and loosened in a diagonal manner meaning after tightening a bolt, tighten the one across from it.

d. Take out the bellows; put it on the holder and lock it (under the fume hood). Take out the O-rings and the gaskets. Mind the delicate surface. Clean the

bellows by rinsing and paper towel (Use of gloves and mask is recommended when working with strong solvents such as THF). Do not use any rough surface to clean the beryllium surface.

e. With a syringe, suck out the contents of the view cell; put it in a beaker and dispose of it in the organic waste bottle.

f. Rinse all parts of the view cell carefully.

g. Open a purge stream (Nitrogen) to the open tubing to clean it from any possible residue (wrap tissue pieces around the tubing head to prevent anything from splashing outside into the cabinet).

Nitrogen Leakage test (Before Each Experiment):

o Pressurize the Nitrogen cylinder to a pressure around 200 Psi.

o Turn on the Monitoring software and observe how bellows move when you change something in the system (this is the fastest way to monitor the system on-line and prevent any damage caused by sudden movements of the bellows).

o Isolate the cell.

o Use the Snoop to check whether the connections are properly tightened or not (beware not to produce bubble with the Snoop). If leakage is spotted, use the appropriate wrench to tighten them.

o When using high pressures, don't just open the valves to pressurize the system in one batch. The following may clarify the proper procedure to pressurize the cell gradually:

a. Open and close the green valve on the outside panel.

b. Open the black valve.

c. Monitor the changes and repeat the procedure above.

d. If no drastic change was observed, open the green valve again and slowly open the black valve to pressurize the cell.

e. Close the connection to the view cell to isolate it from the system.

f. Leave it the pressurized condition for 1 or 2 hours to check whether the pressure changes or not (up to 4 percent loss of pressure is acceptable; also do not forget to wear safety glasses). If the change is significant, the device should be reassembled again.

Vacuuming:

- o Start the instrument air (which operates the solenoids) up to 120 PSI (marked on the pressure indicators).

- o There is a safety mechanical mechanism on the solenoids. A small screw can be utilized for this purpose.

- o Put the liquid nitrogen into the cold trap then put the cap on it and open all the valves on the inside panel in order to make sure that all parts of tubing will be vacuumed.

- o Start the scroll pump→turn on the vacuum switches→scroll the pump switch on the outside panel and give it some time to stabilize→close the scroll switch→turn off the switches.

- o The pressure that can be read for this state is the amount of vacuum produced in this experiment, so record it and subtract the gas pressure inside from the pressure data you may record later for different conditions.

Hydrogen leakage test:

- o Since hydrogen is a combustible gas, before this test vacuuming of the view cell should be done.

- o In this case nitrogen line should be closed (green valve inside the cabin), and black and red valves should be open.

- o Pressurize the cell with hydrogen and leave it for some time.

- o Use the Hydrogen detector on connection, tubing and O-rings to check for hydrogen presence

- o Do not breathe near the detector or it might distort the detecting process.

Liquid Sampling:

- o Take the sampling device (Figure A9) from the cart. Install the gasket on it. Attach it to a syringe. Fill the syringe with the sample and weight it. Then attach it to the sampling line and tighten it thereafter inject the sample.

- o Detach and close the sampling valve.

- o Another vacuuming is needed to be done to purge any air and/or water inside the view cell. This process is to be done quickly to prevent significant loss of the

sample. The elevation of the material is checked before and after vacuuming to ensure no significant loss of sample has occurred.

Fig A9: Sampling device which can be attached to a syringe

Emergency Response and shut down procedure

If there is an explosion or fire during a run, it is urgent to do the following:

1. Turn off the power to furnace

2. Turn x-ray control key (Xylon) to stand by (~).

3. Vacate the area and the building via nearest exit and pull the nearest fire alarm.

4. Proceed to the evacuation assembly area.

5. Notify your supervisor

6. Inform Occupational Health and Safety.

Appendix II: Image Analysis Code

```matlab
%% Clear the Matlab Screen and Memory
clc
clear all,
%% Create the Zero Matrices
imageaverage = zeros(1,600,40);
imageaverage2 = zeros(1,600);
Hold on
%% Digitize the Image and Save in "image"
    image = double(imread('C:\...));
%% Sweep the Rectangle Across The Length of the "image"
    % Column Average
    for x = 10 : 600 % swap vertically
        temp = 0;
        Counter=0;
        for y = 200 : 260  % swap horizontally
            temp = temp + image(y,x);
            Counter=Counter+1;
        end; % of for
        imageaverage(1,x,1) = temp/Counter ;
    end; % of for
    for x = 1 : 600
        temp = 0 ;
        Counter=0;
        temp = temp + imageaverage(1,x,1);
        Counter=Counter+1;
        imageaverage2(1,x) = temp/Counter;
end;% of for
%% Calculate the Internal Standard Amount
IBemean=mean(mean(image(140:160,10:140)));
%% Calculate the Standardized Sample Intensity
    for x = 1 : 600
    imageaverage2(1,x) = imageaverage2(1,x)/IBemean;
    end;% of for
```

```
plot(imageaverage2,'black');
```

Appendix III: Volume Calibrations of the System

Different calibrations have been performed to ensure the accuracy of the calculations:

III-A: Hand Pump Volume Calibration

The hand pump catalogue only provided the volume which is provided by shaft displacement. The Initial volume in the fully open state was not given. Thus a simple experiment was performed to calculate the amount. The pump was pressurized with CO_2 to a known amount and was isolated thereafter. The pressure was recorded, and then with a known number of revolutions, the CO_2 was further pressurized. Since the mass is constant throughout this process the following formula can be written.

$$\rho_0 V_0 = \rho_1 (V_0 - n \frac{volume\ occupied\ by\ the\ travelling\ shaft}{total\ number\ of\ revolutions})$$

In this equation all the parameters are know or can be easily calculated (density of pure CO_2 can be calculated using a simulator such as VMGSim). The only unknown, the initial volume, is then calculated.

III-B: View Cell Liquid Volume Calibration:

Measured amounts of hexane calculated from the masses of a filled and empty syringe were injected to the view cell and an image was taken after each injection. Having the cumulative mass and density, the volume of the injected mass was then calculated and correlated with the elevation (pixel number) of the view cell. Two correlations are developed: one for the insert area, the other for the volume above the stirrer. For the insert area, quadratic extrapolation is used to improve the accuracy of the view cell.

Insert Area: *Volume (cm^3) =0.0443*(Pixel Number) - 0.7478 (R^2=0.99)*

Above the stirrer: *Volume (cm^3) = 0.1763*(Pixel Number) - 23.349 (R^2=0.99)*

III-C: View Cell Total Volume Calibration:

A known amount of CO_2 (from hand pump volume calibration) was injected into the empty and vacuumed view cell. Then by varying the volume, pressure and pixel number of the bellows position were recorded at numerous positions. The amount of dead volume (including the pressure transducer + connections, valves and tubing directly connected to the view cell + Volume trapped between the bellows and the view cell)

was taken into account as invariant dead volume. At each stage, the mass inside cell is conserved; as a result:

$$\rho_0 v_0 = \rho_1 v_1$$

In the above equation v_0 can be calculated at the maximum contraction of the bellows (maximum volume of the view cell - the pressure in the bellows was vacuumed and the length of maximum contraction was measured in order to find the volume). ρ_0 and ρ_1 can be calculated for vapor CO_2 at the temperature and pressure of this experiment using a simulator such as "VMGSim". Thus, the value of v_1 can be calculated for different positions of the bellows and the total volume can be correlated with the pixel number of the bellows as following:

Total Volume: Total Volume (cm^3) =0.1455*(pixel number) + 60.143

The results were verified with another method when we separately calculated the total volume of the view cell according to the following formula:

Total Volume = (Volume under the Bellows) + (Volume Trapped Between the Bellows and the Cell) + (Invariant Dead Volume of the System),

Where Volume under the Bellows was calculated from liquid volume calibration equation);

Volume Trapped Between the Bellows and the Cell was calculated by $(\pi R^2_{Cell} - \pi R^2_{Bellows}) l_{Bellows}$;

R_{Cell} is the Internal Radius of the view cell;

$R_{Bellows}$ is the External Radius of the Bellows;

$R_{Bellows}$ is the Length of the Bellows;

Invariant Dead Volume of the System was estimated as the Volume of the tubing system and pressure transducer which are directly connected to the view cell.

III-D: Height Calibration:

The correlation of the height (elevation in the view cell) with pixel number is developed. A bolt with specific thread length was placed in the view cell vertically and an image was taken; Figure A10 shows the results for the correlation.

Height vs. Pixel Number

$y = 0.0097x - 0.0917$
$R^2 = 1$
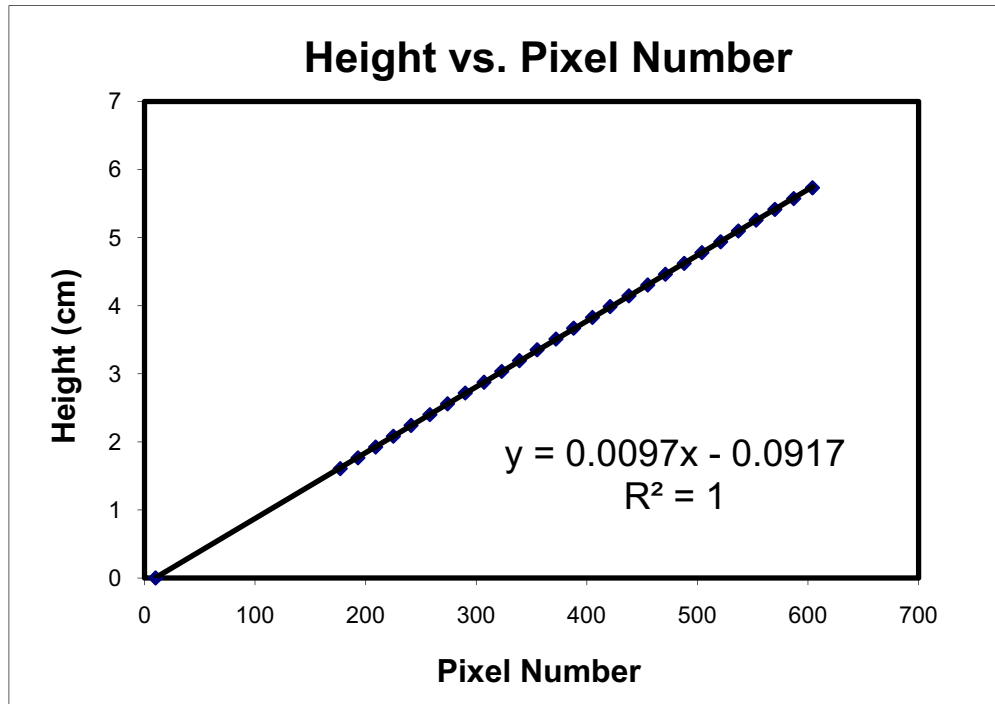
Fig A10: Height calibration in the view cell based on data from a known bolt (each point represents one thread)

Appendix IV: Mole Fraction to Mass Fraction Conversion Formula

Suppose x_i, w_i and MW_i are the mole fraction, mass fraction and molecular weight of component "i" respectively. In a binary mixture of "a" and "b" the following relationships hold:

$$x_a = \frac{n_a}{n_a + n_b}$$

$$wx_a = \frac{m_a}{m_a + m_b} = \frac{n_a MW_a}{n_a MW_a + n_b MW_b} = \frac{n_a}{n_a + \frac{MW_b}{MW_a} n_b}$$

$$\frac{1}{x_a} = \frac{n_b}{n_a} + 1$$

$$\frac{1}{wx_a} = \frac{MW_b}{MW_a} \frac{n_b}{n_a} + 1$$

$$wx_a = \frac{x_a MW_a}{MW_b + x_a(MW_a - MW_b)}$$

Or vice versa:

$$x_a = \frac{wx_a}{\frac{MW_a}{MW_b} + wx_a(1 - \frac{MW_a}{MW_a})}$$

References

1. Masliyah, Jacob, *Fundamentals of Oilsands Extraction*, in *ChE 534 Notes*. 2008: Edmonton.
2. *Enhanced Oil Recovery/CO2 Injection*.   [cited 2010 Feb. 2]; Available from: http://www.fe.doe.gov/programs/oilgas/eor/.
3. Stalkup, F.I., *Carbon Dioxide Miscible Flooding: Past, Present, And Outlook for the Future.* Journal of Petroleum Technology, 1978. **30**(8): p. 1102-1112.
4. Hwang S.C., Lin Y., Hopke S.W., Kobayashi R. *Relation of liquid-liquid equilibrium behacior at low temperatures to vapor-liquid equilibria behavior at high temperatures and elevated pressures*. in *Fifty-Seventh Annual Convention of Gas Processors Association*. 1978: Gas Processors Association.
5. Stalkup, F.I., *Miscible Displacement*. SPE Monograph Series. 1983: SPE Publications.
6. S.J. Abedi, S. Seyfaie and J.M. Shaw *Simultaneous Phase Behavior, Elemental Composition and Density Measurement Using X-Ray Imaging.* Fluid Phase Equilibria, 1999. **Volumes 158-160**: p. 775-781.
7. Zou, Xiangyang, Xiaohui Zhang, and John M. Shaw, *Phase Behavior of Athabasca Vacuum Bottoms + n-Alkane Mixtures.* SPE Production & Operations, 2007. **22**(2): p. 265-272.
8. Levelt Sengers, J., *How fluids unmix: Discoveries by the School of Van derWaals and Kamerlingh Onnes*. 2002.
9. Van Konynenburg, P.H. and R.L. Scott, *Critical lines and phase equilibria in binary Van der Waals mixtures.* Phil. Trans. Roy. Soc. London, 1980. **298**: p. 495-540.
10. R. ENICK, G.D. HOLDER and B.I. MORSI, *Critical and Three Phase Behavior in the Carbon Dioxide/Tridacane System.* Fluid Phase Equilibria, 1985. **22**: p. 209-224.
11. Quifiones-Cisneros, Sergio E., *Phase and critical behavior in type III phase diagrams.* Fluid Phase Equilibria, 1997. **134**: p. 103-112.
12. S.A. Khan, G.A. Pope, K. Sepehrnoori, *Fluid Characterization of Three-Phase CO2/Oil Mixtures*, in *SPE/DOE Enhanced Oil Recovery Symposium*. 1992: Tulsa, Oklahoma.
13. A. BadamchiZadeh, H.W. Yarranton, B.B. Maini, M.A. Satyro, *Phase Behavior and Physical Property Measurements for Vapex Solvents: Part II. Propane, Carbon Dioxide, and Athabasca Bitumen.* Journal of Canadian . Petroleum. Technolgy., 2009. **48**(3): p. 57-65.
14. Polishuk, Ilya, Jaime Wisniak, and Hugo Segura, *Simultaneous prediction of the critical and sub-critical phase behavior in mixtures using equations of state II. Carbon dioxide-heavy n-alkanes.* Chemical Engineering Science, 2003. **58**(12): p. 2529-2550.
15. Miller, Melanie M. and Kraemer D. Luks, *Observations on the multiphase equilibria behavior of CO2-rich and ethane-rich mixtures.* Fluid Phase Equilibria, 1989. **44**(3): p. 295-304.
16. Shaw, John M and E. Behar, *SLLV phase behavior and phase diagram transitions in asymmetric hydrocarbon fluids.* Fluid Phase Equilibria, 2003. **209**: p. 185-206.
17. Vitu, Stéphane, Jean-Noël Jaubert, Jérôme Pauly, and Jean-Luc Daridon, *High-pressure phase behaviour of the binary system {CO2 + cis-decalin} from (292.75*

to 373.75) K. The Journal of Chemical Thermodynamics, 2008. **40**(9): p. 1358-1363.

18. Foreman, Christopher M. and Kraemer D. Luks, *Partial Miscibility Behavior of the Ternary Mixture Carbon Dioxide + n-Tetradecane + Methanol.* Journal of Chemical & Engineering Data, 2000. **45**(2): p. 334-337.

19. Florusse, L. J., T. Fornari, S. B. Bottini, and C. J. Peters, *Phase behavior of carbon dioxide--low-molecular weight triglycerides binary systems: measurements and thermodynamic modeling.* The Journal of Supercritical Fluids, 2004. **31**(2): p. 123-132.

20. Münüklü, P., F. Wubbolts, T. W. De Loos, and P. J. Jansens, *The phase behavior of systems of supercritical CO2 or propane with edible fats and a wax.* The Journal of Supercritical Fluids, 2006. **39**(1): p. 1-5.

21. Fulem, Michal, Mildred Becerra, M. D. Anwarul Hasan, Bei Zhao, and John M. Shaw, *Phase behaviour of Maya crude oil based on calorimetry and rheometry.* Fluid Phase Equilibria, 2008. **272**(1-2): p. 32-41.

22. Bazyleva, Ala B., M. D. Anwarul Hasan, Michal Fulem, Mildred Becerra, and John M. Shaw, *Bitumen and Heavy Oil Rheological Properties: Reconciliation with Viscosity Measurements.* Journal of Chemical & Engineering Data, 2009. **55**(3): p. 1389-1397.

23. Vitu, Stéphane, Jean-Noël Jaubert, Jérôme Pauly, Jean-Luc Daridon, and Danielle Barth, *Bubble and Dew Points of Carbon Dioxide + a Five-Component Synthetic Mixture:‰ Experimental Data and Modeling with the PPR78 Model.* Journal of Chemical & Engineering Data, 2007. **52**(5): p. 1851-1855.

24. Charoensombut-amon, T., Raymond J. Martin, and Riki Kobayashi, *Application of a generalized multiproperty apparatus to measure phase equilibrium and vapor phase densities of supercritical carbon dioxide in n-hexadecane systems up to 26 MPa.* Fluid Phase Equilibria, 1986. **31**(1): p. 89-104.

25. Liphard, K. G. and G. M. Schneider, *Phase equilibria and critical phenomena in fluid mixtures of carbon dioxide + 2,6,10,15,19,23-hexamethyltetracosane up to 423 K and 100 MPa.* The Journal of Chemical Thermodynamics, 1975. **7**(9): p. 805-814.

26. Brunner, Gerd, Carla Saure, and Dieter Buss, *Phase Equilibrium of Hydrogen, Carbon Dioxide, Squalene, and Squalane‰* Journal of Chemical & Engineering Data, 2009. **54**(5): p. 1598-1609.

27. Yokozeki, A., *Solubility correlation and phase behaviors of carbon dioxide and lubricant oil mixtures.* Applied Energy, 2007. **84**(2): p. 159-175.

28. Youbi-Idrissi M, Bonjour J, Terrier MF, Meunier F, and Marvillet C. *Solubility of CO2 in a synthetic oil*. in *international congress of refrigeration*. 2003. Washington DC.

29. Souza, Alexandre T., Marcos L. Corazza, Lúcio Cardozo-Filho, Reginaldo Guirardello, and M. Angela A. Meireles, *Phase Equilibrium Measurements for the System Clove (Eugenia caryophyllus) Oil + CO2.* Journal of Chemical & Engineering Data, 2004. **49**(2): p. 352-356.

30. Hottovy, John D., Kraemer D. Luks, and James P. Kohn, *Three-phase liquid-liquid-vapor equilibriums behavior of certain binary carbon dioxide-n-paraffin systems.* Journal of Chemical & Engineering Data, 1981. **26**(3): p. 256-258.

31. Gutierrez M, Lydia E. and Kraemer D. Luks, *Three-Phase Liquid-Liquid-Vapor Equilibria of the Binary Mixture Carbon Dioxide + 1-Methylnaphthalene.* Journal of Chemical & Engineering Data, 2001. **46**(3): p. 679-682.

32. Kulkarni, Ajit A., Kraemer D. Luks, and James P. Kohn, *Phase-equilibriums behavior of systems carbon dioxide-2-methylnaphthalene and carbon dioxide-n-decane-2-methylnaphthalene.* Journal of Chemical & Engineering Data, 1974. **19**(4): p. 349-354.

33. Lansangan, Roberto M., Adisak Jangkamolkulchai, and Kraemer D. Luks, *Binary vapor---liquid equilibria behavior in the vicinity of liquid---liquid---vapor loci.* Fluid Phase Equilibria, 1987. **36**: p. 49-66.

34. L.L. Larson, M.K. Silva, M.A. Taylor, F.M. Orr, *Temperature Dependence of L1/L2/V Behavior in CO2/Hydrocarbon Systems.* SPE Reservoir Engineering, 1989. **4**(1): p. 105-114.

35. E.A. Turek, R.S. Metcalfe, L. Yarborough, R.L. Robinson Jr., *Phase Equilibria in CO2 - Multicomponent Hydrocarbon Systems: Experimental Data and an Improved Prediction Technique.* SPE Journal, 1984. **24**(3): p. 308-324.

36. Huang, Edward T.S. and Joseph H. Tracht, *The Displacement of Residual Oil By Carbon Dioxide*, in *SPE Improved Oil Recovery Symposium*. 1974: Tulsa, Oklahoma.

37. F.M. Orr, A.D. Yu, C.L. Lien, *Phase Behavior of CO2 and Crude Oil in Low-Temperature Reservoirs.* SPE Journal, 1981. **21**(4): p. 480-492.

38. E.A. Turek, R.S. Metcalfe, R.E. Fishback, *Phase Behavior of Several CO2/ West Texas-Reservoir-Oil Systems.* SPE Reservoir Engineering, 1988. **3**(2): p. 505-516.

39. Bryant, D.W. and T.G. Monger, *Multiple-Contact Phase Behavior Measurement and Application With Mixtures Of CO2 and Highly Asphaltic Crude.* SPE Reservoir Engineering, 1988. **3**(2): p. 701-710.

40. F.M. Orr, C.M. Jensen, *Interpretation of Pressure-Composition Phase Diagrams for CO2/Crude-Oil Systems.* SPE Journal, 1984. **24**(5): p. 485-497.

41. Monger, T.G., *The Impact of Oil Aromaticity on CO2, Flooding.* SPE Journal, 1985. **25**(6): p. 865-874.

42. Monger, Teresa G., *Measurement and prediction of swelling factors and bubble points for paraffinic crude oils in the presence of CO2 and contaminant gases.* Industrial & Engineering Chemistry Research, 1987. **26**(6): p. 1147-1153.

43. Sako, Takeshi, Tsutomu Sugeta, Noriaki Nakazawa, Katsuto Otake, Masahito Sato, Katsuo Ishihara, and Masahiro Kato, *High pressure vapor-liquid and vapor-liquid-liquid equilibria for systems containing supercritical carbon dioxide, water and furfural.* Fluid Phase Equilibria, 1995. **108**(1-2): p. 293-303.

44. S.G. Sayegh, M. Sarbar, *Phase Behavior Properties of CO/Heavy Oil Mixtures for EOR Applications*, in *SPE California Regional Meeting*. 1990, Society of Petroleum Engineers Inc.: Ventura, California.

45. J. L. Creek, J.M. Sheffield, *Phase Behavior, Fluid Properties, and Displacement Characteristics of Permian Basin Reservoir Fluid/CO2 Systems.* SPE Reservoir Engineering, 1993. **Volume 8, Number 1**(February 1993): p. 34-42.

46. R. Eastick, W.Y. Svrcek, A.K. Mehrotra, *Phase behaviour of CO_2 -bitumen fractions.* The Canadian Journal of Chemical Engineering, 1992. **70**(1): p. 159-164.

47.   R.A. DeRuiter, L.J. Nash , M.S. Singletary, *Solubility and Displacement Behavior of a Viscous Crude With CO2 and Hydrocarbon Gases.* SPE Reservoir Engineering, 1994. **9**(2): p. 101-106.

48.   Pollack, Nick and Robert Enick, *The mapping of three phase volumetric behavior of pseudo-binary : Systems on pressure-composition diagrams.* Fluid Phase Equilibria, 1988. **39**(3): p. 325-332.

49.   Jamie L. Fall, Kraemer D. Luks, *Liquid-Liquid-Vapor Phase Equilibria Behavior of Certain Binary Carbon Dioxide + n-Alkylbezene Mixtures.* Fluid Phase Equilibria, 1986. **28**: p. 87-96.

50.   Kokal, Sunil L. and Selim G. Sayegh, *Phase behavior and physical properties of CO2-saturated heavy oil and its constitutive fractions: Experimental data and correlations.* Journal of Petroleum Science and Engineering, 1993. **9**(4): p. 289-302.

51.   A. K. Mehrotra, W.Y. Svrcek, *Properties of Cold Lake Bitumen Saturated with Pure Gases and Gas Mixtures.* THE CANADIAN JOURNAL OF CHEMICAL ENGINEERING, 1988. **66**: p. 656.

52.   J.S. Miller, R.A. Jones, *A Laboratory Study to Determine Physical Characteristics Of Heavy Oil After CO2 Saturation*, in *SPE/DOE Second Joint Symposium on Enhanced Oil Recovery*. 1981, SPE: Tulsa, Oklahoma.

53.   Quail, Beverly, G. A. Hill, and Kamal N. Jha, *Correlations of viscosity, gas solubility, and density for Saskatchewan heavy oils.* Industrial & Engineering Chemistry Research, 1988. **27**(3): p. 519-523.

54.   Miller, Melanie M. and Kraemer D. Luks, *The liquid-liquid-vapor phase equilibria behavior of the CO2 + ethane + n-tetradecylbenzene mixture.* Fluid Phase Equilibria, 1989. **51**: p. 315-326.

55.   Lee, R. J. and K. C. Chao, *Extraction of 1-methylnaphthalene and m-cresol with supercritical carbon dioxide and ethane.* Fluid Phase Equilibria, 1988. **43**(2-3): p. 329-340.

56.   Han, Buxing, Ding-Yu Peng, Cheng-Tze Fu, and George Vilcsak, *An apparatus for phase equilibrium studies of carbon dioxide+heavy hydrocarbon systems.* The Canadian Journal of Chemical Engineering, 1992. **70**(6): p. 1164-1171.

57.   Hong, Seung-Pyo, Kimberly A. Green, and Kraemer D. Luks, *Solubility and volumetric behavior of methane and carbon dioxide plus C7+ pseudocomponents of an oil.* Fluid Phase Equilibria, 1994. **95**: p. 267-280.

58.   Huang, S. H. and M. Radosz, *Phase behavior of reservoir fluids II: Supercritical carbon dioxide and bitumen fractions.* Fluid Phase Equilibria, 1990. **60**(1-2): p. 81-98.

59.   Inomata, H., K. Arai, and Saito S, *Vapor---liquid equilibria for CO2/hydrocarbon mixtures at elevated temperatures and pressures.* Fluid Phase Equilibria, 1987. **36**: p. 107-119.

60.   Kim, Choon Ho, Angela B. Clark, P. Vimalchand, and Marc D. Donohue, *High-pressure binary phase equilibria of aromatic hydrocarbons with carbon dioxide and ethane.* Journal of Chemical & Engineering Data, 1989. **34**(4): p. 391-395.

61.   Gasem, K. A. M., K. B. Dickson, P. B. Dulcamara, N. Nagarajan, and R. L. Robinson, *Equilibrium phase compositions, phase densities, and interfacial tensions for carbon dioxide + hydrocarbon systems. 5. Carbon dioxide + n-tetradecane.* Journal of Chemical & Engineering Data, 1989. **34**(2): p. 191-195.

62. Huie, Nicholas C., Kraemer D. Luks, and James P. Kohn, *Phase-equilibriums behavior of systems carbon dioxide-n-eicosane and carbon dioxide-n-decane-n-eicosane.* Journal of Chemical & Engineering Data, 1973. **18**(3): p. 311-313.

63. Liu, Z. M., G. Y. Yang, Y. Lu, B. X. Han, and H. K. Yan, *Phase equilibria of the CO2-Jiangsu crude oil system and precipitation of heavy components induced by supercritical CO2.* The Journal of Supercritical Fluids, 1999. **16**(1): p. 27-31.

64. A.K. Mehrotra, W.Y. Svrcek, C. Fu, V.R. Puttagunta, *Reconciliation of Bitumen Gas-Solubility Data.* AOSTRA Journal of Research, 1988. **4**: p. 237-243.

65. A.K. Mehrotra, J.A. Nighswander, N. Kalogerakis, *Data and Correlation for CO2-Peace River Bitumen Phase Behavior at 22-200 C.* AOSTRA Journal of Research, 1989. **5**(4): p. 351-358.

66. Yu, J. M., S. H. Huang, and M. Radosz, *Phase behavior of reservoir fluids: Supercritical carbon dioxide and cold lake Bitumen.* Fluid Phase Equilibria, 1989. **53**: p. 429-438.

67. Mohamed, Rahoma S. and Gerald D. Holder, *High pressure phase behavior in systems containing CO2 and heavier compounds with similar vapor pressures.* Fluid Phase Equilibria, 1987. **32**(3): p. 295-317.

68. Morris, William O. and Marc D. Donohue, *Vapor-liquid equilibria in mixtures containing carbon dioxide, toluene, and 1-methylnaphthalene.* Journal of Chemical & Engineering Data, 1985. **30**(3): p. 259-263.

69. R. Simon, A. Rosman, E. Zana, *Phase-Behavior Properties of CO2 - Reservoir Oil Systems.* SPE Journal, 1978. **18**(1): p. 20-26.

70. Novosad, Z., Costain, T.G., *Experimental and Modeling Studies of Asphaltene Equilibria for a Reservoir Under CO2 Injection*, in *SPE Annual Technical Conference and Exhibition*. 1992: New Orleans, Louisiana. p. 599-607.

71. S. L. Kokal, J. Najman, S. G. Sayegh, *Measurement And Correlation Of Asphaltene Precipitation From Heavy Oils By Gas Injection.* Journal of Canadian Petroleum Technology, 1992. **31**(4): p. 24-30.

72. Zabala, Damelys, Carlos Nieto-Draghi, Jean Charles de Hemptinne, and Aura L. LÃ³pez de Ramos, *Diffusion Coefficients in CO2/n-Alkane Binary Liquid Mixtures by Molecular Simulation.* The Journal of Physical Chemistry B, 2008. **112**(51): p. 16610-16618.

73. Upreti, Simant R. and Anil K. Mehrotra, *Experimental Measurement of Gas Diffusivity in Bitumen:â€‰ Results for Carbon Dioxide.* Industrial & Engineering Chemistry Research, 2000. **39**(4): p. 1080-1087.

74. Song, L., A. Kantzas, and J.L. Bryan, *Investigation of CO2 Diffusivity in Heavy Oil Using X-Ray Computer-Assisted Tomography Under Reservoir Conditions*, in *SPE International Conference on CO2 Capture, Storage, and Utilization*. 2010: New Orleans, Louisiana, USA.

75. Yang, Daoyong and Yongan Gu, *Determination of Diffusion Coefficients and Interface Mass-Transfer Coefficients of the Crude Oilâˆ'CO2 System by Analysis of the Dynamic and Equilibrium Interfacial Tensions.* Industrial & Engineering Chemistry Research, 2008. **47**(15): p. 5447-5455.

76. Tharanivasan, Asok Kumar, Chaodong Yang, and Yongan Gu, *Measurements of Molecular Diffusion Coefficients of Carbon Dioxide, Methane, and Propane in Heavy Oil under Reservoir Conditions.* Energy & Fuels, 2006. **20**(6): p. 2509-2517.

77. Zhang, Y. P., C. L. Hyndman, and B. B. Maini, *Measurement of gas diffusivity in heavy oils.* Journal of Petroleum Science and Engineering, 2000. **25**(1-2): p. 37-47.

78. Etminan, S. Reza, Brij B. Maini, Zhangxin Chen, and Hassan Hassanzadeh, *Constant-Pressure Technique for Gas Diffusivity and Solubility Measurements in Heavy Oil and Bitumen.* Energy & Fuels. **24**(1): p. 533-549.

79. Gross, T., J. Buchhauser, and H. D. Ludemann, *Self-diffusion in fluid carbon dioxide at high pressures.* The Journal of Chemical Physics, 1998. **109**(11): p. 4518-4522.

80. Mills, Ian, Tomislav Cvitas, and Klaus Homann, *Quantities, Units and Symbols in Physical Chemistry*. International Union of Pure and Applied Chemistry. 1993: BLACKWELL SCIENCE.

81. Rettich, Timothy R., Y. Paul Handa, Rubin Battino, and Emmerich Wilhelm, *Solubility of gases in liquids. 13. High-precision determination of Henry's constants for methane and ethane in liquid water at 275 to 328 K.* The Journal of Physical Chemistry, 1981. **85**(22): p. 3230-3237.

82. Krichevsky, I. R. and J. S. Kasarnovsky, *Thermodynamical Calculations of Solubilities of Nitrogen and Hydrogen in Water at High Pressures.* Journal of the American Chemical Society, 1935. **57**(11): p. 2168-2171.

83. Zhang, Xiaohui, *The Impact of Multiphase Behaviour on Coke Deposition in Heavy Oil Hydroprocessing Catalysts*, in *Chemical and Materials Engineering*. 2006, University of Alberta: Edmonton.

84. Shaver, R. D., R. L. Robinson, and K. A. M. Gasem, *An automated apparatus for equilibrium phase compositions, densities, and interfacial tensions: data for carbon dioxide + decane.* Fluid Phase Equilibria, 2001. **179**(1-2): p. 43-66.

85. Sato, Yoshiyuki, Yoshinori Tagashira, Daisuke Maruyama, Shigeki Takishima, and Hirokatsu Masuoka, *Solubility of carbon dioxide in eicosane, docosane, tetracosane, and octacosane at temperatures from 323 to 473 K and pressures up to 40 MPa.* Fluid Phase Equilibria, 1998. **147**(1-2): p. 181-193.

86. Roland Span, Wolfgang Wagner, *A New Equation of State for Carbon Dioxide Covering the Fluid Region from the Triple-Point Temperature to 1100 K at Pressures up to 800 MPa.* Journal of Physical and Chemical Reference Data, 1996. **25**: p. 1509-1596.

87. IUPAC. *Volume 15: Carbon Dioxide Series: International Thermodynamic Tables of the Fluid State*. 2010 [cited 2011; Available from: http://www.iupac.org/web/ins/121-17-95.

88. Gregg, C. J. and M. Radosz, *Vapor-liquid equilibria for carbon dioxide and 1-methylnaphthalene: experiment and correlation.* Fluid Phase Equilibria, 1993. **86**: p. 211-223.

89. Mukhopadhyay, Mamata and Shymal K. De, *Fluid Phase Behavior of Close Molecular Weight Fine Chemicals with Supercritical Carbon Dioxide.* Journal of Chemical & Engineering Data, 1995. **40**(4): p. 909-913.

90. Chou, Grace F., Rainald R. Forbert, and John M. Prausnitz, *High-pressure vapor-liquid equilibria for carbon dioxide/n-decane, carbon dioxide/tetralin, and carbon dioxide/n-decane/tetralin at 71.1 and 104.4.degree. C.* Journal of Chemical & Engineering Data, 1990. **35**(1): p. 26-29.

91. Bamberger, Andreas, Jürgen Schmelzer, Dieter Walther, and Gerd Maurer, *High-pressure vapour-liquid equilibria in binary mixtures of carbon dioxide and*

benzene compounds: experimental data for mixtures with ethylbenzene, isopropylbenzene, 1,2,4-trimethylbenzene, 1,3,5-trimethylbenzene, ethenylbenzene and isopropenylbenzene, and their correlation with the generalized Bender and Skjold-Jørgensen's group contribution equation of state. Fluid Phase Equilibria, 1994. **97**: p. 167-189.

92. Sadighian, Ardalan, Mildred Becerra, Ala Bazyleva, and John M. Shaw, *Forced and Diffusive Mass Transfer between Pentane and Athabasca Bitumen Fractions.* Energy & Fuels. **25**(2): p. 782-790.